Durham E-Theses

NMR studies of solid organometallic polymers

Davies, Nicola Anne

How to cite:

Davies, Nicola Anne (1992) *NMR studies of solid organometallic polymers*, Durham theses, Durham University. Available at Durham E-Theses Online: http://etheses.dur.ac.uk/6125/

Use policy

Nicola Davies

NMR studies of solid organometallic polymers

MSc   1992

A series of solid organometallic polymers is known, consisting of octahedrally coordinated $M(CN)_6$ [M=Co, Fe, Ru, Os] centres linked by trigonal bipyramidal connecting rods of the form R_3X [R=Me, Et, Bu] and derivatives thereof. These polymers have open structures with large cavities and channels and therefore could potentially be used as molecular sieves or ion-exchangers. Functionalisation of the rods could also lead to them being used as catalysts.

The polymers are, however, insoluble in water and commonly used solvents making it impossible to use solution-state analytical techniques. Single-crystals are also difficult to grow and therefore X-ray crystallographic studies have only been possible for a few of them.

The research described here is the analysis of the polymers using solid-state nuclear magnetic resonance (NMR) spectroscopy. It has been possible to probe their structures via a number of different nuclei since each polymer contains at least three spin-active nuclei (^{13}C, ^{119}Sn or ^{207}Pb, ^{15}N). Spectra have been obtained at ambient temperatures and for ^{13}C also at lowered and elevated temperatures. A two-dimensional spin-exchange experiment has been used to investigate an interesting exchange process. For those polymers whose structures are known the NMR chemical shift and anisotropy and asymmetry data have been correlated with structural features. This information has then been used to predict the structures of those polymers where X-ray crystallography has not yet been possible.

NMR STUDIES OF SOLID ORGANOMETALLIC POLYMERS

submitted by

Nicola Anne Davies

for the degree of Master of Science

at the University of Durham

Department of Chemistry

1992

2 2 DEC 1992

CONTENTS

FIGURE CAPTIONS

CHAPTER 4

CHAPTER 5

TABLES

Declaration

All the preparative work and the X-ray crystallography was performed at the University of Hamburg by the research group of Professor R. D. Fischer. None of the remainder of the work has been previously submitted for a degree in this or any other University.

Statement of Copyright

ACKNOWLEDGEMENTS

CHAPTER 1

INTRODUCTION

Introduction

Hoskins and Robson[1] predict that infinite three-dimensional frameworks could be constructed if a method could be found to link together octahedral or tetrahedral centres by rod-like connecting units. These frameworks would contain channels and cavities possibly giving them important chemical and physical properties in common with zeolites.

The channels and cavities allow diffusion of species through the framework enabling them to be used as molecular sieves or ion-exchangers. If the connecting rods are rigid enough then the materials may exhibit good thermal, chemical and mechanical properties together with a low density. If the channels and cavities are large enough to allow easy access, then it may be possible to functionalize the connecting rods after the construction of the framework. If one catalytic centre is attached to each rod, each cavity would on average enclose more than one catalytic centre and the open structure would also allow easy access of substrates and release of catalytic products.

In principle the cavities could be made larger than those in zeolites offering better access and a larger concentration of active sites.

Details of the preparation of a series of one-, two- or three-dimensional organometallic polymers have been described by Uson et al[2]. They can be prepared according to the following equation with n = 1, 2 or 3.

$$K_n[M(CN)_{2n}] + n[SnR_3S_2]ClO_4 \longrightarrow nKClO_4 + 2nS + [(R_3Sn)_n)M(CN)_{2n}]$$

S = solvent e.g. acetone, benzene
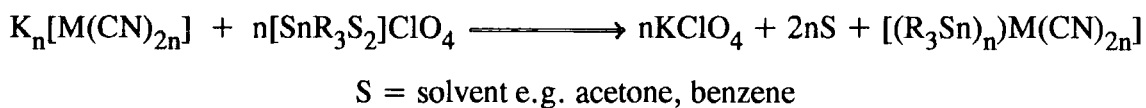
When n = 3 the product is a three dimensional framework with the metal atoms, M (e.g. Fe), as the octahedral centres linked by connecting rods of the form:

$$R \quad R$$
$$-C\equiv N-\underset{\underset{R}{|}}{\overset{\diagdown\diagup}{Sn}}-N\equiv C- \qquad R = Bu, Ph$$
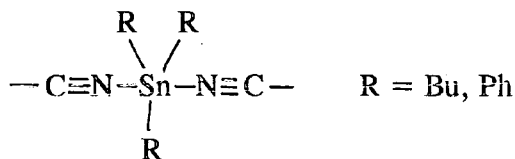
The product is formed by a process known as self assembly[3] in which an organised supramolecular structure is spontaneously formed from its component molecular parts.

The three-dimensional products are insoluble in water and organic solvents such as n-hexane and benzene. Infrared studies have given only one $\upsilon(CN)$ stretching vibration at a higher energy than that normally found for a terminal CN and therefore indicating that all the cyanides are bridging.

The research group of Professor R D Fischer, at the University of Hamburg, has prepared many three-dimensional polymers similar to those described above. The simplest of them have the following general forms.

$$[(R_3X)_3M(CN)_6] \qquad \begin{array}{l} M = Co \\ X = Sn \quad R = Me, Et, Bu \\ X = Pb \quad R = Me \end{array}$$

$$[(R_3X)_4M(CN)_6] \qquad \begin{array}{l} M = Fe, Ru, Os \\ X = Sn \quad R = Me \end{array}$$
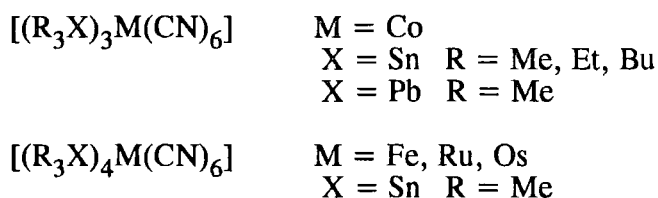
Their structures consist of octahedrally coordinated M atoms linked by trigonal bipyramidal rods of the form $CN-R_3X-NC$. The chains generated are infinite and tend to be non-linear.

$$-\underset{\diagup\;|}{\overset{|\;\diagup}{M}}-C\equiv N_{\diagdown} \atop \hspace{3cm} Sn_{\diagdown} \atop \hspace{4cm} N\equiv C-$$
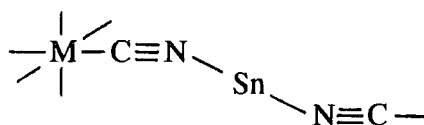
Cavities are formed which have a size of approximately 0.9 nm.

The polymers are insoluble in most commonly used organic solvents making the usual solution-state analytical techniques impossible. Single-crystals are also difficult to grow and the preparation usually leads to a polycrystalline precipitate.

Therefore X-ray crystallographic structure determination has only been possible for a few compounds. The aim of this research was to use multinuclear solid-state magnetic-resonance (NMR) spectroscopy to investigate some of these three-dimensional organometallic polymers. For those compounds where X-ray crystallography has been possible it was hoped that NMR data could be correlated with structural features. This information could then be useful in determining the structures of the other compounds.

The polymers studied have been divided into five groups

Tin and cobalt containing compounds

1    $[(Me_3Sn)_3Co(CN)_6]$

2    $[(Et_3Sn)_3Co(CN)_6]$

3    $[(Bu_3Sn)_3Co(CN)_6]$

Trimethyl tin compounds with different metal atoms

4    $[(Me_3Sn)_4Fe(CN)_6]$

5    $[(Me_3Sn)_4Ru(CN)_6]$

6    $[(Me_3Sn)_4Os(CN)_6]$

Derivatives of $[(Me_3Sn)_4Fe(CN)_6]$

7    $[(Me_3Sn)_4Fe(CN)_6.C_4H_8O_2/H_2O]$

8    $[(Me_3Sn)_4Fe(CN)_6.2H_2O]$

9    $[(Me_3Sn)_4Fe(CN)_6.D(+)glucose]$

Lead containing compounds

10    $[(Me_3Pb)_3Co(CN)_6]$

11    $[(Me_3Pb)_4Ru(CN)_6.2H_2O]$

12    $[(Me_3Pb)_4Fe(CN)_6.2H_2O]$

'Host-guest' systems

13   $[(Cp_2Co)(Me_3Sn)_3Fe(CN)_6]$

14   $[(Et_4N)(Me_3Sn)_3Fe(CN)_6]$
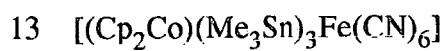
A description of the structures, where known, and the preparations of the polymers are given in chapter 4.

CHAPTER 2

THEORY OF NMR SPECTROSCOPY

2.1 Magnetisation and precession

Consider a sample containing only one type of nucleus with spin 1/2. The nuclear spin will have a magnetic moment. If this magnetic moment is placed in a static field, B_0 (in the z direction), it will tend to precess around B_0 at a frequency known as the Larmor frequency, ω (figure 2.1).

$$\omega = -\gamma B_0 \qquad \gamma = \text{magnetogyric ratio}$$

The magnetic moment will have a static component aligned with B_0 and a component rotating at the Larmor frequency in the xy plane. The magnetic moment interacts with the B_0 field generating two possible energy levels. The difference between the two energy levels ΔE is given by the following equation.

$$\Delta E = \hbar\, \gamma\, B_0$$

The two energy levels can be characterised by the nuclear spin quantum number m_I. Assuming γ is positive, then the state of lower energy has the nuclear magnetic moment aligned with its z component parallel to B_0. It is characterised by $m_I = 1/2$ and is called the α state. The β state, $m_I = -1/2$, is the higher energy state and has the z component antiparallel to B_0 (figures 2.1 & 2.2).

If a large number of nuclei are considered, all with the same Larmor frequency, there is a distribution between the two energy levels. This is a Boltzmann distribution, with more in the level of lower energy according to the following equation.

$$\frac{N_\beta}{N_\alpha} = \exp\left(-\Delta E\, /\, kT\right)$$

The sum of all the z components of magnetisation results in a net magnetisation in the positive z direction. The components precessing in the xy plane have a random distribution, resulting in a net magnetisation of zero. The net magnetisation, M_0, is therefore stationary and is aligned along the z axis.

Any perturbation of the system alters the populations of the two energy levels. The NMR signal is detected as the decay of magnetisation along the y axis which occurs as

a result of the system returning to equilibrium, with a normal Boltzmann distribution of populations in the energy levels, and a magnetisation M_o along z. Therefore, in order to observe an NMR signal, the system must be perturbed in some way. This is done by applying a second magnetic field, B_1, oscillating at a frequency appropriate to the nucleus under observation.

2.2   Rotating frame of reference

A rotating frame of reference is used to apparently eliminate the precession around B_o. The coordinates are chosen such that the z' axis is parallel to B_0 and the x' and y' axes are in the xy plane but are rotating about z' at the radio frequency v_1 and in the same direction. Each magnetic moment then appears to be static and in effect the external B_0 field has disappeared. Since only the rotating frame of reference will be used from now on the axes will be called x, y and z.

2.3   Effect of a pulse

In the rotating frame of reference the net magnetisation of a sample is static and aligned along the z axis (figure 2.3a). If a second magnetic field, B_1, is applied along the the x axis the spins bunch together resulting in phase coherence. The macroscopic view is that B_1 and M_o, being at right angles, exert a force on each other producing a torque. This results in the magnetisation being rotated around the B_1 axis (x) at a speed dependent on the strength of the B_1 field (figure 2.3b).

If the magnetisation is allowed to rotate through an angle θ, it will have a component along the z axis (M_z) and a component along the y axis (M_y).

$$M_z = M_o \cos\theta$$
$$M_y = M_o \sin\theta$$

Maximum magnetisation will be obtained in the y direction if the pulse angle is 90°. The length of time that the B_1 field is applied is called the pulse duration and is usually a few μs.

2.4 Relaxation

2.4.1 Spin-lattice (longitudinal) relaxation

After a 90° pulse the magnetisation will return to equilibrium in the z direction. For this to happen there must be some form of interaction between the spins and their surroundings so that the excess energy can be lost. The rate at which this happens depends on the efficiency of this process and is characterised by the time constant T_1. Following the 90° pulse, the magnetisation grows exponentially in the z direction according to the following equation.

$$M_z = M_0 (1 - e^{-t/T_1})$$

2.4.2 Spin-spin (transverse) relaxation

The process by which the magnetisation in the xy plane decays is characterised by the time constant T_2^* and is frequently dominated by the effects of magnetic field inhomogeneities in B_0. Immediately after a 90° pulse the magnetisation is along the y axis (figure 2.4a). However, different parts of the sample experience slightly different magnetic fields and each group of spins (called isochromats) will precess with its own characteristic Larmor frequency. Some spin isochromats will precess faster than the average and some will precess slower, that is they begin to fan out or dephase (figure 2.4b). The sum of all the components of magnetisation along the y axis is less than maximum and decays exponentially with a time constant T_2^*. This decay of magnetisation is recorded as the Free Induction Decay (FID) (see section 2.6).

An intrinsic relaxation time constant T_2 may be defined in many cases which is characteristic of the magnetisation decay in one of the spin isochromats without any field inhomogeneities. This is called the spin-spin or transverse relaxation time.

2.4.3   Spin-lattice relaxation in the rotating frame

Consider a 90° pulse brought about by a field B_1 along the x axis causing the magnetisation to rotate from the z axis into y. If the B_1 field is then phase shifted by 90° into the y axis it will be acting in the same direction as the magnetisation. The spins are now said to be spin-locked (figure 2.5). $T_{1\rho}$ is the characteristic time constant of the decay of this spin-locked magnetisation.

In the solid-state $T_2 << T_{1\rho} << T_1$ and are of the order of μs, ms and s respectively.

2.5   Single-pulse experiment

The single-pulse experiment (figure 2.6) consists of a 90° pulse after which a free inducion decay (FID) is recorded over a length of time, dependent on T_2^*, called the acquisition time (AT). In order to improve the signal-to-noise ratio the experiment is repeated a number of times, n, called the number of transients (NT). The FID's are then added together before the Fourier transform (FT) is performed. Since the signal will always be in the same place, on addition it will increase in intensity proportional to n. Noise however is random and on addition it will interfere and will increase in intensity proportional to $\sqrt{n}$. The important factor is the signal-to-noise ratio.

$$\frac{S}{N} \propto \sqrt{n}$$

In this single-pulse experiment, if the second 90° pulse is applied directly after the acquisition time then it is unlikely that the magnetisation will have relaxed fully back to M_o in the z direction. Successive 90° pulses will therefore produce a

21

signal less intense than the first. This is called saturation and can be overcome if a delay is left between the acquisition and the next pulse. This delay is called the recycle delay (RD) and its length is dependent on T_1. In order to obtain maximum signal from each transient the RD should be five times T_1 but in practice a shorter value is usually used. This is discussed in section 3.5.

2.6 Free induction decay and the Fourier transform

As described earlier the free induction decay (FID) is a graph of how the intensity of the magnetisation in the y axis decays with time. It is characterised by the time constant T_2^* and, in simple cases, is an exponential decay. The FID is a decaying interferogram of a number of frequencies (all recorded with respect to the radio-frequency) and is usually too complicated to be analysed directly, so it is converted into the frequency domain by a mathematical method called the Fourier transform (FT) (figure 2.7).

2.7 Main interactions affecting the NMR linewidth

NMR signals are the result of the magnetic moments of nuclei interacting with external magnetic fields, i.e. local fields created by the surrounding nuclei and the electronic charge distribution around the nuclei. The main interactions are listed below in frequency units, each being represented by a Hamiltonian, H.

Zeeman interaction

The Zeeman interaction occurs for all nuclei with either an odd atomic mass or odd atomic number. It is an interaction between the magnetic moment of the nucleus and the external magnetic field B_0 and produces the $2I + 1$ energy levels (I = spin of nucleus).

$$H_Z = -\gamma\ \bar{I}.\bar{B}_0 \qquad \gamma = \text{magnetogyric ratio}$$

Dipolar interaction

The dipolar interaction is the direct interaction between the dipoles of two nuclei. It can either be homonuclear between like spins, I, or heteronuclear between two unlike spins I and S.

$$H_D = H_{II} = \frac{\mu_o\ \gamma_I^2\ \hbar\ \bar{I}.\hat{D}.\bar{I}}{4\pi\ r_{II}^3}$$

$$H_D = H_{IS} = \frac{\mu_o\ \gamma_I\ \gamma_S\ \hbar\ \bar{I}.\hat{D}.\bar{S}}{4\pi\ r_{IS}^3}$$

$$D = \text{dipolar coupling tensor}$$

The dipolar interaction is independent of B_0 and it falls off rapidly with internuclear distance r.

Shielding interaction

The shielding interaction is due to the shielding of the nucleus from the external field by the surrounding electrons.

$$H_S = \gamma_I \, \bar{I}.\hat{\sigma}.\bar{B}_o$$

It is the most sensitive interaction to the geometry and surrounding environment of the nucleus.

Spin-spin interaction

This is the indirect interaction between a pair of spins I and S and is often called J coupling.

$$H_J = \bar{I}.\hat{J}.\bar{S}$$

It is independent of the field and is usually small compared to other interactions.

Quadrupolar interaction

The quadrupolar interaction only occurs for nuclei with spin greater than 1/2. It is an interaction between the nuclear electric quadrupolar moment, eQ, and the non-spherically symmetric electric field gradient (efg) around the nucleus.

$$H_Q = \bar{I}.\hat{Q}.\bar{I}$$

It is dependent on the B_o field and if present is often dominating.

The total Hamiltonian can be written as a sum of the Hamiltonians for all the above interactions.

$$H = H_Z + H_D + H_S + H_J + H_Q$$

$\bar{I}$, $\bar{S}$ and $\bar{B}_o$ are all vector quantities, that is they have magnitude and direction. Therefore, any interaction between them will be three-dimensional and must be described by a 3 by 3 matrix or tensor. The tensors $\hat{D}$, $\hat{\sigma}$, $\hat{J}$ and $\hat{Q}$ can all be

converted into a diagonal form and as a result the interactions can be characterised by the three principal elements, for example σ_{xx}, σ_{yy} and σ_{zz}.

2.8 Difference between solution-state and solid-state NMR

In liquids there is fast isotropic motion resulting in an averaging of the interactions. The shielding interaction is averaged to a discrete value giving the chemical shift and the spin-spin interaction averages to give the coupling constant J. Both the dipolar and the quadrupolar interactions are averaged to zero. The result of the motion is therefore to give a high-resolution spectrum containing much useful information.

In the solid-state there is much less motion and therefore the interactions are not averaged completely. This causes broadening of the NMR signals to such an extent that only a broad featureless spectrum is obtained (figure 2.8a).

2.9 Main broadening mechanisms in solids

The nuclei ^{13}C, ^{119}Sn, ^{207}Pb and ^{15}N have a low natural abundance and are called rare spins. This can be a disadvantage since the intensity of the NMR signals will be relatively low. However, there is also a large advantage. Due to the low natural abundance it is unlikely that two spin-active nuclei will be close enough to give any strong homonuclear dipolar interactions. Therefore nearly all homonuclear broadening will be eliminated. The remaining three major broadening mechanisms are as follows.

Heteronuclear dipolar interactions: The strongest are those between the rare spins (^{n}X) and protons (^{1}H) and can be as large as 50 kHz.

Shielding interactions: This interaction is anisotropic, that is it is orientation dependent. In the solution-state molecular motion averages the interaction and an isotropic chemical shift is observed. In the solid-state there is less motion

resulting in a chemical shift that is dependent on the orientation of the molecule within the magnetic field B_o. Typical values of anisotropy for ^{119}Sn are between 20 and 40 kHz and for ^{207}Pb between 80 and 85 kHz.

X-Y interactions: These can be dipolar, J or quadrupolar and are all anisotropic. The J interaction can be averaged to give an isotropic value measurable from the spectrum. Some typical J values are;

$$J_{13C-119Sn} = 450 - 550 \text{ Hz}$$
$$J_{13C-207Pb} = 350 - 450 \text{ Hz}$$

2.10   Removal of broadening mechanisms

In order to obtain chemical shift and other data from a solid sample it is necessary to remove the broadening mechanisms using the following techniques.

2.10.1   High power proton decoupling

By applying a continuous proton radio-frequency (rf) field the heteronuclear coupling of the protons to the rare spins can be removed giving some resolution in the spectrum (figure 2.8b). In the solid-state this rf has to be at a high power of approximately 100 W. Even so if the coupling is strong, such as in a CH_2 group, it will not be completely removed, resulting in some broadening of the signal. A signal from a CH_3 group, however, is sharp by comparison, due to motional averaging. The ethyl region of the ^{13}C spectrum of $[(Et_3Sn)_3Co(CN)_6]$ (figure 5.1.2) illustrates this difference.

High-power proton decoupling also eliminates the indirect (X,H) coupling, J_{XH}.

2.10.2 Magic-Angle-Spinning

Shielding anisotropy

The dominant broadening mechanism is often the shielding interaction. It is an interaction between the nucleus and the surrounding electrons and is three-dimensional.

$\hat{\sigma}$, the shielding tensor, may be expressed by a diagonalised 3 by 3 matrix containing only the principal components σ_{xx}, σ_{yy} and σ_{zz} as described earlier. These three shielding tensor components can then be used to characterise the three-dimensional interaction. Using the convention

$$|\sigma_{zz} - \sigma_{iso}| \geq |\sigma_{xx} - \sigma_{iso}| \geq |\sigma_{yy} - \sigma_{iso}|$$

where σ_{iso} is the isotropic average

$$\sigma_{iso} = 1/3 \ (\sigma_{xx} + \sigma_{yy} + \sigma_{zz})$$

the following parameters are defined.

$$\text{Anisotropy} \quad \beth = \sigma_{zz} - \sigma_{iso}$$

$$\text{Asymmetry} \quad \eta = \frac{\sigma_{yy} - \sigma_{xx}}{\beth}$$

The convention used ensures that the asymmetry will always fall between zero and one.

Figure 2.9 illustrates three possible cases. In case A there is spherical symmetry with a zero value for both the anisotropy and the asymmetry. In case B there is axial symmetry, resulting in a zero asymmetry but an anisotropy differing from zero. This arises due to two of the shielding tensors (σ_{yy} and σ_{xx}) being equal. Case C is the general case with non-zero values for both the asymmetry and the anisotropy.

Consider a single crystal containing a cyanide group. A single sharp ^{13}C signal will be observed for a particular orientation of the crystal in the magnetic field. If the orientation is changed, then the chemical shift of the signal will also change. Figure 2.10a shows two possible orientations of the cyanide in the magnetic field.

In a powdered sample all possible orientations will exist, each producing a signal at a different chemical shift. The signals will overlap to produce a broad powder pattern. In an axially symmetric system such as the cyanide the two shielding tensor components σ_{xx} and σ_{yy} are equal (figure 2.10b). They are usually represented by a single term $\sigma_\perp$ being the component perpendicular to the magnetic field. σ_{zz} is given the symbol $\sigma_{//}$ and is the component of the shielding tensor parallel to the magnetic field. An axially symmetric system will have an asymmetry equal to zero and an anisotropy differing from zero.

In a more general case (figure 2.10c), the shape of the powder pattern depends on all three shielding tensors σ_{xx}, σ_{yy} and σ_{zz}. It is said to be anisotropic and will have non-zero values for both the anisotropy and the asymmetry.

Magic-Angle-Spinning

As discussed in section 2.7, the shielding interaction can be expressed by the following Hamiltonian.

$$H_S = \gamma_I \, \bar{I}.\hat{\sigma}.\bar{B}_o$$

The spatial part of this Hamiltonian is proportional to $(3\cos^2\theta - 1)$ which may be written in a different form.

$$3\cos^2\theta - 1 = \frac{1}{2}(1 - 3\cos^2\beta)(1 - 3\cos^2\chi) + \frac{3}{2}\sin2\beta\sin2\chi\cos(\omega_r t) + \frac{3}{2}\sin^2\beta\sin^2\chi\cos(2\omega_r t)$$

The magic-angle-spinning (MAS) technique[4] involves packing the powdered sample into a cylindrical container (rotor), inclining it at an angle β to the external magnetic field B_o, and then spinning it at a frequency ω_r (figure 2.11). Consider one particular dipole within the sample, in the plane containing B_o and the rotation axis, inclined at an angle θ to B_o. The angle between the dipole and the axis of rotation is χ. In a powder all values of θ will exist and therefore so will all values of χ.

The angle β can be set by the operator and if it is set to an angle 54.7° then the first term in the above equation will equal zero.

$$\frac{1}{2}(1-3\cos^2\beta)(1-3\cos^2\chi) = 0$$

This angle is called the magic angle.

The second and third terms will average to zero if the spin-rate ω_r is much greater than the shielding anisotropy and the spectrum will contain a single line at an isotropic chemical shift. However, the maximum spin-rate possible for the probes used for this research is approximately 14 kHz which is smaller than the shielding interactions in many of the compounds studied. This results in the second and third terms being only partially averaged leading to the appearance of spinning sidebands in the spectrum. The spinning sidebands will have a separation equal to the spin-rate and their intensities will approximately follow the shape of the powder pattern (figure 2.12). Spinning sidebands can be used to obtain values for the shielding anisotropy and asymmetry parameters (section 3.7 and 5.6).

If both high-power proton decoupling and magic-angle-spinning techniques are used then a spectrum can be obtained with good resolution (figure 2.8c).

2.10.3   X-Y coupling

The third broadening mechanism is X-Y coupling which can be due to either a direct dipolar interaction, an indirect spin-spin interaction or a quadrupolar interaction. The anisotropy in J is removed by MAS but the isotropic spin-spin interaction is not removed but is usually quite small. It is observed in the spectrum as J coupling if the linewidth is less than the value for the coupling.

Direct X-H dipolar interactions have already been removed by high-power proton decoupling. Other dipolar interactions and first-order quadrupolar interactions can be removed by MAS since their Hamiltonians also contain a spatial term which is proportional to $3\cos^2\theta$. However, if the strength of the interaction is greater than

29

the spin-rate then it will not be completely removed, but spinning sidebands may appear. Also, second-order quadrupolar effects cannot be removed by MAS and, if present, produce a very complicated spectrum. However, MAS will remove the relatively weak dipolar interactions between the rare (observed) spins.

2.11   Cross-polarisation experiment

Dipolar coupling can also be useful. In the cross-polarisation (CP) experiment[5] it provides a mechanism, under certain conditions, for the transfer of magnetisation from the abundant spins (^1H) to the less abundant (rare) spins (^nX e.g. ^{13}C, ^{119}Sn).

Figure 2.13 shows the pulse sequence for the CP experiment which can be divided into four sections.

1.   Firstly a 90° pulse is applied to the ^1H channel along the x axis which causes the magnetisation to rotate into the y axis.

2.   The proton magnetisation is spin-locked along the y axis by a pulse on the ^1H channel which is 90° out of phase with the first pulse (see section 2.4.3). At the same time a pulse is applied on the X channel. The duration of these simultaneous pulses is called the contact time (CT) and is of the order of ms.

   If the two r.f. magnetic fields (B_{1H} and B_{1X}) are chosen to fulfil the Hartmann-Hahn condition[6] then polarisation transfer can occur from ^1H to ^nX.

$$\text{Hartmann-Hahn condition} : \gamma_H B_{1H} = \gamma_X B_{1X}$$

   During this time the X magnetisation grows and the ^1H magnetisation decays slightly.

3.   The B_{1X} field is then switched off and an FID is recorded over the acquisition time (AT). During this time the B_{1H} field is kept on for heteronuclear decoupling of the ^1H-^nX dipolar interactions.

4. Finally, the B_{1H} field is also switched off and the system is allowed to relax for a recycle delay (RD) before the whole sequence is repeated.

Advantages in using the CP experiment

The CP experiment has two advantages. The first is that in theory there is a gain in signal equal to the ratio of the two gamma values. For ^{13}C the signal is four times that normally obtained following a single 90° pulse.

The second advantage is that the length of the recycle delay is now dependent on the ^1H relaxation rather than that of the X nucleus. Since in most cases the ^1H relaxation is quicker, it is possible to use a shorter RD than would be needed in a single-pulse experiment. There is, therefore, an increase in the signal-to-noise ratio within a given time.

Disadvantage in using the CP experiment

The main disadvantage in using the CP experiment is that the relative intensities of the signals in the spectrum may not always reflect the actual relative number of nuclei in different environments. This is because the rate of polarisation transfer to the different environments may not be the same.

Consider a sample containing an equal number of two very different X nuclei environments. Figure 2.14 shows typical graphs, for two environments, of magnetisation growth and decay with increasing contact time. The equation for this curve[7] is given below.

$$M(t) = M_o \, \lambda^{-1} \, [1 - \exp(\frac{-\lambda t}{T_{CH}})] \, \exp(\frac{-t}{T_{1\rho}^H})$$

$$\text{where} \quad \lambda = 1 + \frac{T_{CH}}{T_{1\rho}^C} - \frac{T_{CH}}{T_{1\rho}^H}$$

31

M_o = equilibrium magnetisation

$M(t)$ = magnetisation at time t

T_{CH} = time constant for the rate of CP under spin-locked conditions

$T_{1\rho}{}^H$ = time constant for the decay of ^1H magnetisation under spin-locked conditions

$T_{1\rho}{}^C$ = time constant for the decay of ^{13}C magnetisation under spin-locked conditions

To simplify the equation, the following approximations are used. Both $T_{1\rho}{}^H$ and $T_{1\rho}{}^C$ are usually long compared to T_{CH} and therefore the second and third terms in the equation for λ approximate to zero resulting in $\lambda = 1$. This simplifies the equation for $M(t)$ as follows:

$$M(t) = M_o \left[1 - \exp(\frac{-t}{T_{CH}})\right] \exp(\frac{-t}{T_{1\rho}{}^H})$$

The first part of the curve, where the magnetisation is increasing, is characterised by the term containing T_{CH} and the second part of the curve, where the magnetisation decays, is dominated by the $T_{1\rho}{}^H$ term.

Figure 2.14 shows two graphs of contact time vs. signal intensity. Both have the same M_o value, in arbitrary units, of 100 but different values for T_{CH} and $T_{1\rho}{}^H$. In a single-pulse experiment the two signals would be expected to be of equal intensity provided adequate relaxation delays are allowed. However, in a CP experiment, if the contact time was optimised for 1 (approximately 1.5 ms) the intensity of signal 2 would be less than half that of 1. A true relative intensity ratio would be found at a point where the two curves cross, i.e. a contact time of approximately 4.5 ms. In practise a series of experiments would be done at different contact times producing graphs like those in fig 2.14. These could then be fitted to the equation by computer resulting in calculated M_o values.

2.12 Two-dimensional spin-exchange experiment

A simple 2-D experiment

Consider first a simple 2-D experiment performed on a sample containing only one environment using the following pulse sequence.

$$90_x \text{——} t_1 \text{——} 90_x \text{——} t_2 \text{——}$$

For one value of t_1, an FID will be acquired over the time t_2, which when transformed will contain only one signal. If a range of t_1 values is used, a series of spectra will be produced each with one signal which will modulate in intensity as t_1 is increased. This process has converted a function in two time domains to a function with one time domain and one frequency domain.

$$f(t_1, t_2) \text{——————} \longrightarrow f(t_1, \nu_2)$$

If the point at the top of the signal is taken from each spectrum and plotted as a function of t_1 then another FID will be produced although it doesn't exist in real time. If the same is done for every point on the spectrum then a whole series of FID's will be produced. A second Fourier transform over the t_1 domain produces a 2-D spectrum with two frequency domains.

$$f(t_1, \nu_2) \text{——————} \longrightarrow f(\nu_1, \nu_2)$$

2-D spin-exchange experiment

The 2-D spin-exchange experiment allows exchange processes to be observed. The solid-state experiment[8] described here is analogous to the solution-state experiment[9] except that the first 90° pulse has been replaced by a cross-polarisation preparation. The pulse-sequence is given in figure 2.15 and can be divided into four sections.

Preparation

This is a cross-polarisation preparation as described in section 2.11 and results in the ^{13}C magnetisation being spin-locked in the xy plane.

Evolution

During the evolution time t_1 the B_1^H field is kept on for high-power proton decoupling and the ^{13}C spins experience the shielding interaction. A 90° pulse at the end of this time transfers the magnetisation into the z direction. Each ^{13}C spin isochromat has in effect been labelled with its chemical shift.

Mixing time

The mixing time allows communication to take place between the ^{13}C spins. If exchange (or spin diffusion) does take place, a particular ^{13}C spin will be labelled with a new chemical shift as a result of its new environment. The 90° pulse then transfers the magnetisation back into the xy plane.

Acquisition time

The acquisition takes place over a time t_2. A recycle delay is left before the sequence is repeated.

A 2-D Fourier transform results in a spectrum which contains the ordinary CP spectrum along the diagonal and off-diagonal cross-peaks indicating exchange processes occurring between any two or more sites (see section 5.2.5 and figure 5.2.7a).
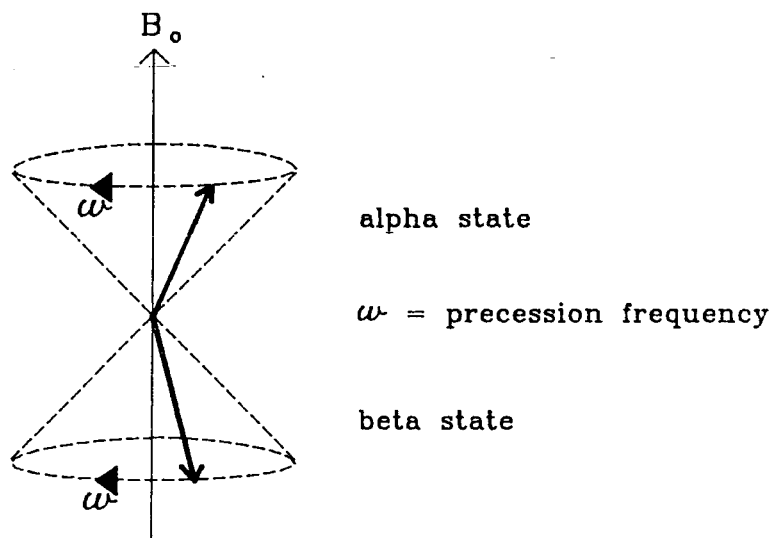
Figure 2.1   Precession of magnetic moments about a static magnetic field B_o
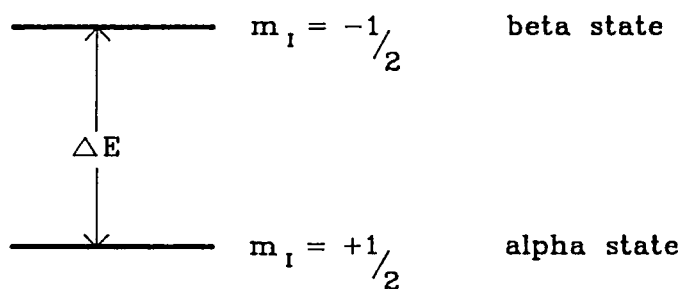
Figure 2.2   Energy levels generated by one spin-1/2 nucleus in B_o
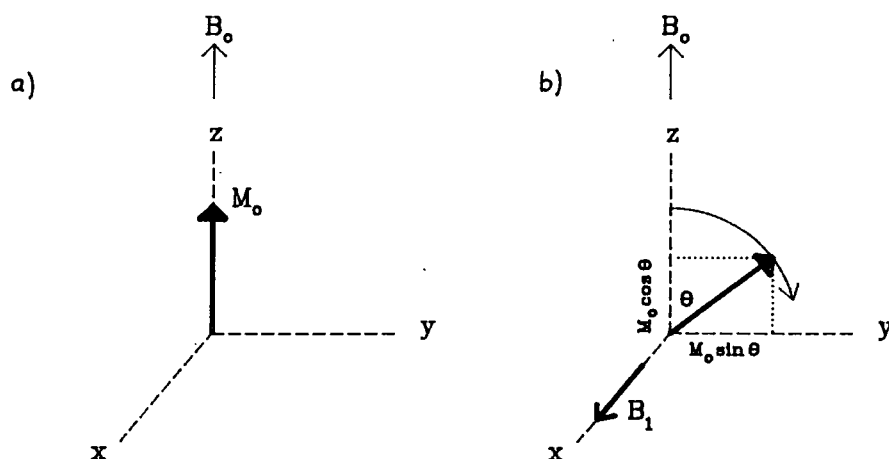
Figure 2.3   Effect of a pulse

Immediately after
a 90 pulse

A short time later
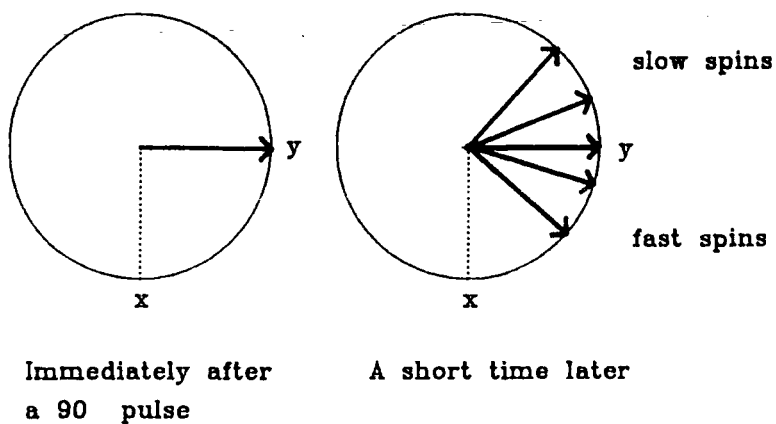
Figure 2.4   Dephasing of the spins leading to spin-spin (transverse) relaxation

Co-ordinate system used
in the diagrams below
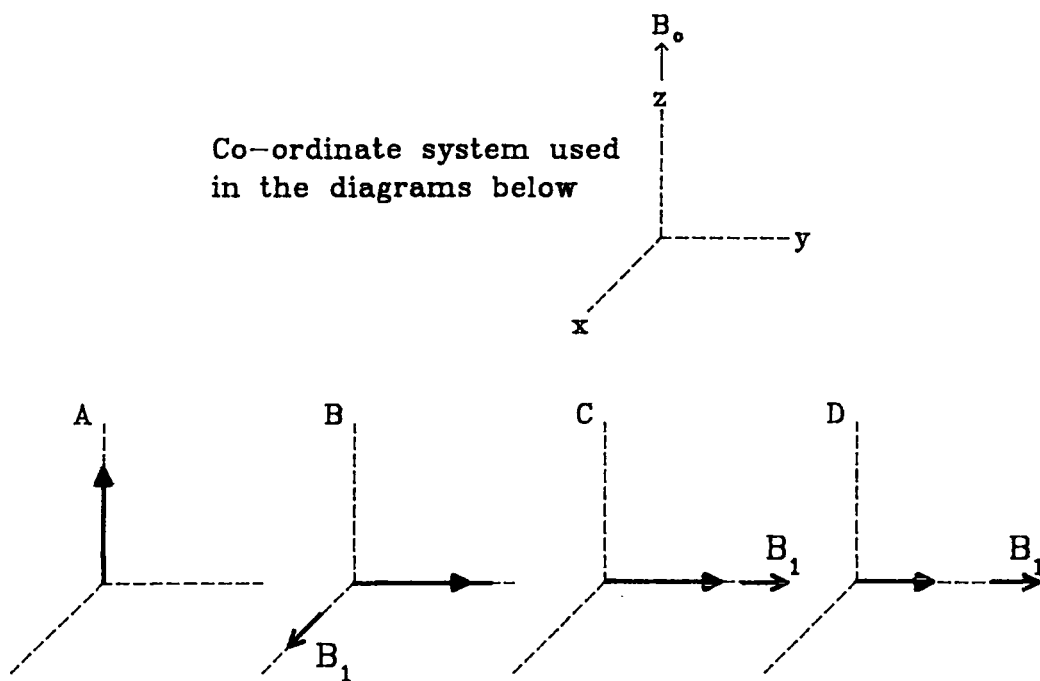
A   Magnetisation at equilibrium

B B_1 field rotates magnetisation into the y axis (90° pulse)

C 90° phase shift of B_1 field produces spin-locking pulse

D   Magnetisation decays with time

Figure 2.5   Spin-lattice relaxation in the rotating frame

90°
pulse

←——— Acquisition time ———✕——— Recycle delay ———→
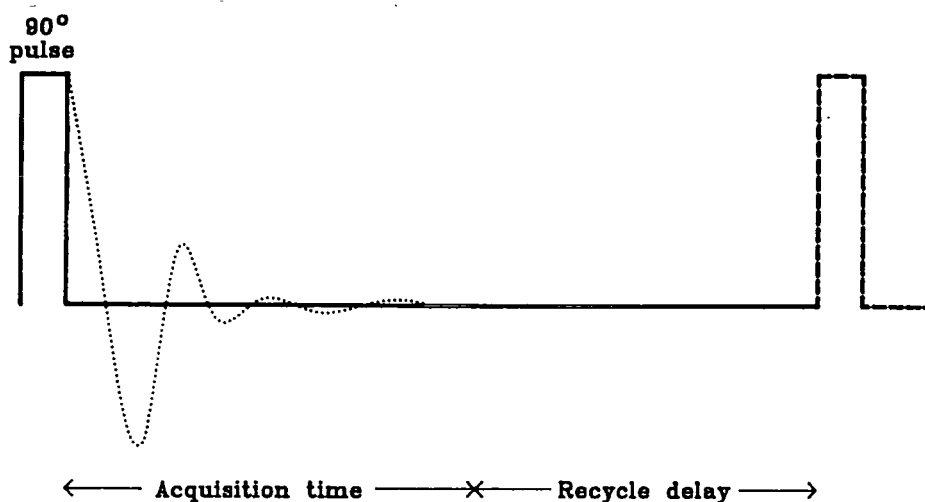
Figure 2.6   Pulse sequence for a single-pulse experiment

a)

2 ms

b)

350   300   250   200   150   100   50   0   −50 PPM−100
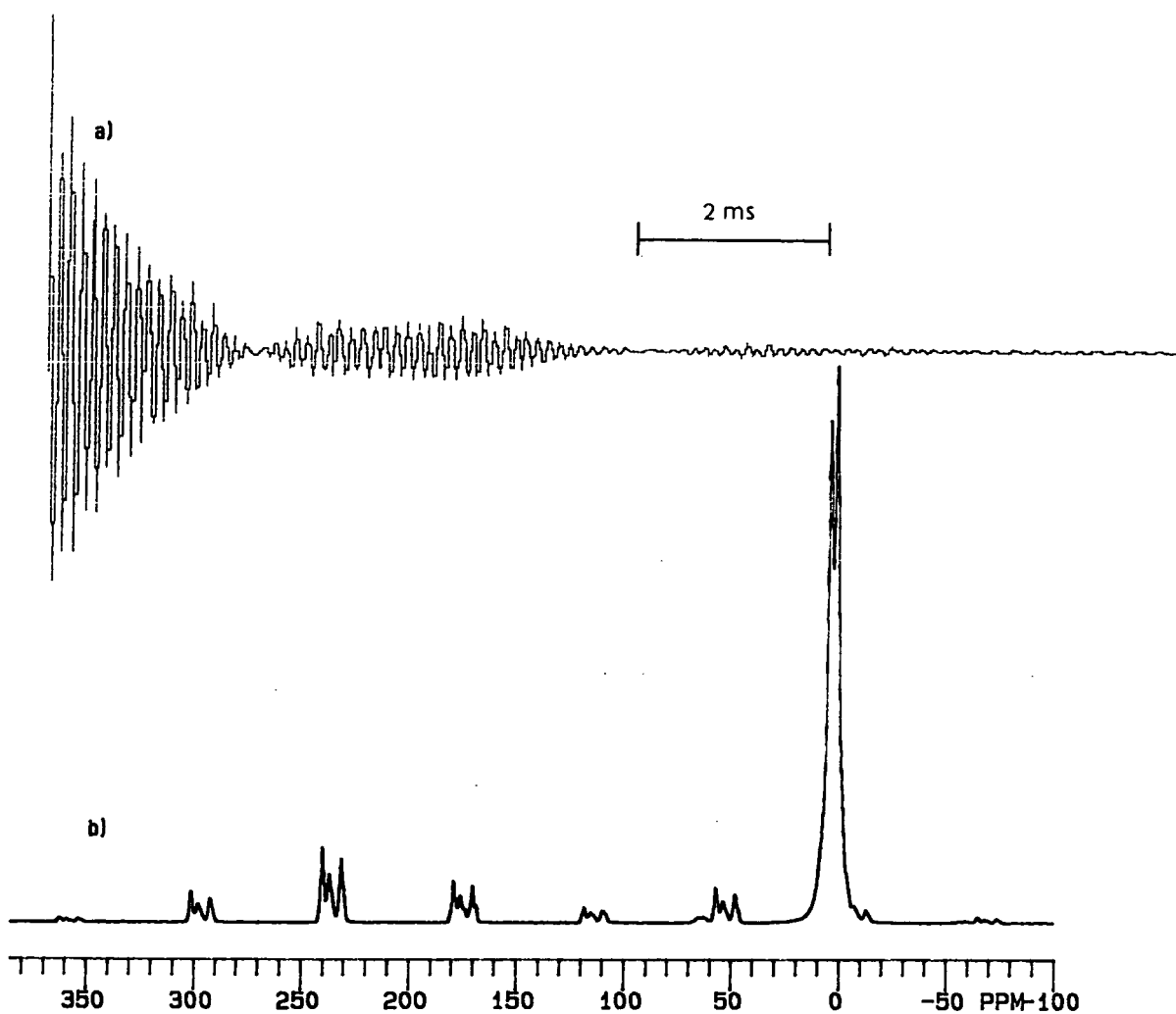
Figure 2.7   a) A ^{13}C free induction decay for $[(Me_3Sn)_4Fe(CN)_6]$ and b) the
resulting ^{13}C spectrum following a Fourier transform

37
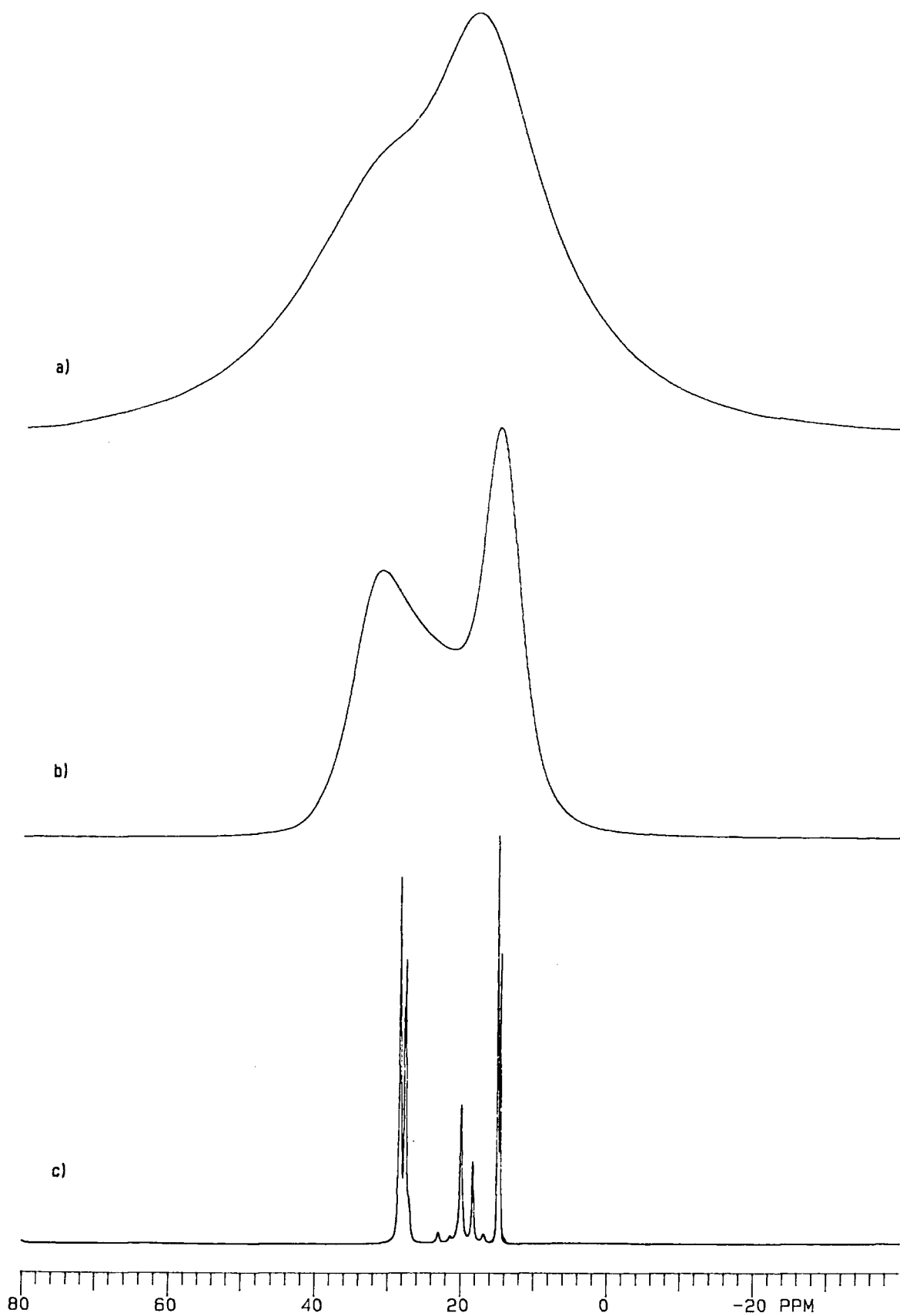
Figure 2.8 ^{13}C solid-state spectrum of $[(Bu_3Sn)_3Co(CN)_6]$ a) static with no
decouping   b) static with high-power proton decoupling and
c) with decoupling and MAS

Case A :   spherical symmetry
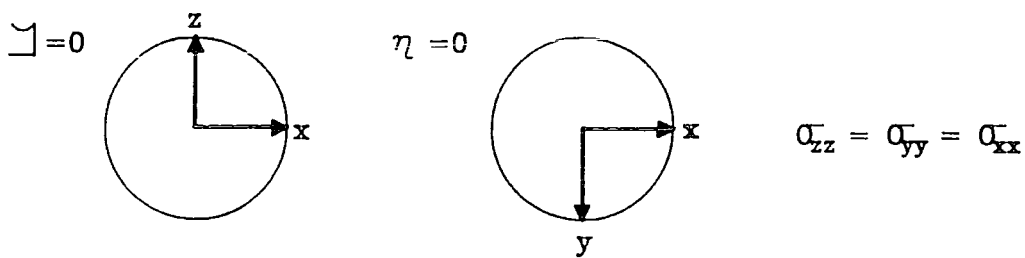
$\beth = 0$ $\eta = 0$ $\sigma_{zz} = \sigma_{yy} = \sigma_{xx}$

Case B :   axial symmetry

$\beth \neq 0$ $\eta = 0$ $\sigma_{zz} > \sigma_{yy} = \sigma_{xx}$

Case C :   asymmetry

$\beth \neq 0$ $1 \geqslant \eta \geqslant 0$ $\sigma_{zz} > \sigma_{yy} > \sigma_{xx}$
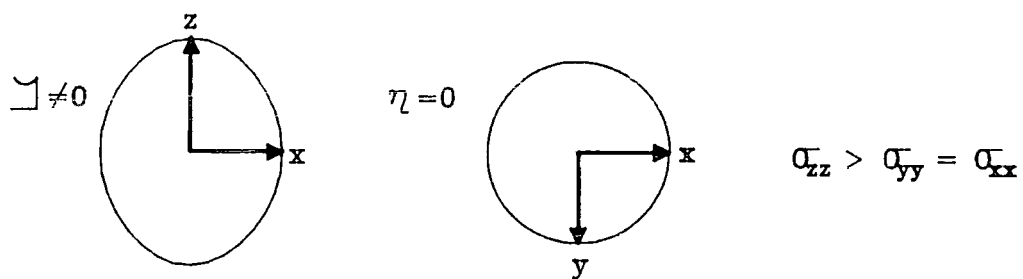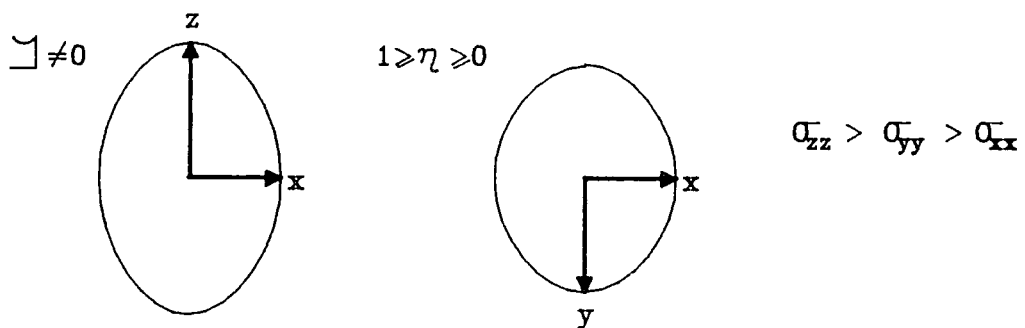
$\beth$ = anisotropy

η = asymmetry

$\sigma_{zz}, \sigma_{yy}, \sigma_{xx}$ = shielding tensor components

Figure 2.9   Illustration of the three-dimensional nature of shielding anisotropy
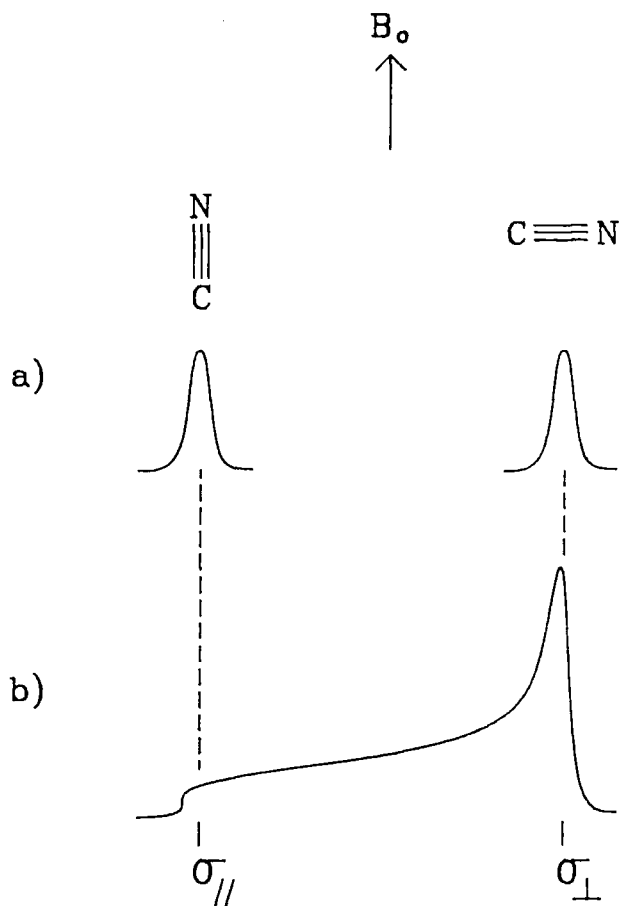
$\sigma_{//}$ = shielding tensor component parallel to B_o

$\sigma_{\perp}$ = shielding tensor component perpendicular to B_o
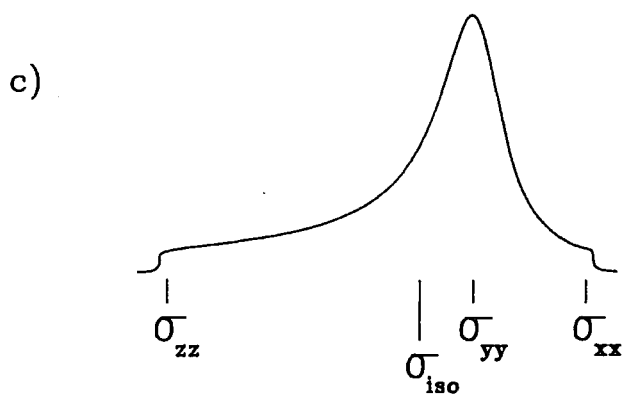
Figure 2.10   a) NMR signal from a single crystal in two particular orientations to B_o
b) A powder pattern for an axially symmetric system
c) A powder pattern for a generally asymmetric system
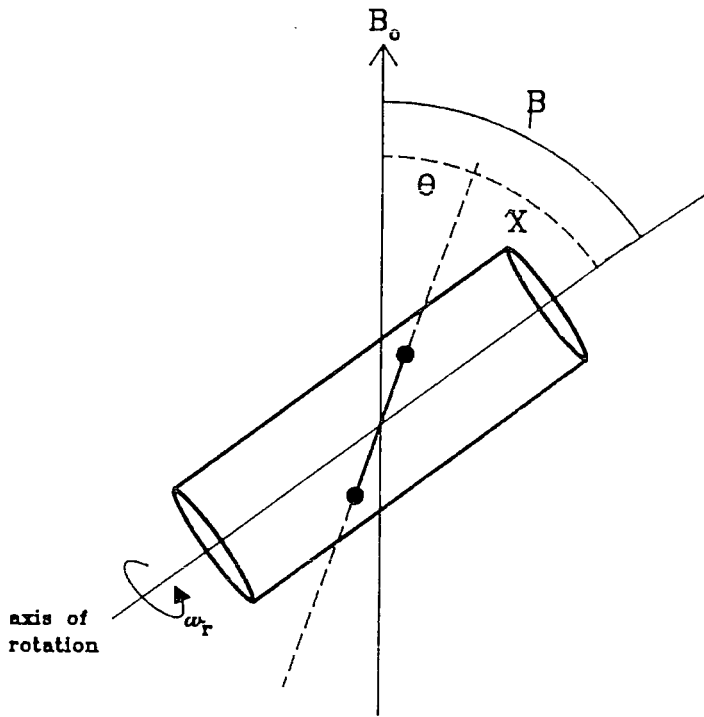
Figure 2.11   Magic-angle-spinning
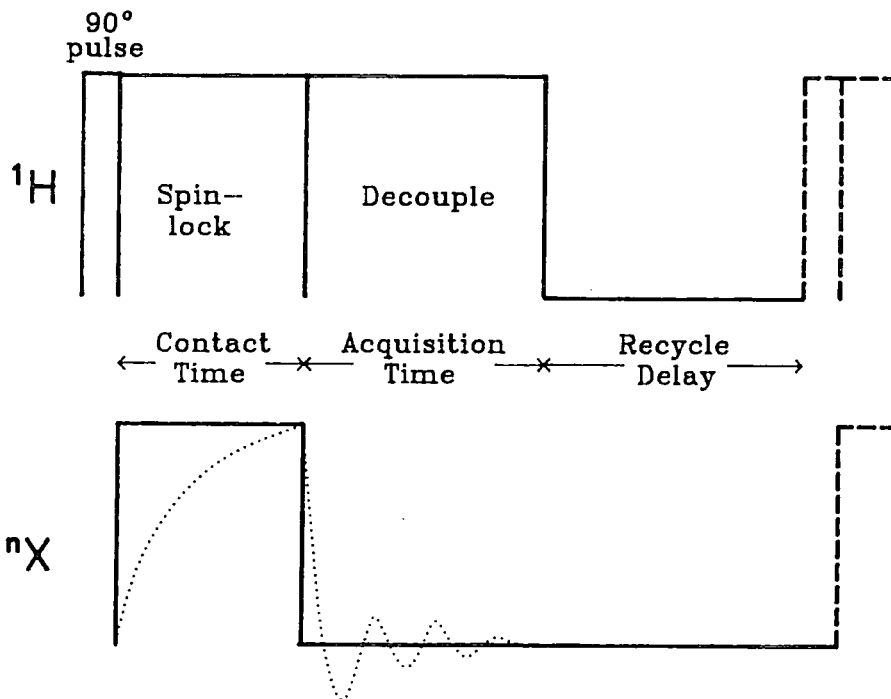
Figure 2.13   Pulse-sequence for a cross-polarisation experiment

41
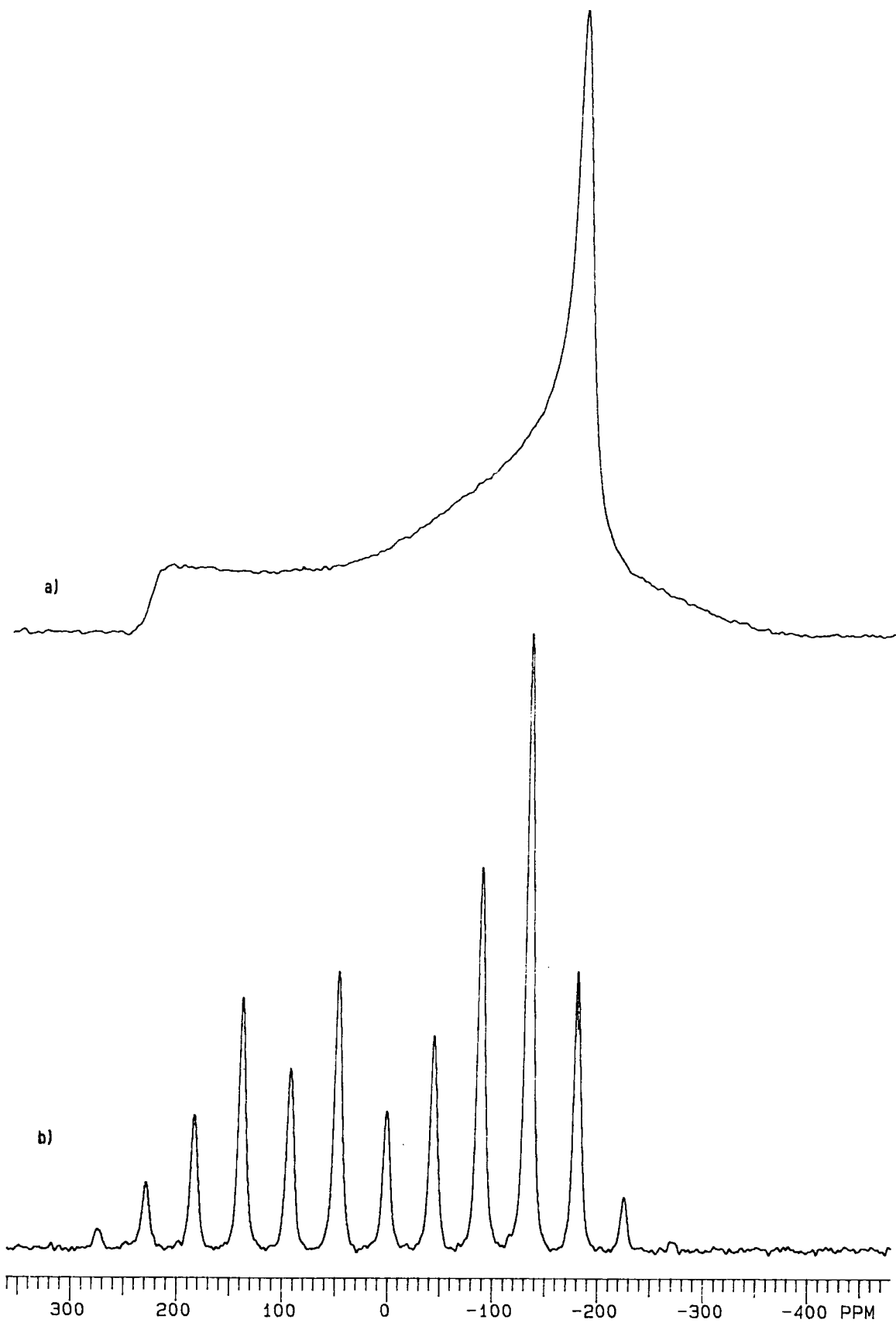
Figure 2.12 ^{119}Sn spectrum of [(Bu$_3$Sn)$_3$Co(CN)$_6$] a) static with decoupling and b) with decoupling and MAS

$$M(t) = M_o[1-\exp(\frac{-t}{T_{CH}})] \exp(\frac{-t}{T_{1\rho}^H})$$
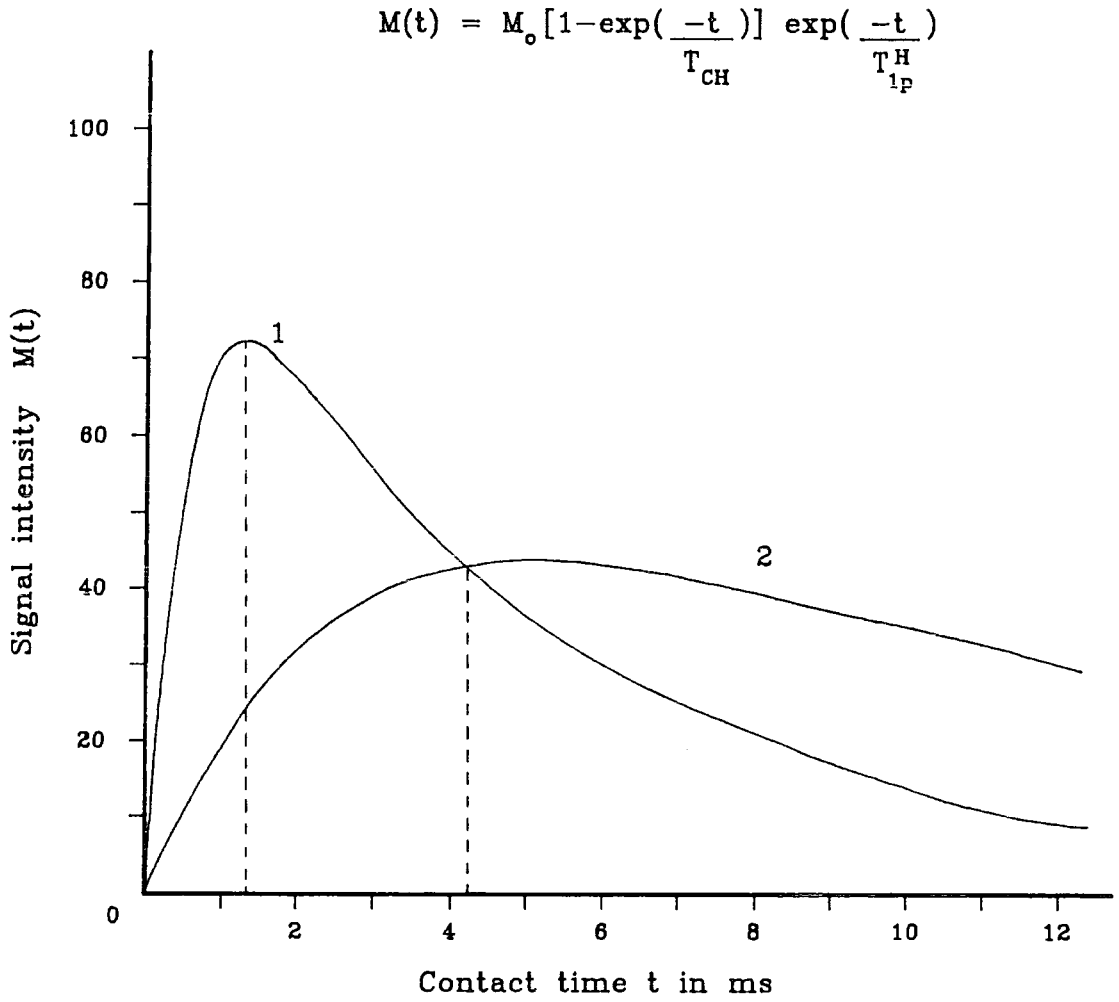
Figure 2.14 A graph of how the intensity of the signal varies with contact time in a cross-polarisation experiment

Below the graph:

1: $M_o = 100$ $T_{CH} = 0.5$ ms $T_{1\rho}^H = 5$ ms

2: $M_o = 100$ $T_{CH} = 4.0$ ms $T_{1\rho}^H = 10$ ms
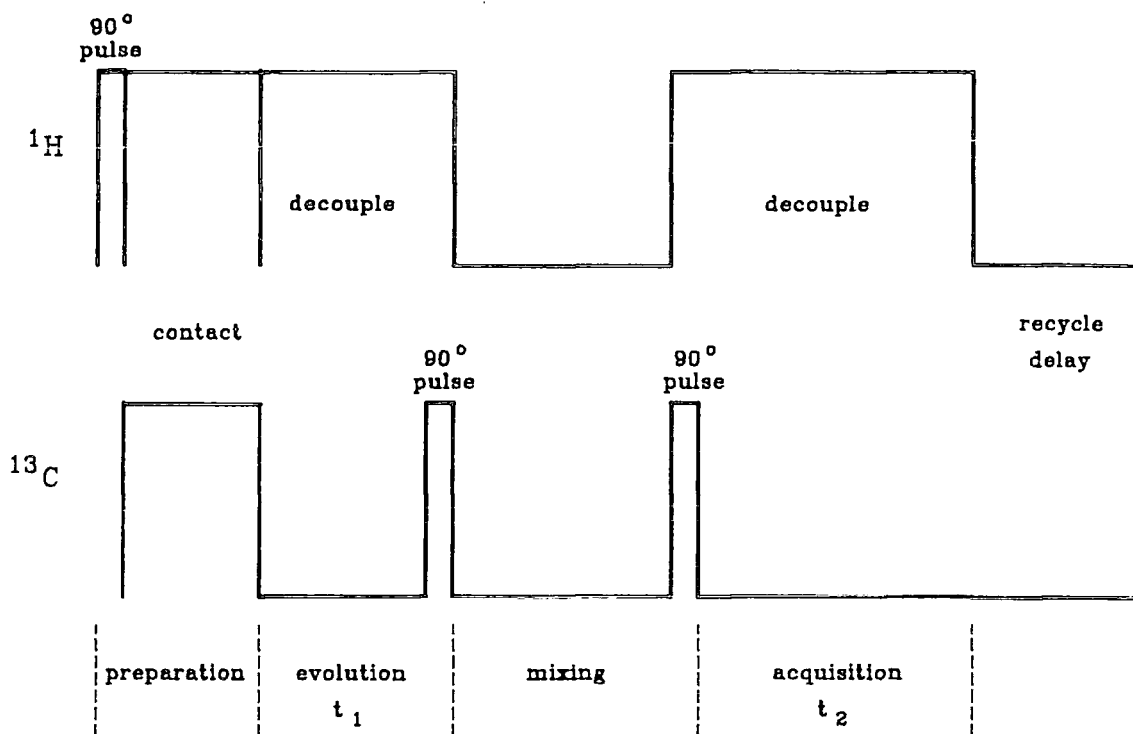
Figure 2.15   Pulse-sequence for a two-dimensional spin-exchange experiment

CHAPTER 3

EXPERIMENTAL

3.1 Spectrometer

All spectra were obtained using a Varian VXR-300 spectrometer and an Oxford Instruments magnet with a B_0 field of 7.05 T (300 MHz for protons).

Two different probes were used, both of which were manufactured by Doty Scientific. The ^{13}C, ^{15}N, ^{59}Co and some of the ^{119}Sn spectra were obtained using a probe capable of spin-rates up to about 5 kHz. The rotors used were made from sapphire, with an outside diameter of 7 mm and held between 250 and 300 mg of sample. The endcaps used were made from kel-F (a perfluorinated plastic). The second probe was used for some of the ^{119}Sn spectra and the ^{207}Pb spectra. Silicon nitride rotors with vespel endcaps were used. These had an outside diameter of 5 mm, held between 100 and 150 mg of sample and could reach spin-rates up to 14 kHz. The spin-rates on both probes were measured using the tribo-electric effect[10].

Both probes have zirconia stators and there were no background signals from the stator, rotors or endcaps for any of the nuclei studied.

The spinning gas used for normal room temperature operation was dry air.

3.2 Referencing

Five different nuclei have been studied: ^{13}C, ^{119}Sn, ^{207}Pb, ^{15}N and ^{59}Co. The important NMR parameters are given in table 3.1. The resonant frequency quoted for each nucleus is the absolute frequency of the centre of the spectral width which is the position of the transmitter. However, some spectra were recorded with a transmitter offset so that the transmitter was closer to the signals being observed.

Before each spectrum was run the spectrometer was referenced. The reference samples with their chemical shifts are given in table 3.2. The standard references for ^{13}C, ^{119}Sn and ^{207}Pb are tetramethylsilane (TMS), tetramethyltin and tetramethyllead respectively. However, in practice, secondary references were used because all three

standard references are volatile liquids at room temperature and therefore cannot be used to set the cross-polarisation Hartmann-Hahn match conditions. The secondary references used were the CH_2 signal from adamantane, $(C_6H_{11})_4Sn$ and Ph_4Pb. For ^{15}N a sample of ^{15}N doubly enriched ammonium nitrate was used with the nitrate line referenced to 0 ppm (shift of $NH_4^+ = -353.3$ ppm). In solution state ^{15}N NMR spectroscopy the nitromethane scale is more commonly used[11]. The chemical shift of the nitrate signal of solid NH_4NO_3 is -5.8 ppm relative to CH_3NO_2.

Signals from these secondary references could easily be seen in only four transients using recycle delays of between 10 and 40 seconds.

For ^{59}Co a 0.26 M solution of $K_3Co(CN)_6$ in H_2O was used since a solid reference sample was not needed because only single-pulse ^{59}Co spectra were obtained.

The reference samples were also used to set the Hartmann-Hahn match conditions for the CP experiment. Both the observe field and the CP field could be varied via the computer keyboard. In practice the ^1H CP field was kept constant (1.4 mT or 60 kHz for ^{13}C, ^{119}Sn and ^{207}Pb; 0.6 mT or 25 kHz for ^{15}N) and a series of short experiments, each of four transients with a recycle delay of between 10 and 40 seconds, were run with different observe fields. The one which gave the maximum signal was then chosen as the match. The decoupler field was the same for all the nuclei at 1.4 mT.

The ^1H 90° pulse duration was also measured in the CP experiment, using the reference samples, by varying its length until maximum signal was obtained. Typical values were 4 μs for ^{13}C, ^{119}Sn and ^{207}Pb and 10 μs for ^{15}N. ^{59}Co has a spin of 7/2 and therefore only a 22° pulse angle was used in order to excite only the central transition[12].

3.3   Setting the magic angle

In order to set the magic-angle of 54.7° the ^{15}N reference sample of ammonium nitrate was used. The linewidth of the nitrate signal is very sensitive to the angle. The angle of the stator was altered by turning a small screw until the minimum linewidth (approximately 10 Hz) of the nitrate signal was obtained.

3.4   Sample preparation

All the samples were prepared at the University of Hamburg and were already in a powdered form, therefore no further preparation was required. Some of the samples were ground slightly using a pestle and mortar to eliminate the occasional small lump.

3.5   Experimental parameters

The experimental parameters used to obtain the spectra in figures 5.1.1 to 5.5.6 in chapter 5 are given in table 3.3. Most spectra were obtained with spin-rates below 5.5 kHz except for some of the tin and all of the lead spectra. The number of transients needed for a good signal-to-noise ratio was high for the majority of the spectra (60000 transients at a 1 s recycle delay $=$ 16.5 hrs). In the case of ^{13}C this was in order to observe the carbon of the cyanide groups which were difficult to see, partly due to their intensity being spread into a manifold of spinning sidebands and also because the CP rate was low. The choice of recycle delay (RD) and contact time (CT) is discussed below.

In most cases the ^{13}C spectrum was obtained for each compound first. RD's were chosen by running a series of short experiments each with a different RD from which a rough estimate of the proton T_1 was made. If an RD of five times T_1 is used then almost maximum signal will be obtained from each transient. However, in choosing an appropriate RD it must be taken into account that if the RD is halved, then double

the number of transients can be accumulated within a given time. Although reducing the RD will reduce the signal from each transient it would result in an improved signal-to-noise ratio in a given time. It can be shown that the optimum RD is $1.2 \times T_1$[13].

Choosing an appropriate contact time (CT) for the ^{13}C spectra was often a compromise since the compounds contained two very different carbon environments each requiring different CT's for maximum signal. The cyanides have no directly bonded protons and therefore a relatively long CT of 5 to 15 ms should be used to allow time for the cross-polarisation to take place. Longer times could not be used because the pulse would begin to cause heating of the probe. In some cases, where $T_{1\rho}^H$ was short, a short contact time had to be used because the magnetisation decayed away at longer times. The R groups have directly bonded protons and only required a short CT of about 1 ms for maximum signal. In practice, a series of short experiments, each with a different CT, were performed in which only the signals from the R groups were seen. If the signals from the R group had not decreased too much at long CT's then a long CT was used. If the signals from the R group decayed very quickly then a shorter CT was used.

In general, the signals from the ^{119}Sn, ^{207}Pb and ^{15}N in the compounds could not be seen immediately. Therefore choosing an RD and a CT was more difficult than for the ^{13}C. In a CP experiment, the relaxation of the nucleus being observed (^nX) is dependent upon the ^1H T_1 and not the ^nX T_1. Therefore the same RD can be used as for the ^{13}C spectrum. The CT chosen for the ^{119}Sn and ^{207}Pb spectra was in general shorter than for the CN region of the ^{13}C spectra since the protons are not so far away. For the ^{15}N spectra a longer CT was chosen because the protons are further away.

The ^{59}Co spectra were obtained using a single-pulse experiment and therefore only the RD had to be optimised. A value of 0.5 s was used since this gave almost maximum signal and allowed for a large number of transients in a short space of time. Single-pulse

experiments were also used for some ^{119}Sn and ^{13}C spectra to achieve more accurate relative intensities of signals.

3.6   Data obtained from the spectra

The most important data obtained from the spectra were the chemical shifts, the accuracy of which depends, to a certain extent, on the linewidths. The low frequency regions of the ^{13}C spectra contained the sharpest signals and here the chemical shifts are given to one decimal place and are accurate to $+/- 0.2$ ppm. All other chemical shifts have been rounded to the nearest ppm and are accurate to $+/- 1$ ppm. Internal shift differences are, however, more accurate than the absolute values.

The spectra in figures 5.1.1 to 5.5.6 were plotted with varying amounts of line-broadening. However all linewidths were measured without any line broadening.

For some signals coupling constants could be calculated. Since from solid-state spectra the signs of the coupling constants are not known they are all given as magnitudes in both the text and the tables.

3.7   Spinning sideband analysis

The anisotropies and asymmetries were all calculated using a sideband fitting program[14] based on the theory described by Maricq and Waugh[15]. Initial guesses were made for the anisotropy and asymmetry from the sideband patterns. These were entered into the program along with the intensities of the signals, which were in most cases found by measuring the peak heights with a ruler. Only the signals which were multiplets (e.g. ^{119}Sn spectrum of $[(Et_3Sn)_3Co(CN)_6]$) were integrated using the spectrometer computer. Figure 3.1 shows both the entered data and the fitted data for the 46 ppm ^{119}Sn centreband and spinning sidebands for the compound $[(Me_3Sn)_4Fe(CN)_6]$. The intensities of the two sets of lines agree very closely as is reflected by the low SDSQ (sum of the differences squared) of 1. Figure 3.2 shows a

similar sideband manifold for the -73 ppm signal from the compound $[(Me_3Sn)_4Fe(CN)_6.Dioxan/H_2O]$. Here the intensities of the fitted lines vary considerably from the entered values resulting in a higher SDSQ of 45. The accuracy of the results can therefore be gauged by comparing the values of SDSQ in the tables in section 5.6.

Asymmetry values below 0.2 are quite inaccurate because the intensity differences between the sideband patterns of axial ($\eta = 0$) and slightly non-axial ($\eta = 0.2$) systems are very small[16]. Therefore calculated values below 0.2 are usually taken to be zero indicating axial symmetry.

3.8   Variable temperature (VT) studies

^{13}C CPMAS spectra were obtained at temperatures both above and below room temperature. In order to elevate the temperature, the required value was set using the computer keyboard. The spin gas (dry air) was then heated and the temperature close to the sample was sensed by a thermocouple. The heating was computer controlled in order to maintain a stable temperature.

To obtain spectra below room temperature was slightly more complicated. Here nitrogen, used as the spin gas, was cooled by passing it through a heat exchanger which was situated in a dewar of liquid nitrogen (capacity of 50 litres). The gas was then also heated to maintain a stable temperature.

3.9   Calibration of the VT system

The temperature sensed by the thermocouple was that close to the sample, and not actually the temperature in the sample itself. To investigate this difference a sample of samarium acetate was used as a 'thermometer'. Samarium acetate contains three signals in the ^{13}C CPMAS spectrum all of which have chemical shifts which are temperature dependent[17]. However, the high-frequency carbonyl signal is the most

51

sensitive and so its chemical shift (δ_{ppm}) was recorded at 17 computer-set temperatures (T_c) between -70 and $60\ ^{\circ}C$. The following equation, as published in the literature, was then used to calculate the actual sample temperature (T_s).

$$\delta_{ppm} = \frac{-4867}{T_s} + 209 \qquad T_s = \text{sample temperature / K}$$

$$T_s = \frac{4867}{209 - \delta_{ppm}}$$

The computer-set temperature (T_c) was then plotted against the calculated sample temperature (T_s). From these points the following straight line equation was calculated using the least squares method[18].

$$T_s = (T_c \times 1.1) + 6.6 \qquad T_s \text{ and } T_c \text{ in } ^{\circ}C$$

This equation was then used to calculate the actual sample temperature in all the VT experiments as shown in the example below.

Computer-set temperature $\quad T_c = 40\ ^{\circ}C$

Actual sample temperature $\quad T_s = (40 \times 1.1) + 6.6\ ^{\circ}C = 51\ ^{\circ}C$

The thermocouple senses an ambient temperature of 22.3 $^{\circ}C$ which equates to an actual sample temperature of 31 $^{\circ}C$ at moderate spin-rates (see below). It is estimated that these calculated sample temperatures are accurate to approximately $+/-$ 2 $^{\circ}C$.

At moderate spin-rates of up to 5 kHz sample temperatures appear to remain roughly constant but at the higher spin-rates used for tin and lead there can be considerable heating of the sample (at spin-rates of 12 kHz, temperature $> 60^{\circ}C$[19]). This heating could cause decomposition of the sample although all the compounds studied here should be stable to at least 200 $^{\circ}C$. Heating effects can also cause a slight loss of intensity in the signal according to the Curie Law[20]. However, a much larger loss of intensity is sometimes caused by the fast spinning (> 10 kHz). This is due to weak dipolar interactions being averaged by the spinning resulting in the cross-polarisation process not being so effective. If the dipolar interactions are much stronger then fast spinning will have little effect.

3.10   Deconvolution

The methyl regions of the 51 °C ^{13}C spectra for 4, 5 and 6 were deconvoluted using in house software running on an a Archimedes 440 computer. The program requires initial guesses for the position, linewidth and intensity of each signal and then, by using a simplex routine, finds the best fit to the data.

3.11   Finding the centreband

For the ^{13}C, ^{15}N and ^{59}Co spectra, the centreband was easily identifiable due to its large magnitude in comparison to the spinning-sidebands. In the case of ^{119}Sn and ^{207}Pb the centreband was not always the most intense signal. Therefore spectra were run at two different spin-rates as shown in figure 3.3. Since the spacing of the spinning sidebands is equal to the spin-rate, the centreband is the only signal which remains in the same position when the spin-rate is changed (marked by an arrow). In some compounds, however, there were three or four different species each with a centreband and a manifold of spinning-sidebands. In chapter 5, figures 5.3.7 and 5.3.8 show how this can produce a very complicated spectrum. In this case the fourth species was not noticed until a third spin-rate was done because of the overlap of spinning-sidebands from the other species.
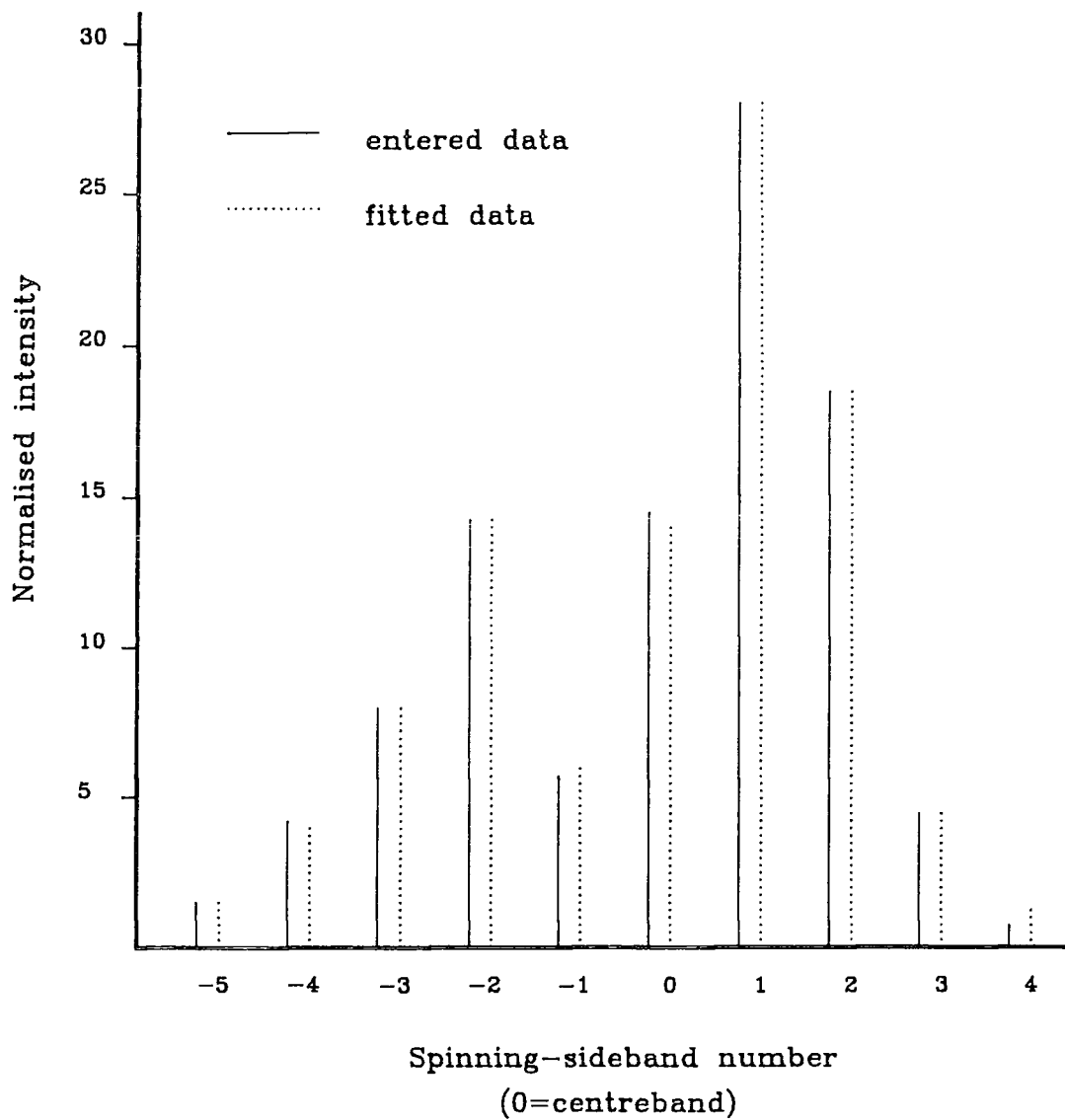
Figure 3.1 Entered and fitted SSB analysis data for the 46 ppm tin signal from the [119]Sn spectrum of [(Me$_3$Sn)$_4$Fe(CN)$_6$]
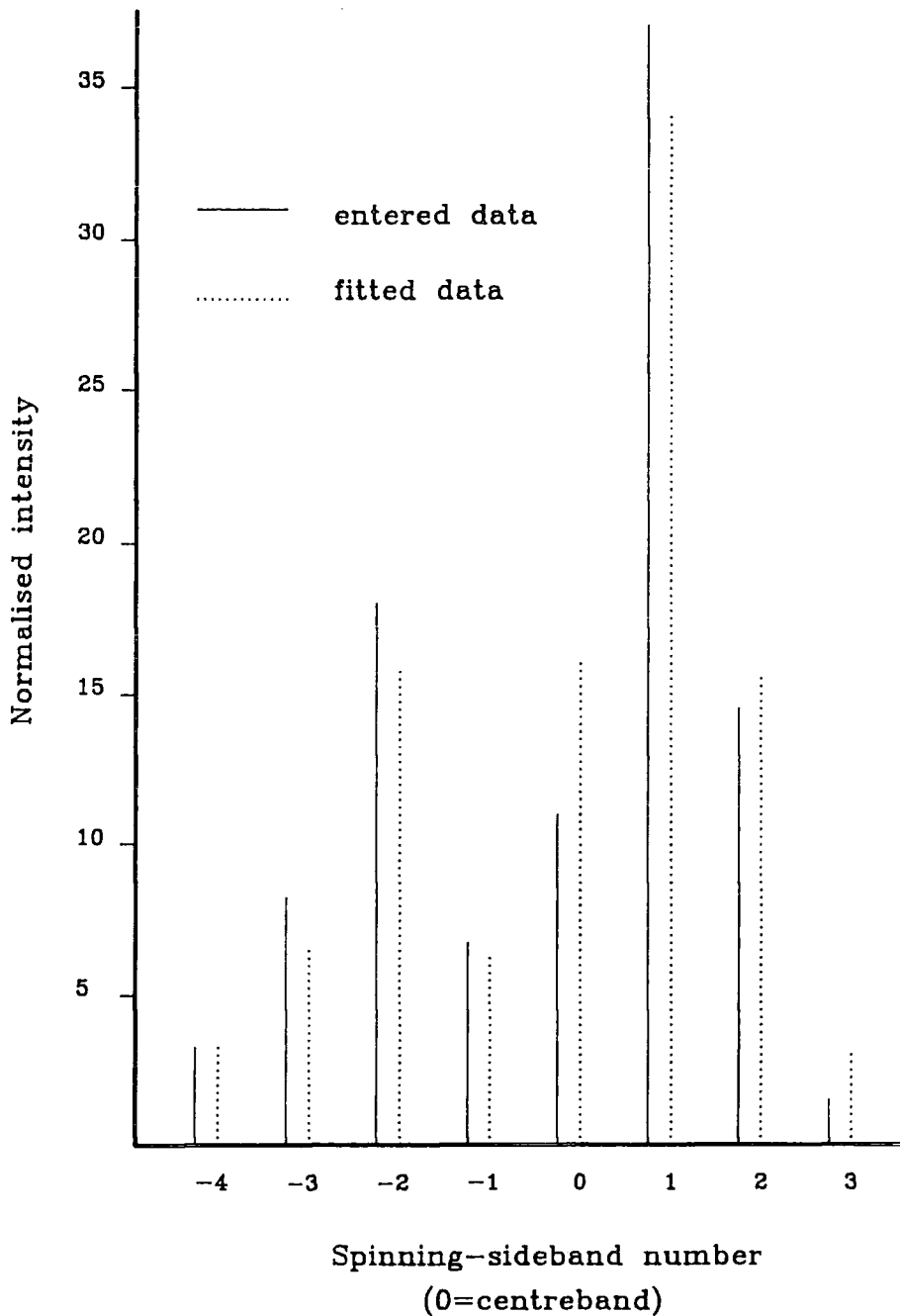
Figure 3.2 Entered and fitted SSB analysis data for the −73 ppm tin signal from the ^{119}Sn spectrum of $[(Me_3Sn)_4Fe(CN)_6.C_4H_8O_2/H_2O]$
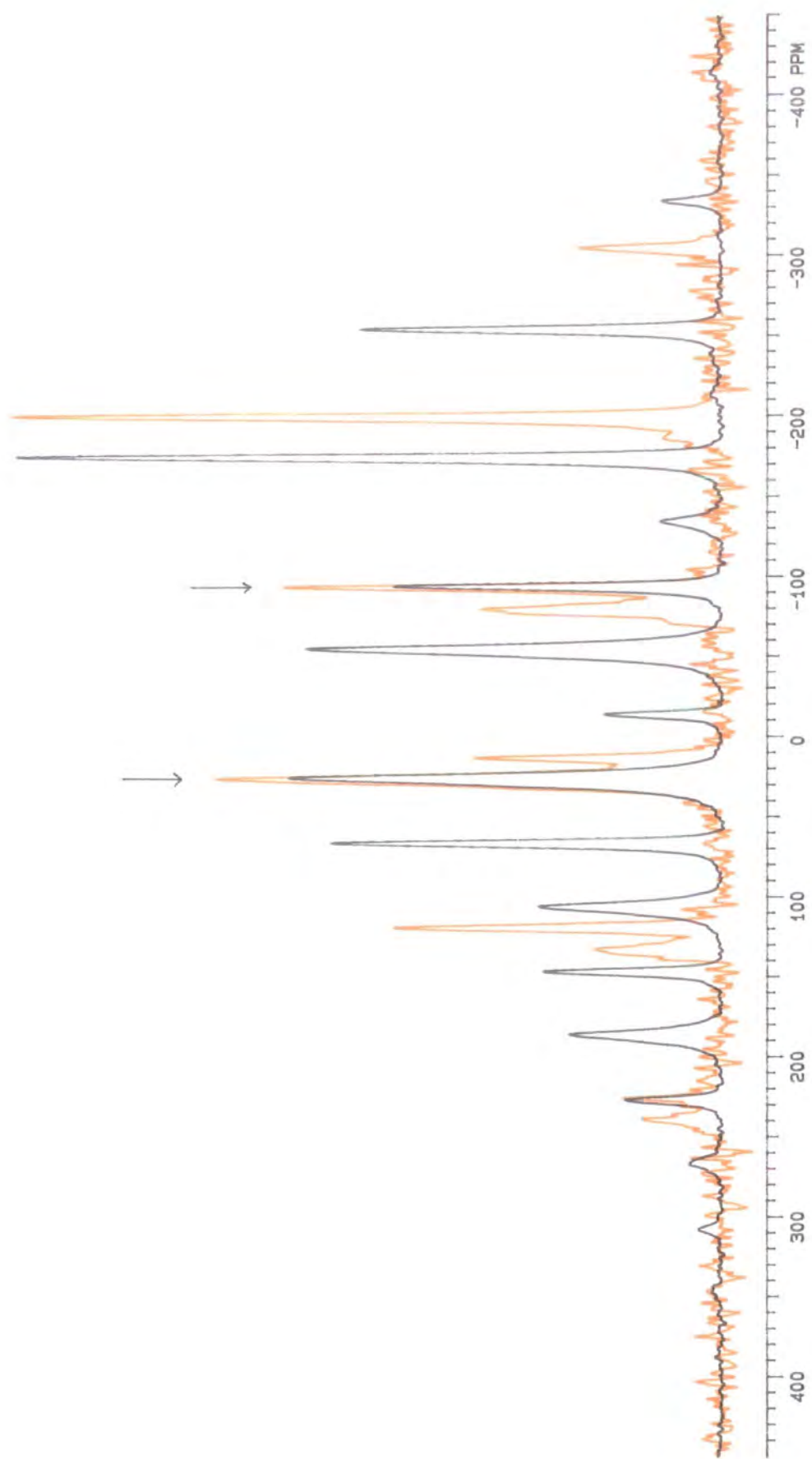
Figure 3.3   119Sn spectra of [(Me3Sn) 4Fe (CN) 6] at two different spin-rates

Table 3.1   Important NMR parameters

Nucleus	Resonant Frequency/MHz	Spin	% natural abundance
^{13}C	75.431	1/2	1.1
^{119}Sn	111.862	1/2	8.6
^{207}Pb	62.740	1/2	22.6
^{15}N	30.405	1/2	0.4
^{59}Co	71.160	7/2	100

Table 3.2   Primary and secondary references

Nucleus	Primary reference	δ/ppm	Secondary reference	δ/ppm
^{13}C	$(CH_3)_4Si$	0.0	CH_2 line of adamantane	38.4
^{119}Sn	$(CH_3)_4Sn$	0.0	$(C_6H_{11})_4Sn$	−97.4
^{207}Pb	$(CH_3)_4Pb$	0.0	Ph_4Pb	−156.5
^{15}N	$^{15}NH_4{}^{15}NO_3$	0.0		
^{59}Co	0.26M $K_3Co(CN)_6$	0.0		

Table 3.3 Experimental parameters

Figure	Compound	Nucleus	RD/s	CT/ms	NT	SR/Hz
5.1.1a	1	^{13}C	2	5	1000	4120
b	1	^{13}C	2	7	500	3630
5.1.2	3	^{13}C	1	10	57300	4970
5.1.4	2	^{13}C	2	15	27450	4870
5.1.5	1	^{119}Sn	2	5	12500	5020
5.1.6	3	^{15}N	1	10	67000	4650
5.1.7	1	^{59}Co	0.5	-	200	4760
5.1.10	2	^{119}Sn	5	10	1000	4500
5.2.1a	4	^{13}C	2	3	28320	4600
b	5	^{13}C	1	2.5	52800	5000
c	6	^{13}C	1	7	52400	5030
5.2.2a	4	^{13}C	2	3	28320	4600
b	4a	^{13}C	2	8	4600	4900
c	5	^{13}C	1	2.5	52800	5000
d	6	^{13}C	1	7	52400	5030
5.2.3	4	^{119}Sn	1	2.5	16800	12600
5.2.4a	6	^{15}N	1	7	66500	5020
b	4a	^{15}N	5	8	332	3690
5.2.5a	5	^{13}C	2	1	300	4340
b	5	^{13}C	1	2.5	500	4530
c	5	^{13}C	5	5	300	3700
d	5	^{13}C	5	5	500	3790
e	5	^{13}C	5	5	440	3680
f	5	^{13}C	5	5	200	3600
5.2.6	4	^{13}C	2	1	300	4370
5.2.7a	4	^{13}C	1	1	198	2100
b	4	^{13}C	2	1	420	4080
c	4	^{13}C	2	1	300	4370

58

Table 3.3 continued

Figure	Compound	Nucleus	RD/s	CT/ms	NT	SR/Hz
5.3.1	7	^{13}C	1	5	55520	4890
5.3.2	7	^{13}C	1	5	55520	4890
5.3.3	7	^{119}Sn	1	2.5	42000	9200
5.3.4	7	^{15}N	1	3	70000	4890
5.3.5	9	^{13}C	5	1	10300	4900
5.3.6a	8	^{13}C	2	3	14000	4940
b	9	^{13}C	5	1	10300	4900
5.3.7a	8	^{119}Sn	1	2.5	52000	12650
b	8	^{119}Sn	1	2.5	6852	12000
5.3.8a	9	^{119}Sn	1	2.5	34000	12600
b	9	^{119}Sn	1	2.5	1000	11100
5.3.9	9	^{15}N	1	3	71500	4630
5.4.1	10	^{13}C	1	10	53540	4140
5.4.2	10	^{207}Pb	2	5	29520	10360
5.4.3a	11	^{13}C	1	7.5	54400	4960
b	12	^{13}C	1	7.5	35640	4830
5.4.4a	11	^{13}C	1	5	54400	4960
b	12	^{13}C	1	5	35649	4830
5.4.5a	11	^{207}Pb	1	5	53200	11180
b	12	^{207}Pb	1	5	53300	11300
5.4.6a	11	^{15}N	1	7.5	73000	4840
b	12	^{15}N	1	5	161300	4780
5.5.1a	13	^{13}C	1	7	57500	4920
b	13	^{13}C	1	7	57500	4920
5.5.2	13	^{119}Sn	1	7	55400	13340
5.5.3	13	^{15}N	1	7	75000	4500
5.5.4a	14	^{13}C	1	10	20500	4860
b	14	^{13}C	1	10	20500	4860
5.5.5	14	^{119}Sn	1	2.5	23400	11750
5.5.6	14	^{15}N	1	5	73000	4930

CHAPTER 4

STRUCTURAL INFORMATION

Introduction

In general, all the compounds investigated are organo-metallic three-dimensional co-ordination polymers and they were all prepared at the University of Hamburg. The single crystal X-ray studies, which provided all the structural information and the figures in this chapter, were also performed in Hamburg. All the compounds contain octahedrally co-ordinated $M(CN)_6$ units (M = Co, Fe, Ru, Os) linked by trigonal-bipyramidal bridging units of the form R_3E (R = Me, Et, Bu E = Sn, Pb). This creates a three-dimensional lattice of infinite chains which intersect at the M atoms.

4.1   Tin- and cobalt- containing compounds

1   $[(Me_3Sn)_3Co(CN)_6]$

2   $[(Et_3Sn)_3Co(CN)_6]$

3   $[(Bu_3Sn)_3Co(CN)_6]$

1 forms in aqueous solution according to the following equation and is thermally stable up to 335 $^\circ$C[21].

$$3Me_3SnCl + K_3[Co(CN)_6] \xrightarrow[-3KCl]{H_2O} [(Me_3Sn)_3Co(CN)_6]$$
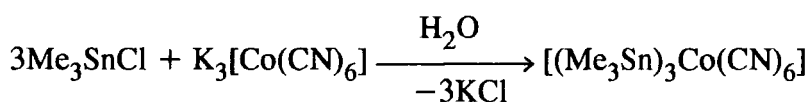
2 and 3 are analogues of 1, and all three are fine white powders which are insoluble in commonly used solvents.

A single crystal X-ray structure determination[21,22] has only been done for the methyl compound. This indicates the presence of distorted octahedral units of $Co(CN)_6$ and trigonal bipyramidal co-ordination for the Me_3Sn units within a three-dimensional lattice. This lattice consists of three infinite chains intersecting at the Co atoms.

$$...-N-C-\underset{\diagup\,|}{\overset{|\diagup}{Co}}-C-\underset{|\,\cdot}{\overset{R\quad R}{\underset{\diagdown\,\diagup}{N-Sn-N}}}-C-\underset{\diagup\,|}{\overset{|\diagup}{Co}}-...$$
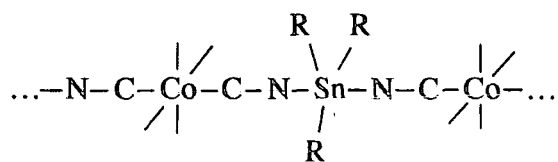
A structure is created containing long channels and large cavities lined by the organic R groups. The cavaties have a maximum diameter of 0.68 nm[23].

Figure 4.1 shows the elementary cell and atomic numbering scheme, while figures 4.2 and 4.3 show the lattice viewed along, and perpendicular to, the main channels. It is necessary to describe the lattice in terms of three intersecting chains A, B and C.

Chain A [Co1-C2-N2-Sn1-N4-N4-Co2-C4-N4-Sn1-N2-C2]

Chain B [Co2-C5-N5-Sn2-N6-C6-Co2-C6-N6-Sn2-N5-C5]

Chain C [Co1-C1-N1-Sn3-N3-C3-Co1-C3-N3-Sn3-N1-C1]

Table 4.1 contains bond angles and bond lengths for 1.

In terms of the N-Sn bond lengths, chain C has the most asymmetric N-Sn-N bridge, whereas the corresponding bridges in chains A and B are more symmetric. Chain C is also the most bent with a Sn-N-C angle of 134°. Crystallographically this structure contains 9 CH_3, 6 CN, 3 Sn and 2 Co environments within the asymmetric unit.

4.2   Trimethyl tin compounds with different metal atoms

4   $[(Me_3Sn)_4Fe(CN)_6]$

5   $[(Me_3Sn)_4Ru(CN)_6]$

6   $[(Me_3Sn)_4Os(CN)_6]$

The iron-containing compound can be prepared according to the following equation[24]. Compounds 5 and 6, which are analogues of 4, can be prepared in a similar way.

$$K_4[Fe(CN)_6] + 4Me_3SnCl \xrightarrow{\;H_2O\;} [(Me_3Sn)_4Fe(CN)_6] + 4KCl$$

The crystal structure is not known for any of these three compounds but it is proposed that the basic structure is similar to that of the cobalt-containing compounds as discussed in 4.1. This would have three infinite chains consisting of octahedrally co-ordinated $M(CN)_6$ units (M = Fe, Ru, Os) and bridging trigonal-bipyramidal trimethyl tin groups with the chains intersecting at the metal atom forming a three-dimensional lattice.

$$-N-C-M-C-N-\overset{\overset{\displaystyle Me \quad Me}{|}}{\underset{\displaystyle Me}{Sn}}-N-C-M-C-N- \qquad M = Fe, Ru, Os$$

However, this type of lattice only accounts for three out of the four Me_3Sn groups. It is not known how the fourth group is bonded in the lattice but it has been shown that 4, 5 and 6 undergo ion exchange reactions readily.

$$[(Me_3Sn)_4(CN)_6] \xrightarrow[-[Me_3Sn(H_2O)_2]^+]{[A^+/H_2O]} [A(Me_3Sn)_3Fe(CN)_6]$$

$$A = Et_4N^+, NH_4^+, (C_5H_5)_2Co^+$$

This fourth Me_3Sn unit is therefore probably 'ionic', i.e. only weakly bonded to the lattice and thus may be more mobile than the others. It will also be in a very different environment to the Me_3Sn in the lattice, but this difference has not shown up in the ^{119}Sn Mössbauer spectrum[24]. The NMR spectra of this class of compounds also reveal discrepancies with the idea of one 'ionic' Me_3Sn group. This matter will be further discussed in section 5.2.6.

4.3 Derivatives of [(Me₃Sn)₄Fe(CN)₆]

<div>

    7   $[(Me_3Sn)_4Fe(CN)_6.C_4H_8O_2/H_2O]$

    8   $[(Me_3Sn)_4Fe(CN)_6.2H_2O]$

    9   $[(Me_3Sn)_4Fe(CN)_6.D(+)glucose]$

</div>

These are all derivatives of compound 4. The crystal structure has only been solved for compound 7. It can be prepared in the same way as 4, but dioxane and water are also added, which inhibits the spontaneous precipitation of 4 and instead compound 7 crystallises out[24].

$$4(Me_3SnCl) + K4[Fe(CN)_6] \xrightarrow[-4KCl]{2H_2O.Dioxane} [(Me_3Sn)_4Fe(CN)_6.2H_2O.Dioxan]$$

The crystal structure indicates that the fourth Me_3Sn unit of 4 is now incorporated into chains of the type

The incorporation of the Me_3Sn into the chain is also confirmed by the fact that 7 will undergo practically no ion-exchange reactions[24].

Figure 4.4 shows the elementary cell and the atomic numbering scheme for 7. The X-ray study[25,22] indicates a three-dimensional network composed of two different non-linear chains, A and B, intersecting at the octahedrally co-ordinated Fe atoms.

Chain A   Sn2-N1-C1-Fe-C1-N1-Sn2-N3-C3-Fe-C3-N3-

Chain B   Sn1-O1···O2(C2H4)O2···O1-Sn1-N2-C2-Fe-C2-N2- O1=H₂O

The structure contains twice as many chains of type A as there are of type B which results in an equivalent number of tin atoms in each of the two environments. All Fe atoms and midpoints of dioxane molecules lie on centres of symmetry. Table 4.2 shows

some angles and bond lengths for 7, from which it can be seen that the Me_3Sn units in chain A are almost trigonal bipyramidal (Me-Sn-N = 89.9°) but the units in chain B are distorted (Me-Sn-N = 94.1°). The tin atoms in chain A are also in a more symmetric environment (Sn-N = 0.237, 0.228 nm) than in chain B (Sn-N = 0.216 nm, Sn-O = 0.245nm). Chain B is also more bent (Sn-O-O = 126°) than chain A (C-N-Sn = 148°, 159°).

Compounds 8 and 9 have not had their structures solved but they are analogous to 7 and can be prepared in a similar way from $[(Me_3Sn)_4Fe(CN)_6]$.

4.4   Lead-containing compounds

10    $[(Me_3Pb)_3Co(CN)_6]$

11    $[(Me_3Pb)_4Ru(CN)_6.2H_2O]$

12    $[(Me_3Pb)_4Fe(CN)_6.2H_2O]$

4.4.1 $[(Me_3Pb)_3Co(CN)_6]$

$[(Me_3Pb)_3Co(CN)_6]$ is analogous to the first compound discussed, the difference being that the tin has been replaced by lead. It can be prepared in a similar way, as shown in the following reaction equation.

$$3(Me_3PbCl) + K_3[Co(CN)_6] \xrightarrow{\quad H_2O \quad} [(Me_3Pb)_3Co(CN)_6] + 3KCl$$
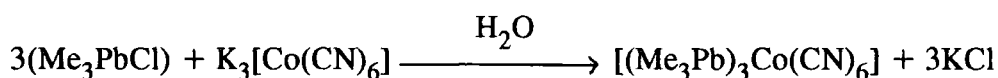
The product, however, is not as thermally stable as compound 1 and decomposes above 230 °C[26,22].

A single-crystal X-ray structure determination[26,22] indicates that the structure of 10 is similar to that of 1. It is a three-dimensional lattice consisting of three infinite chains.

```
                      Me  Me
              |  /     \  /      |  /
    — N — C — Co — C — N — Pb — N — C — Co — C — N —
              /  |              |         /  |
                               Me
```
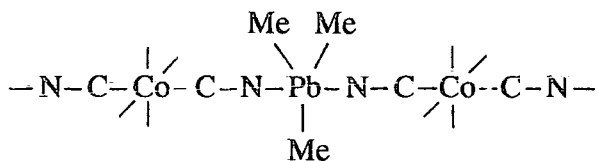
The $Co(CN)_6$ units have nearly octahedral symmetry and the bridging trimethyl-lead groups are trigonal-bipyramidal. Figure 4.5 shows the elementary cell and atomic numbering scheme, while figures 4.6 and 4.7 show the lattice viewed parallel to and perpendicular to the main channels. The bond lengths and bond angles for the three chains A, B and C are given in table 4.1.

From table 4.1 it can be seen that all three chains have near linear N-Pb-N fragments. The lead atoms in chains A and B are also in almost symmetric environments but in chain C the two Pb-N bond lengths are different (Pb-N = 0.252, 0.246 nm) creating a more asymmetric environment. All three chains are bent at the N atom, to a greater degree than they were in the Sn analogue. Chain B is the most bent, with one Sn-N-C angle of 125°. The asymmetric unit contains 9 CH_3, 6 CN, 3 Pb and 2 Co environments.

4.4.2 [(Me₃Pb)₄Ru(CN)₆.2H₂O] and [(Me₃Pb)₄Fe(CN)₆.2H₂O]

Both compounds 11 and 12 can be prepared in a similar way to 10.

$$4(Me_3PbCl) + K_4[M(CN)_6] \xrightarrow{\quad 2H_2O \quad} [(Me_3Pb)_4M(CN)_6.2H_2O] + 4KCl$$
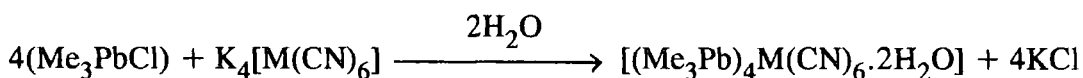
They have both had their structures determined by X-ray diffraction[2] and figures 4.8 and 4.9 show the elementary cell and atomic numbering scheme for each. Table 4.3 contains some bond lengths and bond angles for the two compounds.

The structures of 11 and 12 are very similar, each containing two different types of chains, both with octahedrally co-ordinated $M(CN)_6$ units. Chain A is similar to the chains of compound 10 and contains trigonal-bipyramidal bridging Me_3Pb units.

66

```
                        Me  Me
                     | /   \ /      | /
Chain A           — M—C—N—Pb—N— C—M—       M = Fe, Ru
                     / |       |       / |
                             Me
```
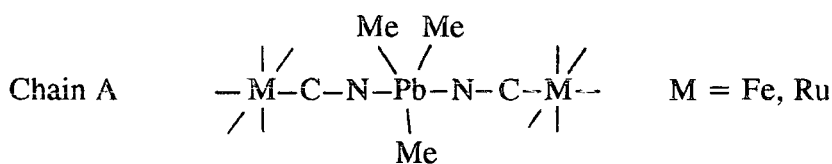
Chain B also contains penta-coordinate lead atoms, but here the lead is bonded to a nitrogen atom on one side and to the oxygen of the water on the other side.

```
            H      \ /      | /     \ /      H
Chain B      \    O—Pb—N— C—M—C—N—Pb—O /
            H /    |       / |      |      \ H
```
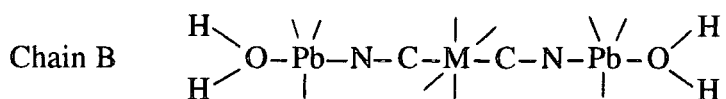
A hydrogen bond forms between the H_2O and the nitrogen of the closest cyanide group. The lattice contains twice as many chains of type A as there are of type B. However, between two $M(CN)_6$ units in chain B there are two $Pb(Me)_3$ units, whereas in chain A there is only one. This results in equal numbers of lead atoms in the two different environments.

In both the Ru- and the Fe- containing compounds chain A has a fairly symmetrical N-Pb-N bridge and is bent both at the nitrogen atom (Pb-N-C = 121° (Ru), 120° (Fe)) and at the lead atom (N-Pb-N = 173° (Ru), 171° (Fe)). Chain B in both cases contains an asymmetric environment for the lead atom (Pb-N = 0.232 nm (Ru), 0.235nm (Fe), Pb-O = 0.268nm (Ru), 0.266 (Fe)) and is bent both at the nitrogen atom by 175° and at the lead atom (N-Pb-N = 177° (Ru), 179° (Fe)).

13   $[(Cp_2Co)(Me_3Sn)_3Fe(CN)_6]$

14   $[(Et_4N)(Me_3Sn)_3Fe(CN)_6]$
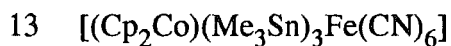
Crystallographic studies have been done for compound 13[27] and the number of crystallographically different atoms are given in the table below.

Fe	Sn	N	C,(CH$_3$)	C,(CN)	C,(Cp$_2$Co)
1	2	3	6	3	5

It is thought that the $(Me_3Sn)_3Fe(CN)_6$ part of the compound forms a three-dimensional lattice similar to that of compound 1 which acts as a 'host' to the Cp_2Co - the 'guest'.

It might be expected for compound 14 to possess a similar structure since the formulae are similar. However, it is possible that the Cp_2Co, being larger than Et_4N will distort the lattice and produce different spectra.

Both host-guest systems can be prepared via an ion-exchange reaction from $[(Me_3Sn)_4Fe(CN)_6]$ according to the following equations[24].

$$[(Me_3Sn)_4Fe(CN)_6] \xrightarrow[\;H_2O\;]{Et_4NCl} [(Et_4N)(Me_3Sn)_3Fe(CN)_6] + Me_3SnCl + H_2O$$

$$[(Me_3Sn)_4Fe(CN)_6] \xrightarrow[\;H_2O\;]{Cp_2CoCl} [(Cp_2Co)(Me_3Sn)_3Fe(CN)_6] + Me_3SnCl + H_2O$$
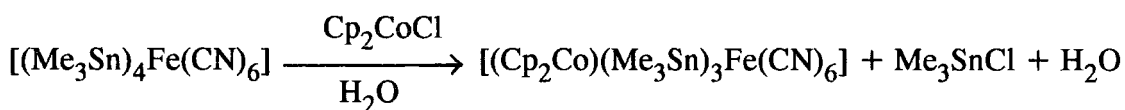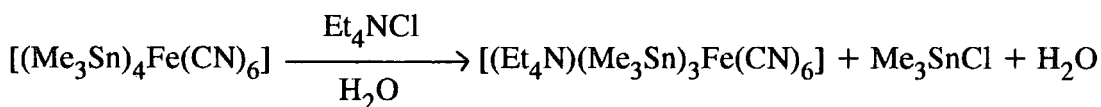
This exchange reaction occurs after only a few hours at room temperature.
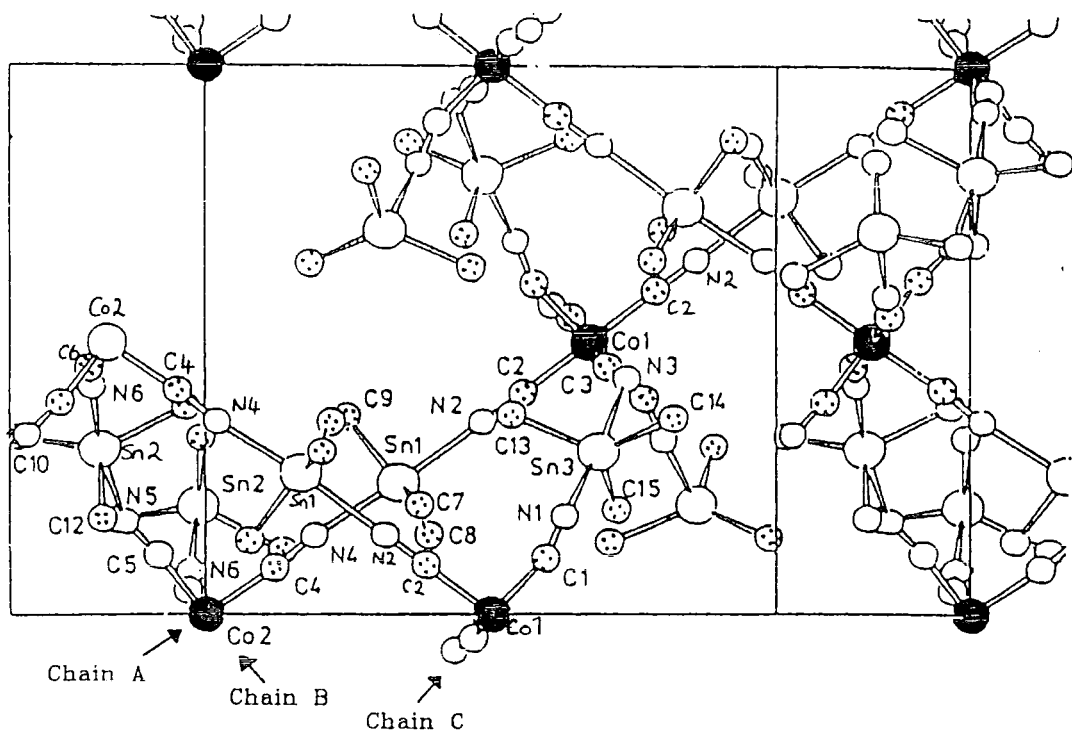
Chain A   Co2–C4–N4–Sn1–N2–C2–Co1–C2–N2–Sn1–N4–C4–

Chain B   Co2–C5–N5–Sn2–N6–C6–Co2–C6–N6–Sn2–N5–C5–

Chain C   Co1–C1–N1–Sn3–N3–C3–Co1–C3–N3–Sn3–N1–C1–

Figure 4.1   Elementary cell and atomic numbering scheme for $[(Me_3Sn)_3Co(CN)_6]$
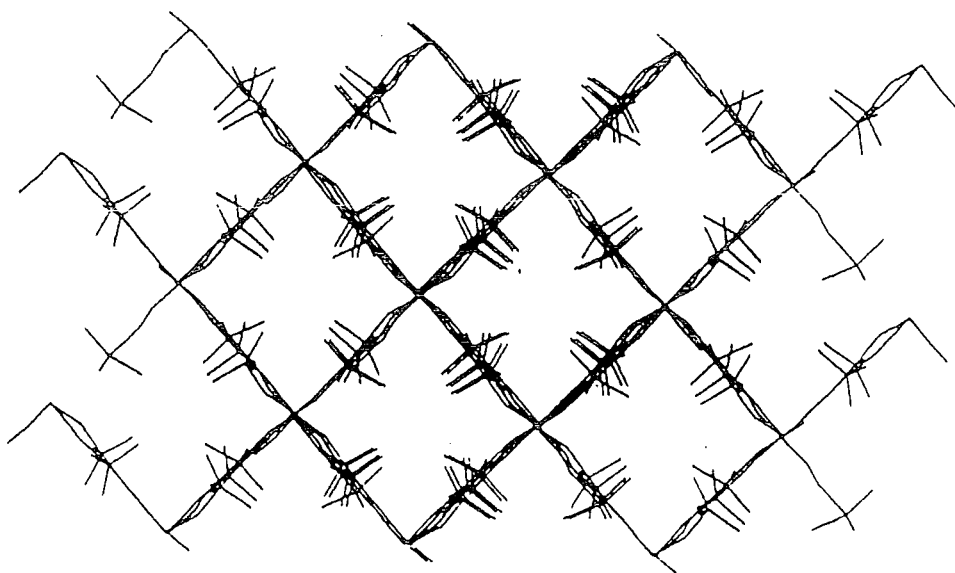
Figure 4.2   Lattice of [(Me$_3$Sn)$_3$Co(CN)$_6$] viewed along the main channels
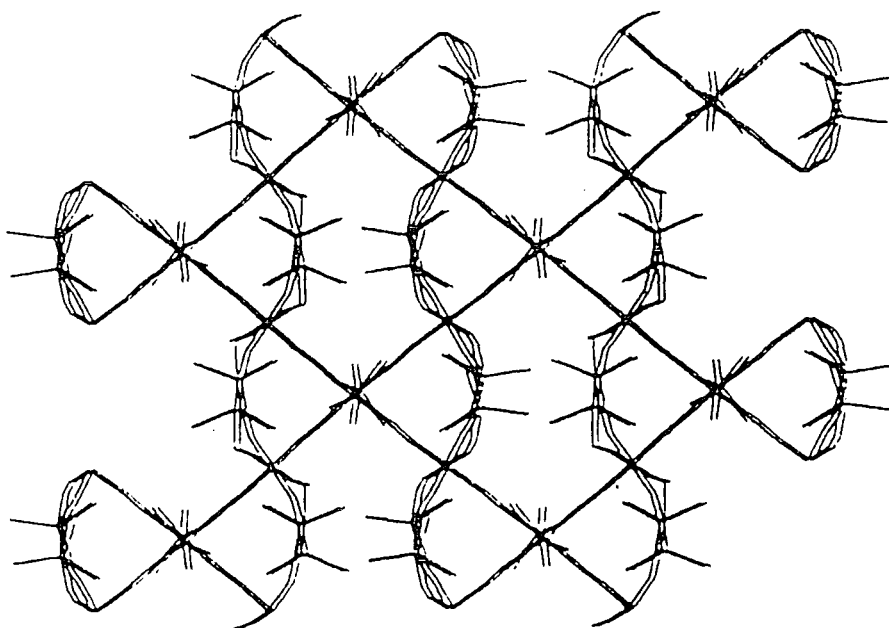
Figure 4.3   Lattice of [(Me$_3$Sn)$_3$Co(CN)$_6$] viewed perpendicular to the main channels
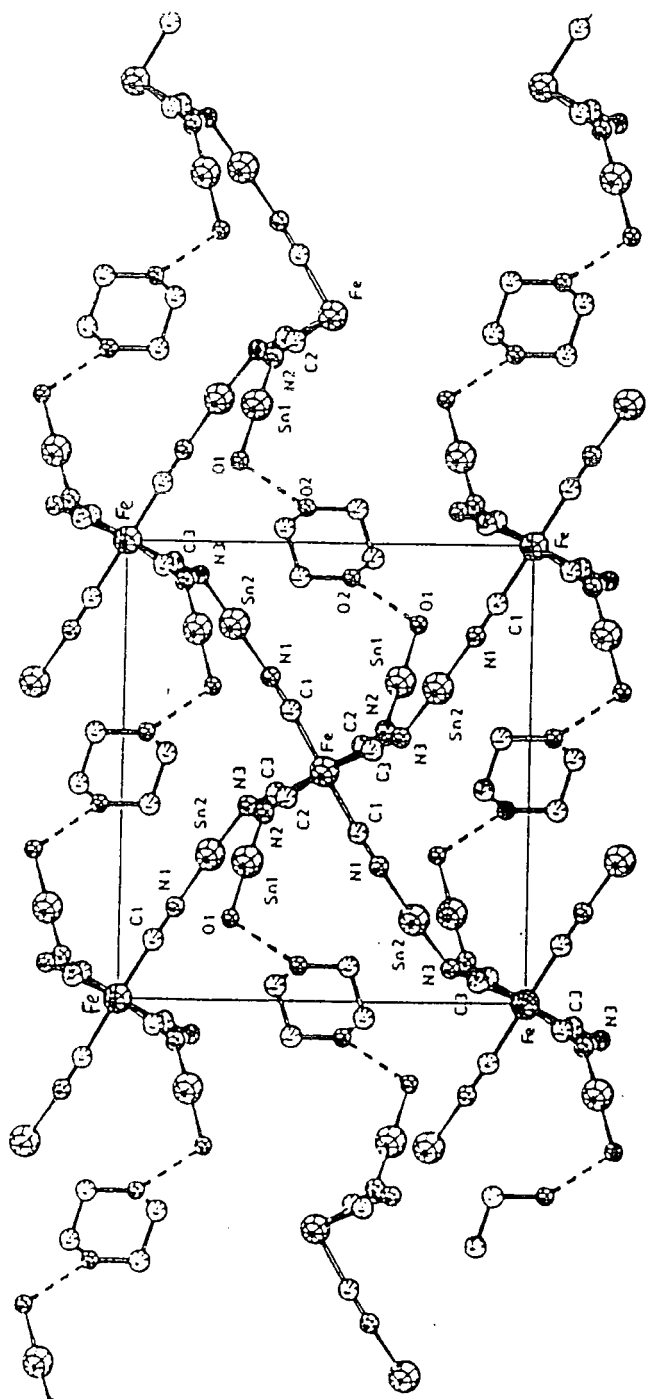
Figure 4.4   Elementary cell and atomic numbering scheme for $[(Me_3Sn)_4Fe(CN)_6 \cdot C_4H_8O_2/H_2O]$

71
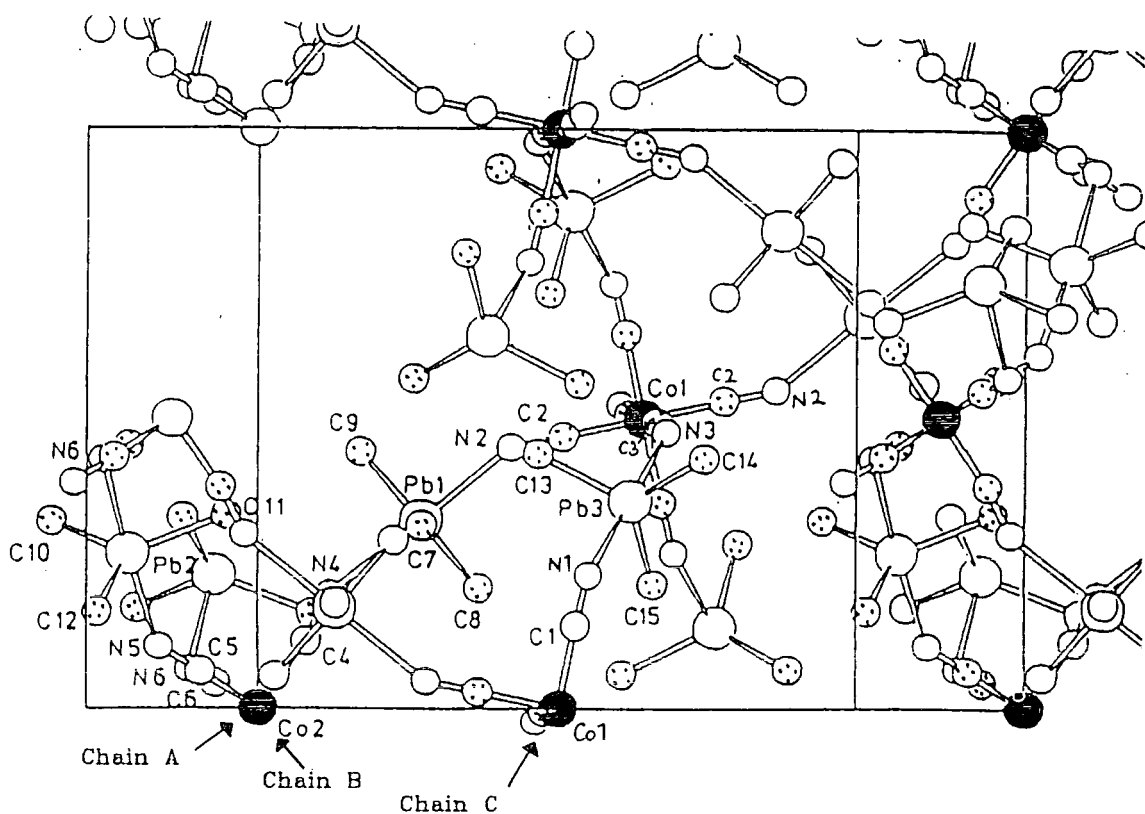
Chain A	Co2—C4--N4—Pb1—N2—C2—Co1—C2—N2—Pb1—N4--C4 —
Chain B	Co2—C5--N5—Pb2--N6--C6—Co2—C6—N6--Pb2—N5—N6--
Chain C	Co1—C1--N1--Pb3—N3—C3--Co1—C3—N3--Pb3--N1--C1--

Figure 4.5   Elementary cell and atomic numbering scheme for $[(Me_3Pb)_3Co(CN)_6]$
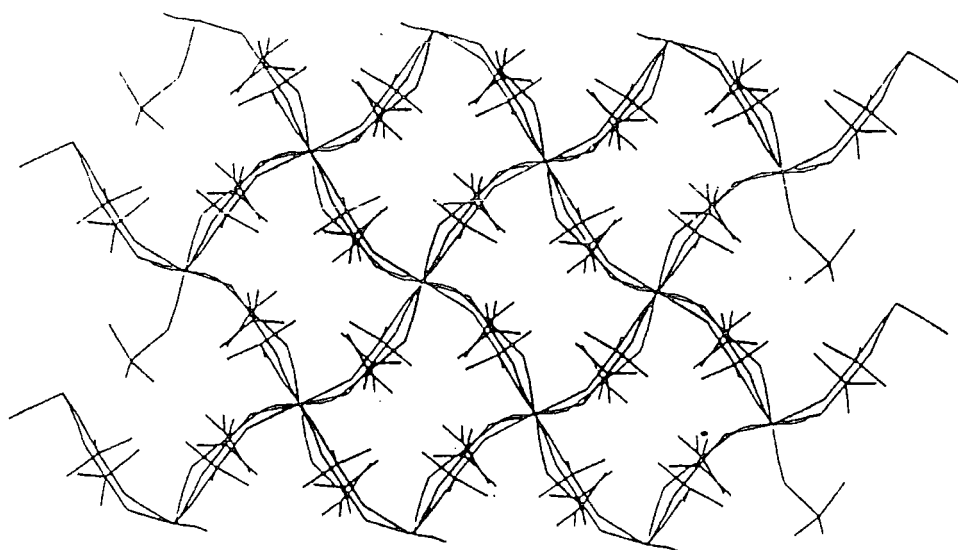
Figure 4.6　Lattice of $[(Me_3Pb)_3Co(CN)_6]$ viewed along the main channels
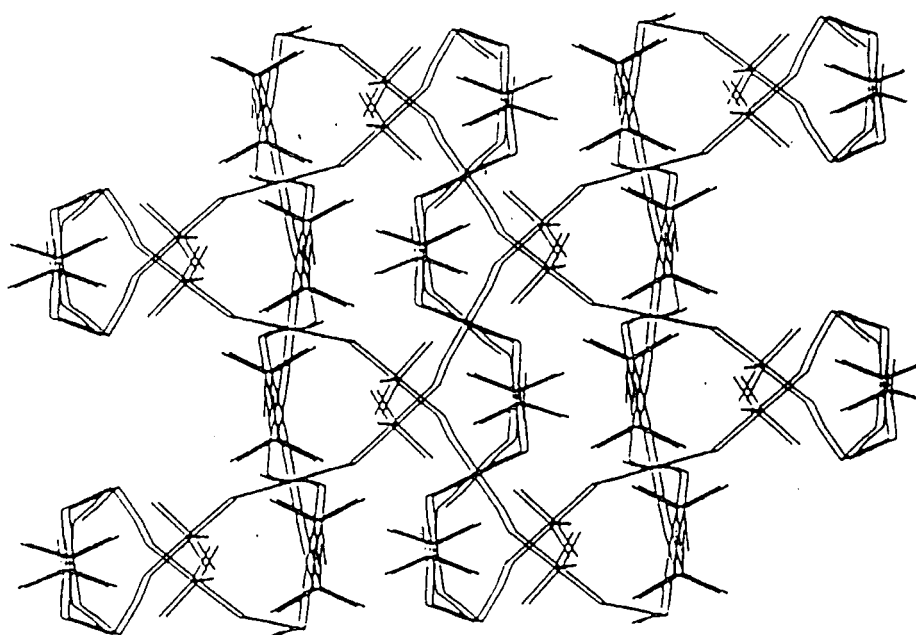
Figure 4.7　Lattice of $[(Me_3Pb)_3Co(CN)_6]$ viewed perpendicular to the main channels

Figure 4.9   Elementary cell and atomic numbering scheme for
[(Me₃Pb)₄Fe(CN)₆.2H₂O]

Figure 4.8   Elementary cell and atomic numbering scheme for
[(Me₃Pb)₄Ru(CN)₆.2H₂O]

74

Table 4.1 Bond lengths and bond angles for 1 and 10

1   [(Me₃Sn)₃Co(CN)₆]

10   [(Me₃Pb)₃Co(CN)₆]
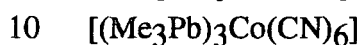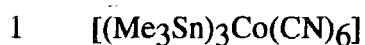
Chain A   [Co1-C2-N2-M1-N4-C4-Co2-C4-N4-M1-N2-C2]

Chain B   [Co2-C5-N5-M2-N6-C6-Co2-C6-N6-M2-N5-C5]

Chain C   [Co1-C1-N1-M3-N3-C3-Co1-C3-N3-M3-N1-C1]

		Bond lengths / nm		Bond angles / °		
		M = Sn	M = Pb		M = Sn	M = Pb
Chain A	Co1-C2	0.186	0.179	Co1-C2-N2	166	176
	C2-N2	0.116	0.116	C2-N2-M1	171	149
	N2-M1	0.236	0.252	N2-M1-N4	175	180
	M1-N4	0.223	0.252	M1-N4-C4	172	154
	N4-C4	0.115	0.115	N4-C4-Co2	172	172
	C4-Co2	0.191	0.181			
Chain B	Co2-C5	0.191	0.182	Co2-C5-N5	163	171
	C5-N5	0.115	0.116	C5-N5-M2	159	145
	N5-M2	0.220	0.254	N5-M2-N6	170	177
	M2-N6	0.234	0.252	M2-N6-C6	152	125
	N6-C6	0.115	0.116	N6-C6-Co2	174	178
	C6-Co2	0.188	0.190			
Chain C	Co1-C1	0.192	0.189	Co1-C1-N1	161	175
	C1-N1	0.115	0.114	C1-N1-M3	159	145
	N1-M3	0.228	0.252	N1-M3-N3	175	175
	M3-N3	0.253	0.246	M3-N3-C3	134	140
	N3-C3	0.116	0.116	N3-C3-Co1	171	172
	C3-Co1	0.180	0.191			

Table 4.2   **Bond lengths and bond angles for 7**

7    $[(Me_3Sn)_4Fe(CN)_6.C_4H_8O_2/H_2O]$

Chain A

```
            Me   Me
              \  /
Fe — C1 — N1 — Sn2 — N3 — C3 —
              |
             Me
```
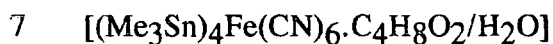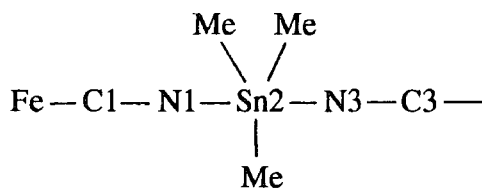
Bond lengths /nm		Bond angles / °	
Fe-C1	0.191	C1-N1-Sn2	148.2
C1-N1	0.114	N1-Sn2-N3	177.3
N1-Sn2	0.237	Sn2-N3-C3	159.2
Sn2-N3	0.228	C3-Fe-C2	90.2
N3-C3	0.114	C2-Fe-C1	88.9
C3-Fe	0.191	C3-Fe-C1	90.5
C(Me)-Sn2	0.212	C(Me)-Sn2-N1	89.9

Chain B

```
            Me   Me
              \  /
Fe — C2 — N2 — Sn1 — O1····O2
              |
             Me
```
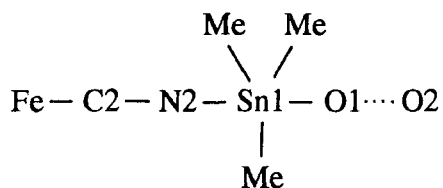
Bond lengths / nm		Bond angles / °	
Fe-C2	0.188	C2-N2-Sn1	157.4
C2-N2	0.117	N2-Sn1-O1	177.2
N2-Sn1	0.216	Sn1-O1-O2	126.0
Sn1-O1	0.245	C(Me)-Sn1-N2	94.1
O1-O2	0.278		
C(Me)-Sn1	0.211		
O1-N1	0.312		

Table 4.3   **Bond lengths and bond angles for 11 and 12**

> 11 $[(Me_3Pb)_4Ru(CN)_6.H2O]$
>
> 12 $[(Me_3Pb)_4Fe(CN)_6.H2O]$

Chain A

```
              C6
              |        | /
    — Pb1— N1— C1— M — C3—N3—Pb1—
            / \        / |
          C5    C4
```
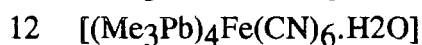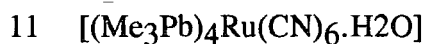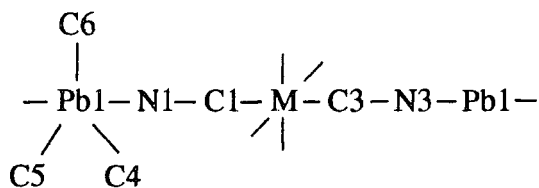
Bond lengths / nm			Bond angles / °		
	M = Ru	M = Fe		M = Ru	M = Fe
Pb1-N1	0.255	0.251	C4-Pb1-N1	87	87
N1-C1	0.119	0.121	C5-Pb1-N1	88	89
C1-M	0.200	0.188	C6-Pb1-N1	92	92
M-C3	0.203	0.189	Pb1-N1-C1	121	120
C3-N3	0.115	0.116	N1-C1-M	177	179
N3-Pb1	0.254	0.256	M-C3-N3	180	176
Pb1-C4	0.218	0.221	C3-N3-Pb1	124	126
Pb1-C5	0.220	0.220	N3-Pb1-N1	173	171
Pb1-C6	0.218	0.220			

Chain B

```
              C9   C7
               \  /        | /
    O1— Pb2 — N2— C2 — M — C2—N2—Pb2— O1
               |          / |
              C8
```
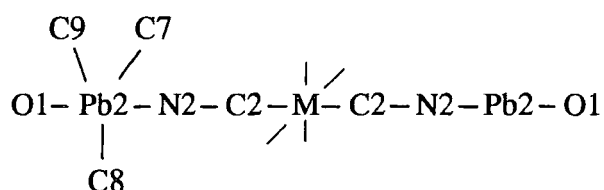
Bond lengths / nm			Bond angles / °		
	M = Ru	M = Fe		M = Ru	M = Fe
O1-Pb2	0.268	0.266	O1-Pb2-C7	82	84
Pb2-N2	0.232	0.235	O1-Pb2-C8	95	83
N2-C2	0.115	0.111	O1-Pb2-C9	86	92
C2-M	0.203	0.192	O1-Pb2-N2	177	179
Pb2-C7	0.215	0.222	Pb2-N2-C2	175	175
Pb2-C8	0.222	0.222	N2-C2-M	177	178
Pb2-C9	0.222	0.222	C2-M-C2	180	180
O1..N1	0.285	0.294			
O1..N3	0.300	0.298			

77

CHAPTER 5

NMR RESULTS AND DISCUSSION

5.1 Tin- and cobalt- containing compounds

$$[(Me_3Sn)_3Co(CN)_6] \quad 1$$

$$[(Et_3Sn)_3Co(CN)_6] \quad 2$$
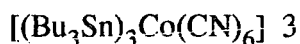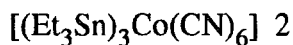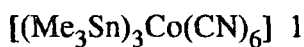
$$[(Bu_3Sn)_3Co(CN)_6] \quad 3$$

The NMR data are given in table 5.1.

5.1.1 ^{13}C spectra

The first compound to be discussed is $[(Me_3Sn)_3Co(CN)_6]$, 1. The single-crystal X-ray structure determination indicates nine crystallographically inequivalent methyl groups, three around each tin in the three different chains. However, the room temperature methyl region of the ^{13}C spectrum (figure 5.1.1a) contains only two signals with an intensity ratio of 2:1. This would suggest that the three methyls bonded to any one tin atom are indistinguishable, probably due to a rapid rotation of the trimethyl-tin group around the N-Sn-N axis. As discussed earlier (section 4.1), chains A and B are both relatively linear and have symmetric bridges compared to chain C. Therefore the signal of double intensity at 0.8 ppm can probably be assigned to the methyls in the two chains A and B (with accidental near-degeneracy of the chemical shifts) and the signal at −0.5 ppm can be assigned to the methyls in chain C. An alternative assignment would be that the three Me$_3$Sn groups are all equivalent in NMR, but two of the methyls within a given Me$_3$Sn, are different from the third. This, however is unlikely, in view of the results from the ^{119}Sn NMR spectrum (see section 5.1.2).

In order to investigate further the difference in the number of inequivalent methyl groups as predicted by NMR and X-ray work, a series of spectra were obtained at temperatures ranging from room temperature to −59°C. As the temperature was lowered the signals shifted slightly until at −59°C (figure 5.1.1b) the high-frequency signal split into two. This signal was earlier assigned to the methyls of chain A and B.

79

Lowering the temperature has caused the two signals to be resolved but it is not enough to stop any proposed rotation or exchange process.

The carbon of the methyl is directly bonded to a tin atom and coupling of the ^{13}C to the tin can be seen as satellites around the methyl signals in both the room-temperature and the low-temperature spectra (figure 5.1.1a & b). Each satellite signal is split into two due to coupling to both ^{119}Sn and ^{117}Sn. This is shown to be true because the ratio of the two gamma values is equal to the ratio of the coupling constants.

$$\frac{\gamma^{117}Sn}{\gamma^{119}Sn} = \frac{-9.578 \times 10^7}{-10.021 \times 10^7} = 0.956$$

Methyl 1 at 0.8 ppm,   ratio of J/Hz $= \frac{532}{561} = 0.95$

Methyl 2 at -0.5 ppm,   ratio of J/Hz $= \frac{551}{579} = 0.95$

The values of J are typical of a penta-coordinated trimethyl tin system[28].

In the second compound the R group is ethyl and the ^{13}C spectrum indicates the presence of only one type of ethyl in the lattice (figure 5.1.2). There is one CH_2 signal at 11.7 ppm with satellites due to direct coupling of the ^{13}C to the ^{119}Sn ($^1J_{(13C-119Sn)} = 503$ Hz). The CH_3 resonance is at 10.2 ppm and also has satellites, but here the coupling is over two bonds and is therefore much smaller ($^2J_{(13C-19Sn)} = 34$ Hz). It is interesting to note that the linewidth of the CH_3 (8 Hz) resonance is much smaller than that of the CH_2 (28 Hz), probably because the CH_3 is more mobile than the CH_2.

In the third compound, the R group is n-butyl and the low-frequency region of the ^{13}C spectrum (figure 5.1.3) contains at least seven lines. Some of them are overlapping but they can be divided into four groups. The first group contains two methyl signals at 14.5 ppm and 14.9 ppm and the five CH_2 signals can be divided into three separate groups (18.3, 19.9 ppm, 27.5, 27.6 ppm and 28.2 ppm). These signals indicate the presence of two crystallographically different butyl groups. The two

CH_2 signals at 18.3 and 19.9 ppm are resolved enough to allow an intensity ratio of 2:1 to be calculated; the higher frequency signal being of double intensity. This indicates that there are in fact three different butyls within the unit cell but two of them are indistinguishable by NMR. The two CH_2 signals at 18.3 and 19.9 ppm also have satellites with coupling constants $^1J_{(13C-119Sn)} = 467Hz$ and therefore they can be assigned to CH_2's directly bonded to the tin. No two-bond J coupling is seen for the other CH_2 signals because the signals are overlapping and are also broader than the CH_3 signal of 2.

Comparison of the low-frequency regions of the three spectra shows that the number of inequivalent R groups changes from two, for R=Me, to one, for R=Et, and back to two, for R=Bu. It is possible that as the steric bulk of the R group increases (Me to Et), the chains are all forced to become more linear and equivalent. Seeing only a single type of ethyl in the spectrum of 2 is consistent with this. However, it would be expected that the trend would continue when the steric bulk of the R group is increased again, by replacing ethyl with butyl, leading to resonances from only one type of butyl in the ^{13}C spectrum of 3, but this is not the case.

The only other ^{13}C signals present in the spectra from these three compounds are those from the carbon in the cyano groups (figure 5.1.4). These signals are similar for all three compounds, with the centreband appearing at about 135 ppm. Crystallographically there are six different CN groups within the asymmetric unit for compound 1. However the centreband for both the methyl and ethyl compounds is split into more than six lines. This complicated splitting pattern is discussed in section 5.1.5. In the butyl compound the lines are too broad for the splitting pattern to be resolved.

5.1.2 ^{119}Sn spectra

The crystal structure of 1 indicates three different tin atoms within the unit cell. The ^{119}Sn spectrum (figure 5.1.5) contains two overlapping sideband manifolds with an overall intensity ratio of 2:1 indicating that, out of the three chains A, B and C, two are indistinguishable by NMR. The signal of double intensity (-88 ppm) can therefore, tentatively, be assigned to the tin atoms in chains A and B with the relatively symmetric bridges (as for the ^{13}C spectrum), and the second signal (-118 ppm) to the tin atoms in chain C with the more asymmetric bridge.

For 2, only one ^{119}Sn signal is seen at -75 ppm, from which it is inferred that all the chains are now equivalent, which is in agreement with the ^{13}C spectrum. The chemical shift of the centreband is similar to that assigned to chains A and B for 1 (-88 ppm). From this it is possible to draw the conclusion that all the equivalent chains in 2 are very similar to chains A and B of 1. The centrebands and sidebands for both 1 and 2 are split, but 2 shows this the most clearly, with each signal split into five lines. This is discussed in section 5.1.6.

Compound 3 also gives a ^{119}Sn spectrum containing only one signal, suggesting that this also has three equivalent chains. However, this signal shows no sign of any splittings. The chemical shift of the centreband (-42 ppm) is at a higher frequency than that for 2, possibly indicating the chains are becoming more linear, or the bridges are more symmetric. The single ^{119}Sn resonance for 3 suggests that, in the ^{13}C spectrum, the two different signals for the CH_3 and CH_2's are likely to be due to differences in the n-butyl groups on one particular tin atom. It is a possibility that the large steric bulk of the butyl has caused the proposed rotation about the N-Sn-N threefold axis to slow down or stop, allowing differences to be seen between the butyl groups. This could be investigated further by obtaining high temperature spectra of the methyl region of the ^{13}C spectrum.

5.1.3 ^{15}N spectra

The nitrogen spectrum of 1 contains three signals of approximately equal intensity. This is not in agreement with the crystal structure which predicts all six CN groups to be different. Since the intensity of the signals in the ^{15}N spectrum are approximately equal, each signal must arise from two N atoms in very similar environments.

The nitrogen spectra of both 2 and 3 contain only one signal, implying that the three chains are equivalent, which is in agreement with the ^{13}C and ^{119}Sn NMR data. The spectrum of 3 (figure 5.1.6) has a particularly good signal-to-noise ratio, allowing satellite signals to be seen due to coupling of the ^{15}N to ^{119}Sn ($^1J_{(15N-119Sn)} = 147$ Hz).

5.1.4 ^{59}Co spectra

The ^{59}Co spectra of the three compounds are similar, containing an intense centreband with many spinning sidebands (figure 5.1.7). There is, however a difference in the linewidths (table 5.1). ^{59}Co is a quadrupolar spin-7/2 nuclei. The intense centreband in the spectrum is due to the central 1/2, -1/2 transition and the spinning sidebands are a result of the other possible transitions (-3/2,-1/2; 7/2,5/2 etc.). In each case the spectra suggest the asymmetric unit contains a single cobalt atom whereas the X-ray data for compound 1 predicted two. The possibility that different signals are obscured by the substantial linewidths is unlikely given the very high sensitivity of cobalt chemical shifts to changes in environment.

The room temperature spectra of all the different nuclei indicate that the number of crystallographically inequivalent sites in the asymmetric unit for 1 differs from the number of observed resonance lines in the NMR spectra as shown below.

	CH$_3$	-C-	N	Sn	Co
XRS	9	6	6	3	2
NMR	2		3	2	1

The origin of these discrepancies is unclear.

5.1.5   CN region of ^{13}C spectrum of (Et$_3$Sn)$_3$Co(CN)$_6$

The centreband of the CN region is split into at least nine lines as shown in figure 5.1.4. The carbon is directly bonded to both cobalt and nitrogen so there is a possibility of coupling to both the quadrupolar spin-7/2 ^{59}Co and the spin-1 ^{14}N. Indirect (J) coupling between a spin-1/2 nucleus and a quadrupolar nucleus, with spin S, would give a first-order splitting pattern with 2S+1 lines of equal intensity. Therefore coupling of ^{13}C to ^{59}Co would give eight lines of equal intensity separated by $J_{13C-59Co}$, and further coupling to ^{14}N would split each of these lines into three, resulting in a total of 24 lines. This simple case only occurs if the Zeeman interaction greatly exceeds the quadrupolar interaction of the S spin. If this is not so, second-order features, which cannot be removed by MAS, can be transferred to the spectrum of the spin-1/2 nucleus by dipolar coupling[29]. This can give rise to the coupling pattern being distorted and also the intensity distribution in the sidebands changing[30]. The CN centreband and sidebands exhibit some of these features with a considerable amount of overlapping of the lines reducing the number from 24 to 9.

In the case of ^{13}C coupling to a spin-1 ^{14}N, $J_{13C-14N}$ is very small and therefore the simple first order splitting pattern would consist of three lines very close together (figure 5.1.8B). It is known that quadrupolar effects cause the two outermost lines

to shift in the same direction and by the same amount (Δ) and the middle line to shift by twice as much (2Δ) and in the opposite direction to the others. This results in a pattern of two lines in the intensity ratio 2:1 (figure 5.1.8C).

If this type of ^{14}N splitting pattern is superimposed onto the 8 lines from the coupling of ^{13}C to ^{59}Co (figure 5.1.9B) with the nitrogen splitting approximately equal to $J_{13C-59Co}$ then a pattern of 9 lines will be obtained with in the intensity ratio 2:3:3:3:3:3:3:3:1 (figure 5.1.9C). Looking at the cyanide region of the ^{13}C spectrum of 2 (figure 5.1.4), even if the intensities of the signals in the sidebands are taken into account, the ratios do not seem to add up to those predicted. This is most likely due to quadrupolar effects from the ^{59}Co which have not been taken into account.

5.1.6 ^{119}Sn spectrum of [(Et$_3$Sn)$_3$Co(CN)6]

Figure 5.1.10 shows the ^{119}Sn spectrum of 2 and figure 5.1.11 shows expansions of the centreband and some of the spinning sidebands with the positions of each signal in Hz. The tin atoms in compound 2 are directly bonded to two equivalent nitrogen atoms.
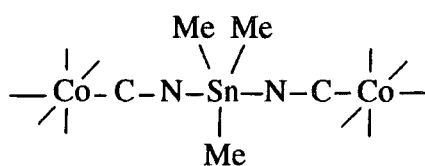
In a simple first order spectrum, coupling of the ^{119}Sn to one ^{14}N would give three lines of equal intensity separated by the coupling constant J (figure 5.1.12B). Coupling to the second ^{14}N atom splits each of these lines, also into three lines of equal intensity, separated by J. This results in some of the lines overlapping and forming a pattern of five lines, separated by J, with an intensity ratio of 1:2:3:2:1.

Due to quadrupolar effects the lines are all shifted slightly. The two outermost lines in figure 5.1.12B are shifted by $-\Delta$ and the central line is shifted by $+2\Delta$ where Δ is small compared to J (figure 5.1.12C). If each of these slightly shifted lines (labelled 1, 2 and 3) are split into three due to coupling to the second ^{14}N then figure 5.1.12D is obtained. Perturbations due to quadrupolar effects again occur resulting in figure 5.1.12E. The central three lines are split by 6Δ, however this splitting is very small compared to the linewidth of the central line in each sideband of approximately 100 Hz. The theory, therefore, predicts a pattern of five lines with an intensity ratio of 1:2:3:2:1, as in the first order case, but with slight shifts in the line positions.

Values for $J+3\Delta$, $2J$ and $J-3\Delta$ can be read from the positions of the signals in the sidebands and the centreband of the ^{119}Sn spectrum and hence J and Δ can be calculated as follows.

$J+3\Delta$	$2J$	$J-3\Delta$
140.4	250.3	109.8
137.5	250.2	116.0
148.5	250.3	109.8
140.4	244.1	116.0
131.7*	269.9*	97.7*
140.5	250.3	109.8
140.4	250.3	103.8

Mean 140.4   249.3   110.9

(* not included in the mean because the signal is of low intensity and therefore inaccurate)

$2J = 249.3\,Hz$ $J = 124.6\,Hz$ i.e. $J = 125\,Hz$

$J+3\Delta = 140.9\,Hz$ $\Delta = 5.43\,Hz$

$J-3\Delta = 110.9\,Hz$ $\Delta = 4.57\,Hz$

i.e. $\Delta = 5\,Hz$

According to perturbation theory $\Delta = \dfrac{-3}{10}\dfrac{D\chi}{\upsilon}$

D = dipolar coupling constant
χ = quadrupolar coupling constant
υ = Larmor frequency of S nucleus

Assuming no anisotropy in J, the dipolar coupling constant D can be calculated as follows.

$$D = \frac{\mu}{4\pi} \gamma_{119Sn} \, \gamma_{14N} \, \hbar \, (r_{Sn-N})^{-3}$$

$$= -265 \text{ Hz}$$

$$\gamma_{119Sn} = -9.98 \times 10^7 \text{ radT}^{-1}\text{s}^{-1}$$
$$\gamma_{14N} = 1.93 \times 10^7 \text{ radT}^{-1}\text{s}^{-1}$$
$$\hbar = 1.05 \times 10^{-34} \text{ Js}$$
$$\frac{\mu}{4\pi} = 1 \times 10^{-7} \text{ Hm}^{-1}$$
$$r_{Sn-N} \simeq 0.23 \text{ nm}$$

Hence χ can be calculated

$$\Delta = \frac{-3}{10} \frac{D\chi}{\upsilon} \qquad \chi = \frac{-10}{3} \frac{\Delta \upsilon}{D} \qquad \upsilon = 21.7 \text{ MHz}$$

$$\chi = 1.36 \text{ MHz}$$

The calculated values for both D and χ are approximate since only an approximate bond length was used. However, 1.36 MHz is high for χ, probably due to the fact that the anisotropy in J cannot be ignored. However, even though there is no strictly linear geometry for the cyanide nitrogen the colinearity of tensors and the axiality of q (electric field gradient) are likely to be reasonably good.
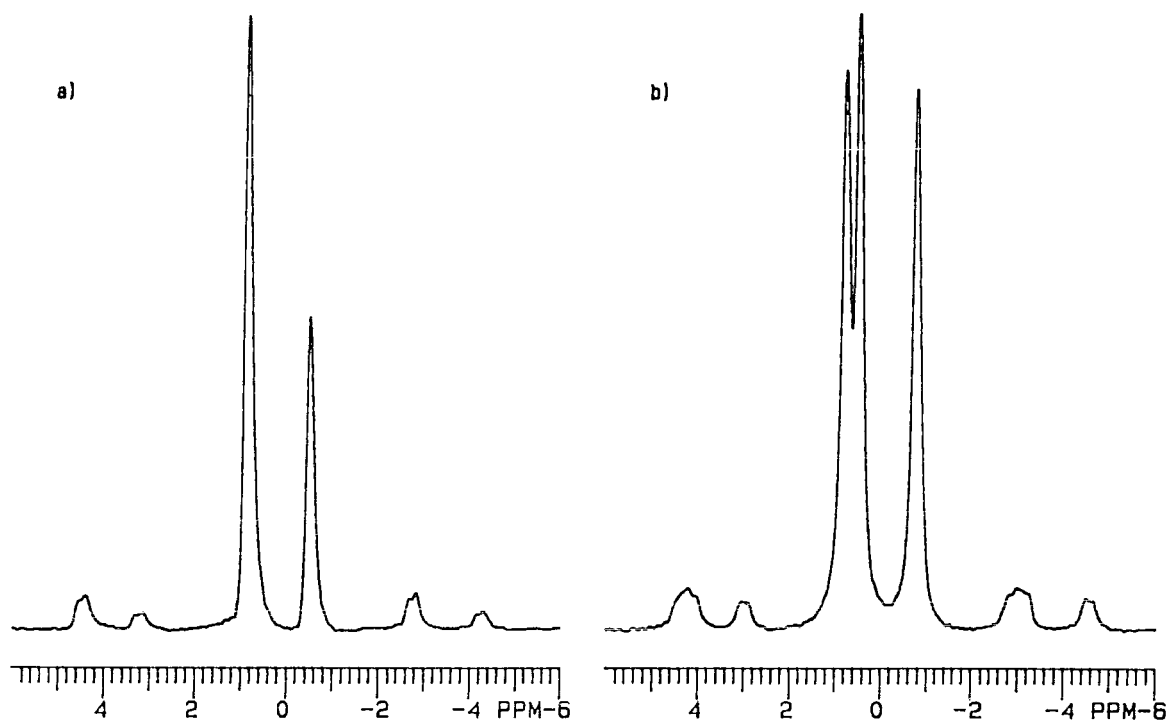
Figure 5.1.1   Methyl region from ^{13}C spectrum of [(Me$_3$Sn)$_3$Co(CN)$_6$] at a) room
temperature b) −59°C
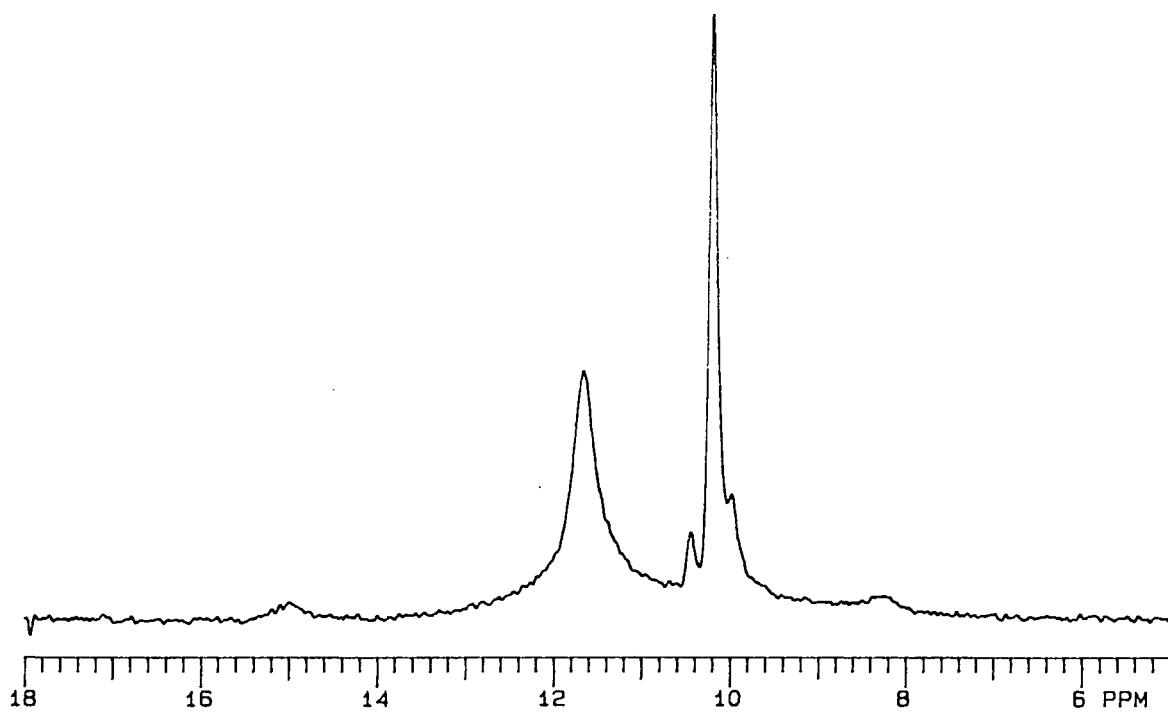
Figure 5.1.2   Ethyl region from ^{13}C spectrum of [(Et$_3$Sn)$_3$Co(CN)$_6$]
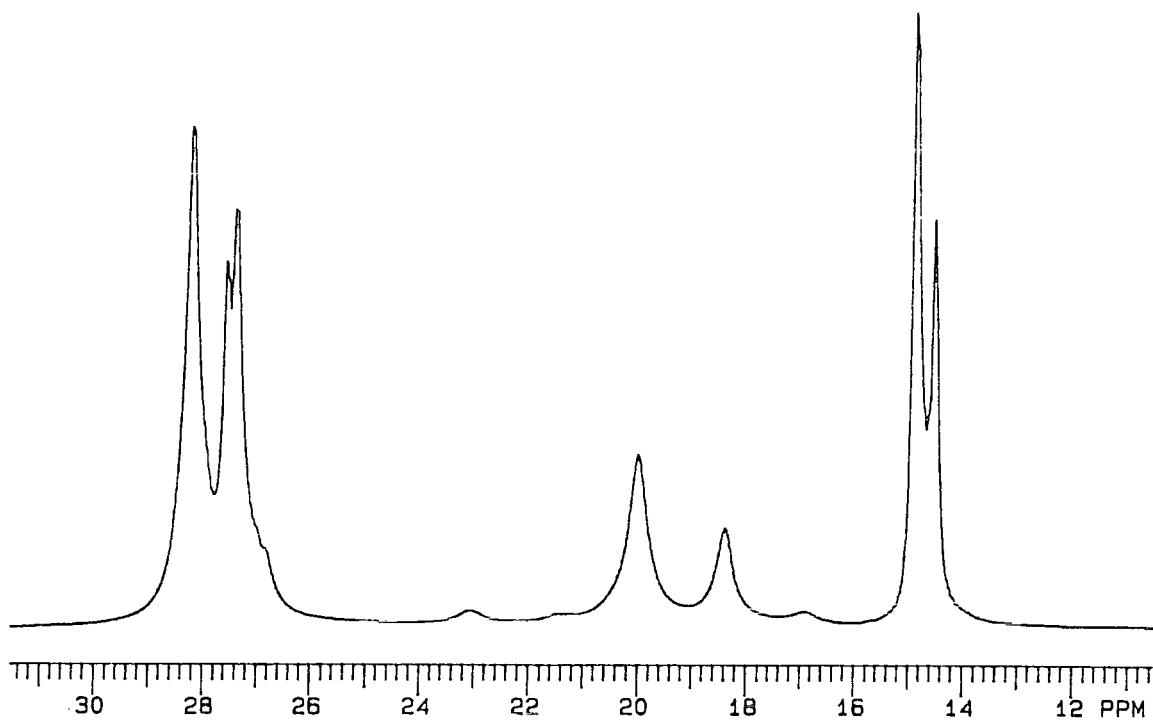
Figure 5.1.3   Butyl region from ^{13}C spectrum of $[(Bu_3Sn)_3Co(CN)_6]$
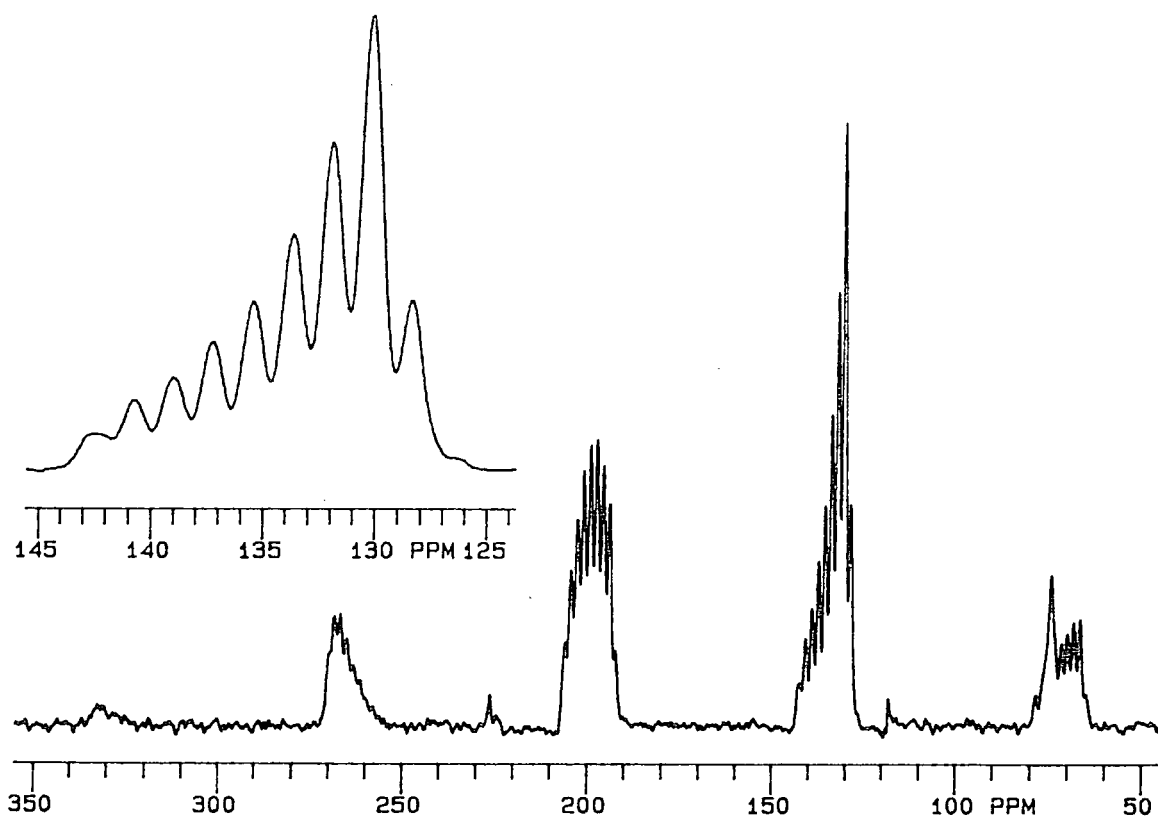
Figure 5.1.4   CN region from ^{13}C spectrum of $[(Et_3Sn)_3Co(CN)_6]$ and an expansion of the centreband
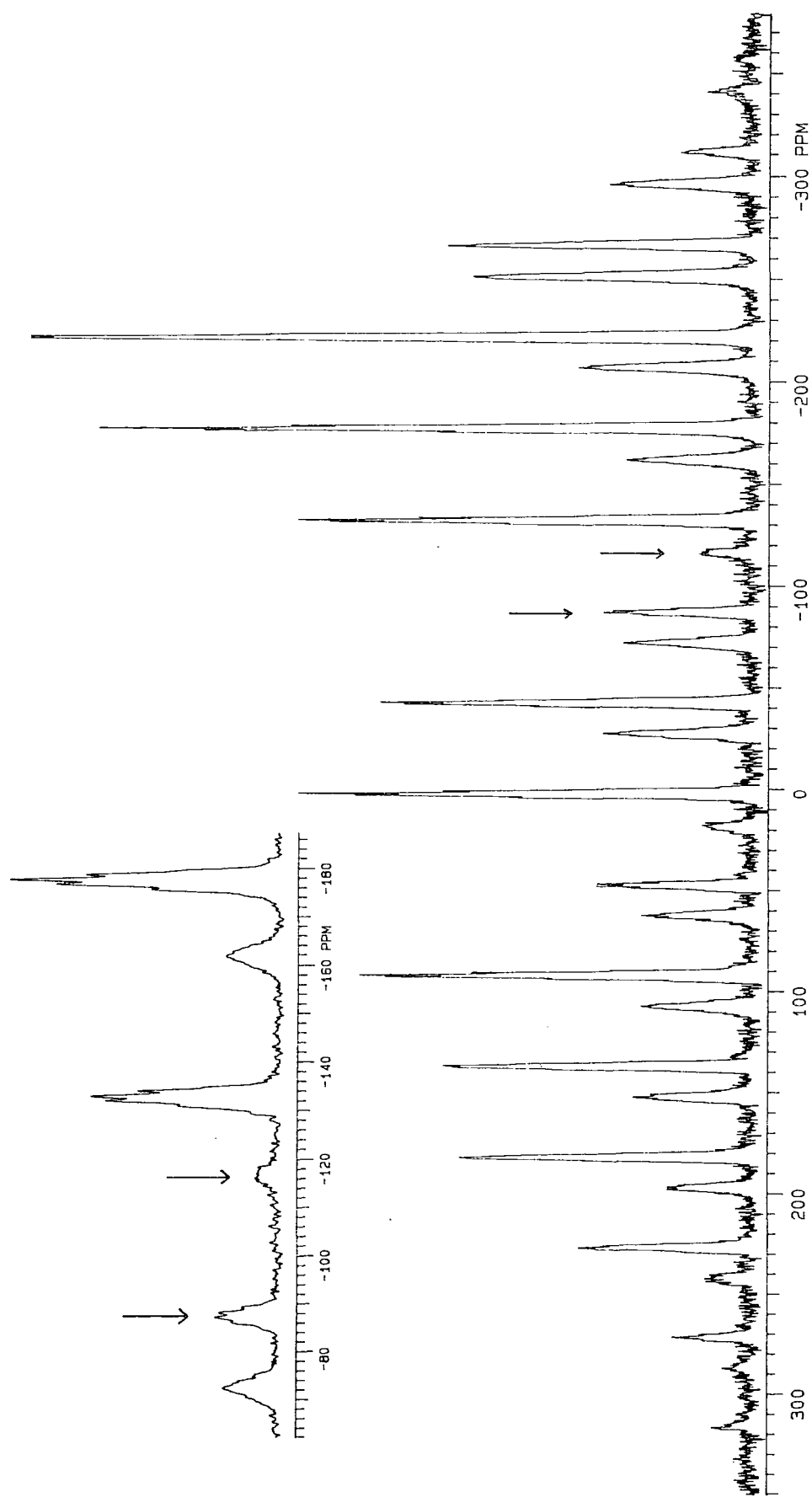
Figure 5.1.5 ^{119}Sn spectrum of $[(Me_3Sn)_3Co(CN)_6]$ and an expansion of the centreband and some spinning-sidebands

90
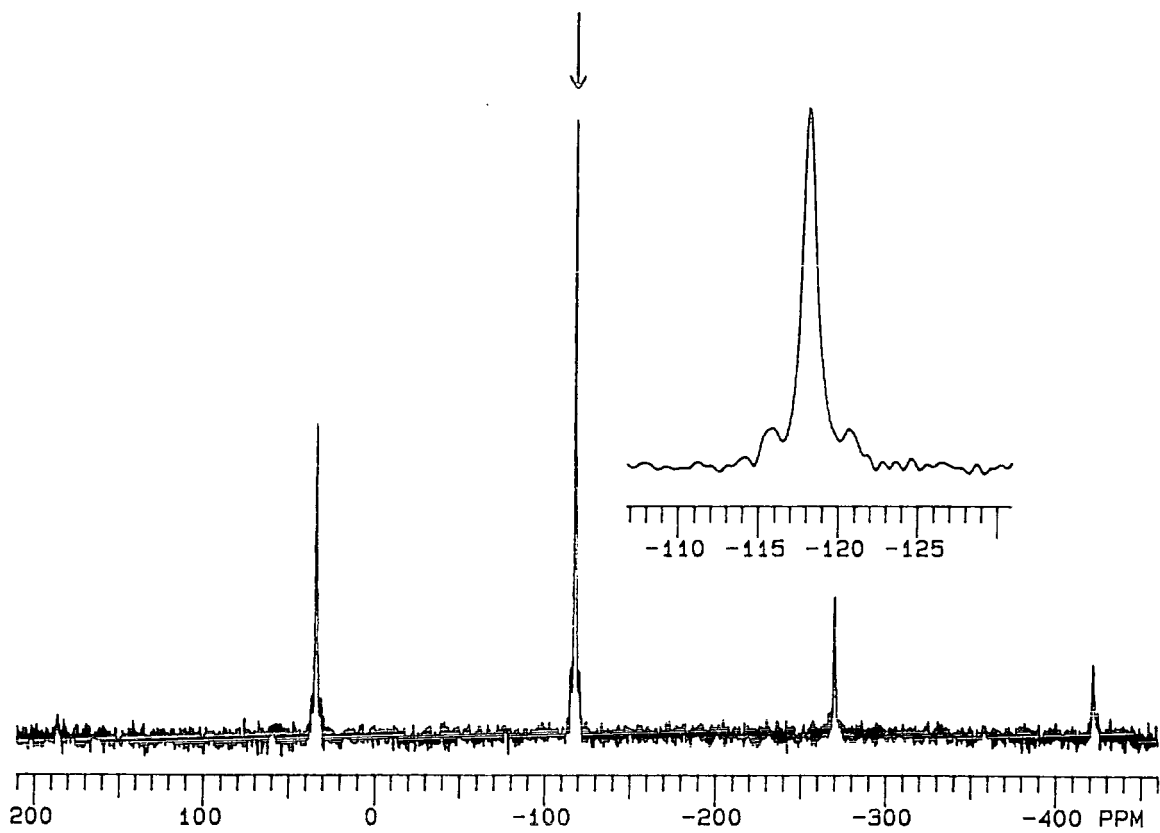
Figure 5.1.6 ^{15}N spectrum of [(Bu$_3$Sn)$_3$Co(CN)$_6$] and an expansion of the centreband
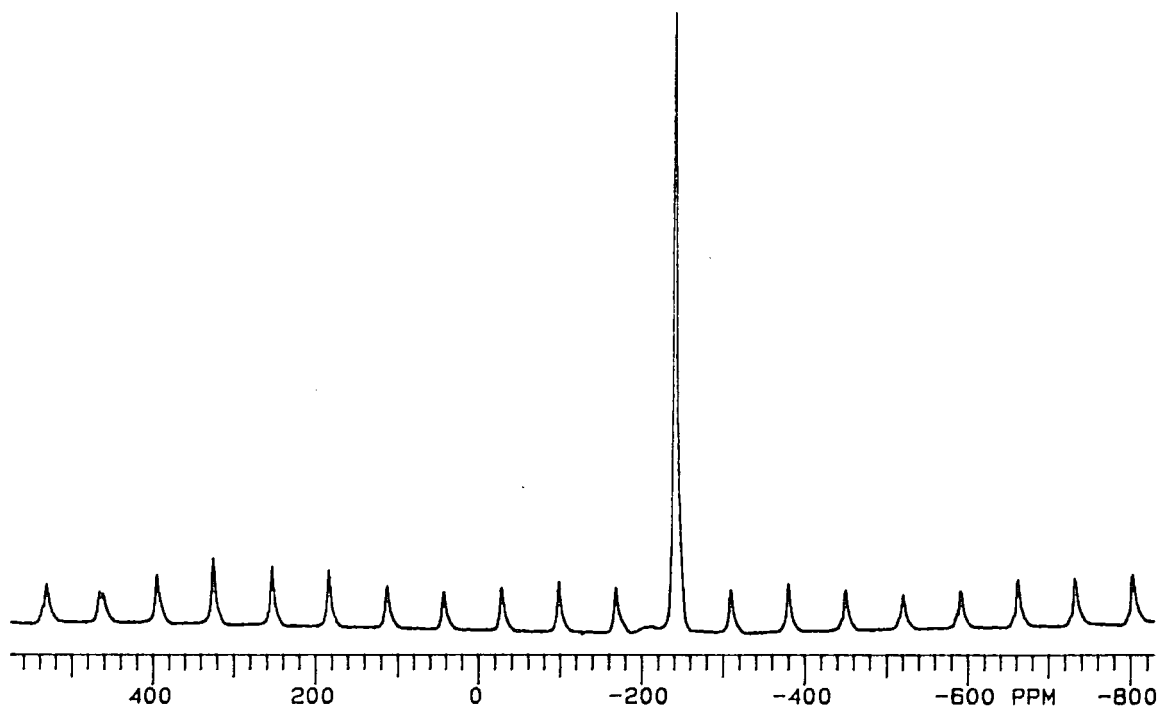
Figure 5.1.7 ^{59}Co spectrum of [(Et$_3$Sn)$_3$Co(CN)$_6$]
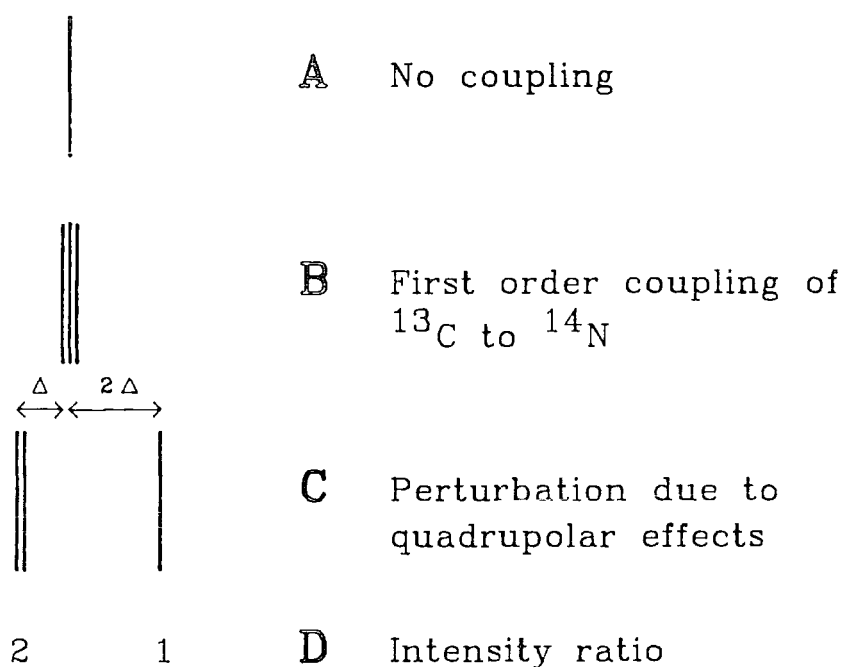
Figure 5.1.8   Theoretical splitting pattern for ^{13}C coupling to ^{14}N
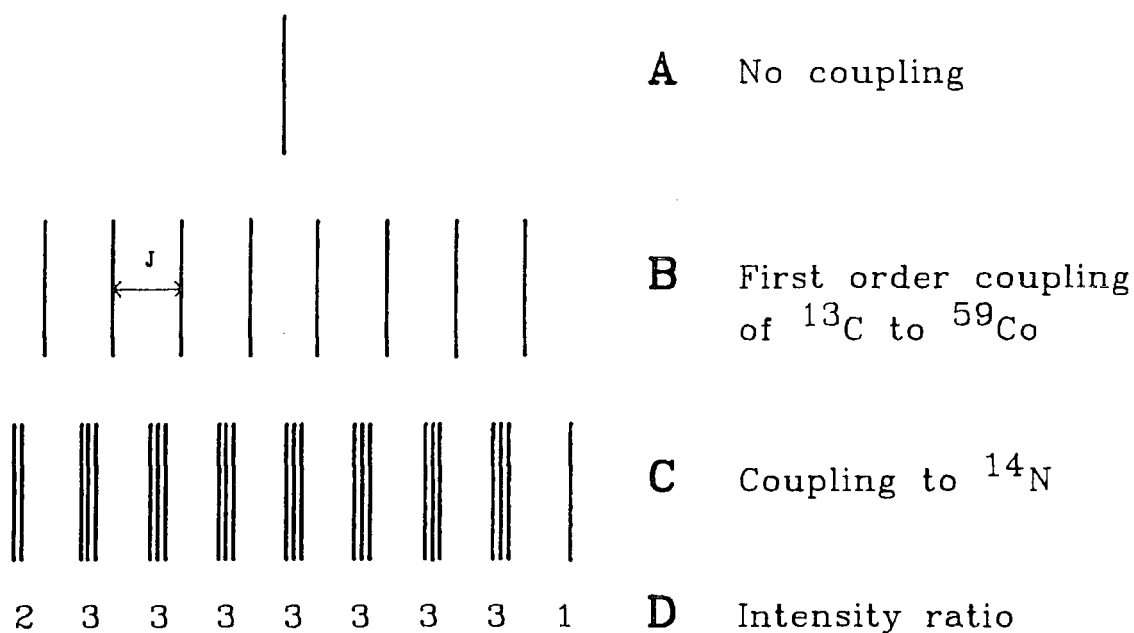
Figure 5.1.9   Theoretical splitting pattern for ^{13}C coupling to both ^{59}Co and ^{14}N
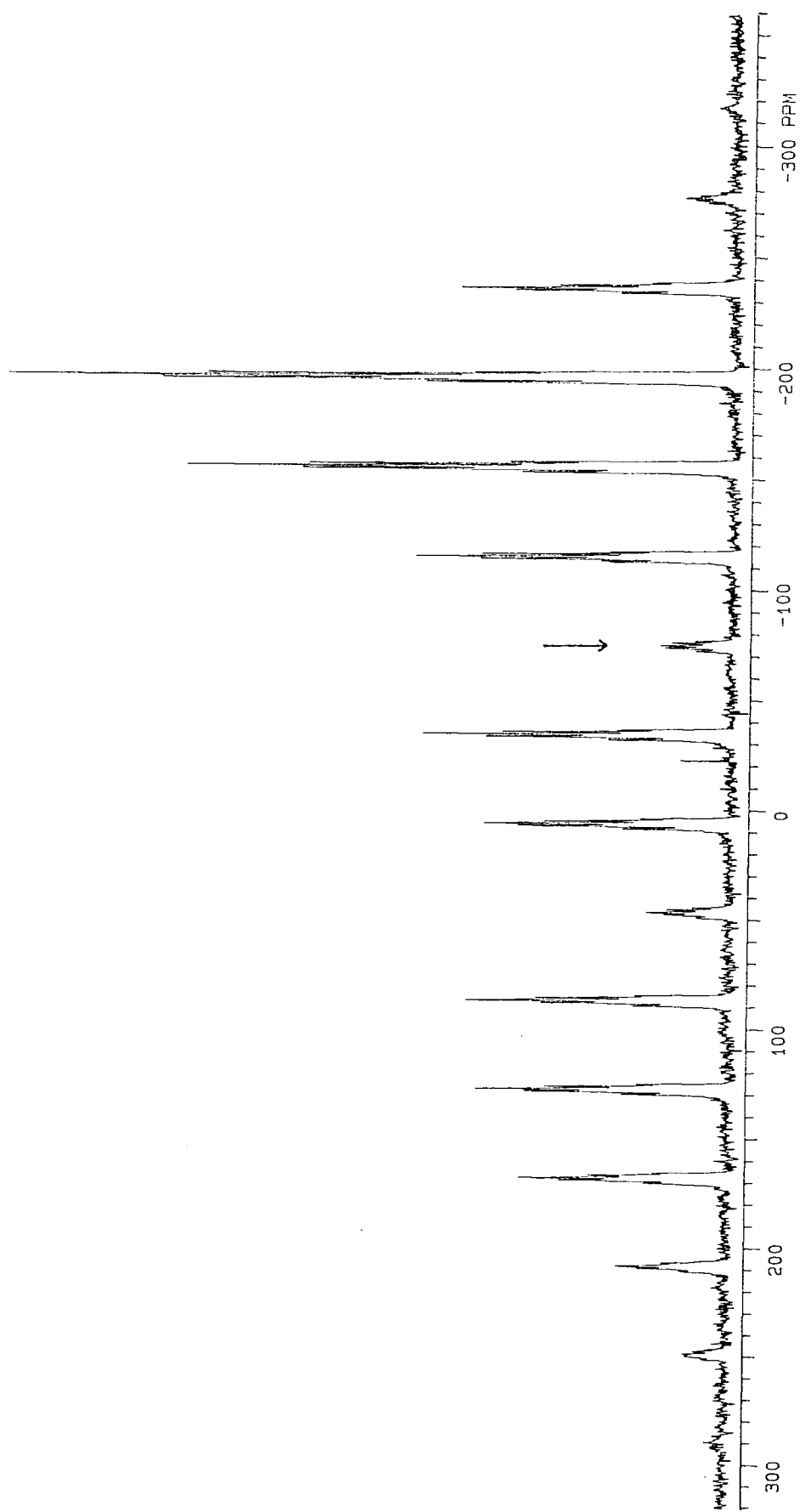
Figure 5.1.10 ^{119}Sn spectrum of $[(Et_3Sn)_3Co(CN)_6]$
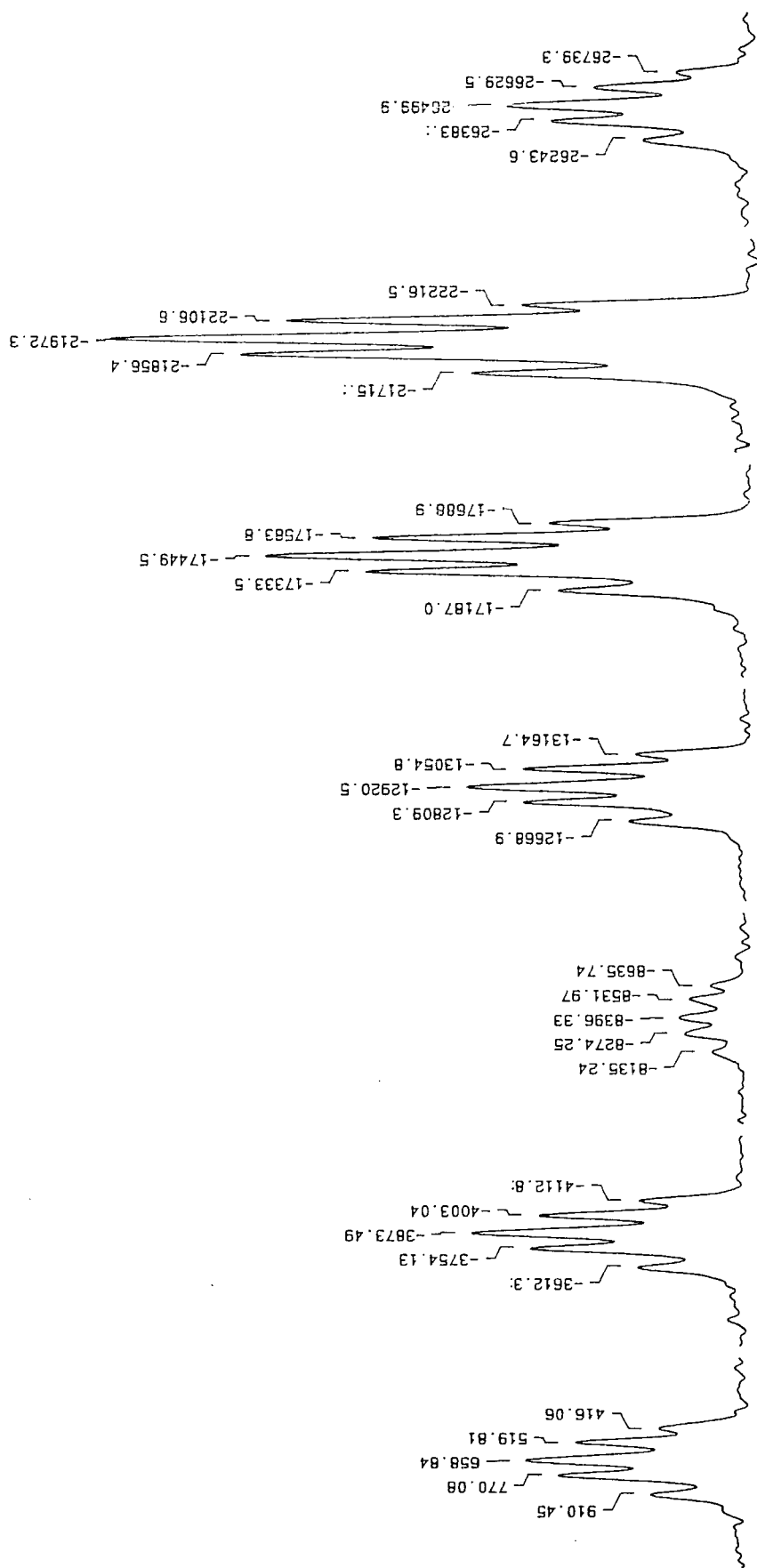
Figure 5.1.11 A selection of spinning-sidebands from the ^{119}Sn spectrum of $[(Et_3Sn)_3Co(CN)_6]$ with peak picking in Hz

94
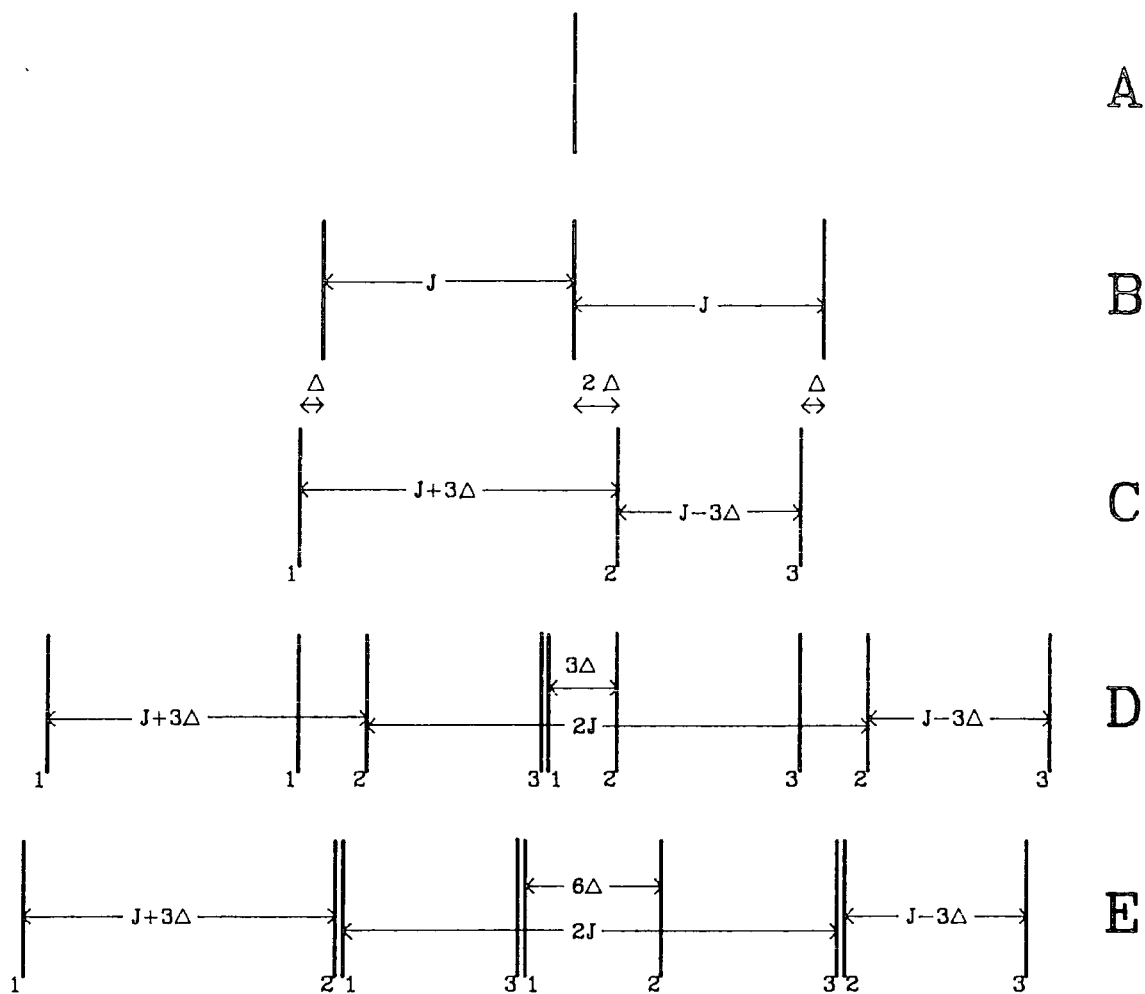
A   No coupling

B   First order coupling of ^{119}Sn to ^{14}N

C   Perturbation due to quadrupolar effects

D   Coupling to the second ^{14}N

E   Perturbation due to quadrupolar effects

Figure 5.1.12   Theoretical splitting pattern for one ^{119}Sn coupling to two ^{14}N

Table 5.1   NMR data for 1, 2 and 3

1	$[(Me_3Sn)_3Co(CN)_6]$	
2	$[(Et_3Sn)_3Co(CN)_6]$	
3	$[(Bu_3Sn)_3Co(CN)_6]$	

	δ/ppm	I_{rel}	J/Hz	Δυ1/2/Hz	assignment
13C					
1	−0.5	1.0	551[b] 579[c]	19	CH3
	0.8	1.9	532[b] 561[c]	19	CH3
	135[a]				CN
2	10.2	1.0	34[d]	8	CH3
	11.7	1.3	503[c]	28	CH2
	135[a]				CN
3	14.5 14.9	1.2		11 11	CH3
	18.3 19.9	1.0	467[c] 467[c]	18 22	CH2
	27.5 27.6	1.1		24 24	CH2
	28.2	1.1		15	CH2
	128[a]				CN
119Sn					
1	−118[a]	1.0			Chain C
	−88[a]	2.2			Chain A+B
2	−75[a]				
3	−45			800	
15N					
1	−116	1.0		22	
	−119	1.2		17	
	−123	1.0		24	
2	−120			20	
3	−118		147[e]	33	
59Co					
1	−244			558	
2	−233			344	
3	207			2500	

a   multiplet, therefore only approximate δ   c ^1J 13C-119Sn

b ^1J 13C-117Sn   d ^2J 13C-119Sn

                                                       e ^1J 15N-119Sn

5.2   Trimethyl tin compounds with different metal atoms

$$4 \quad [(Me_3Sn)_4Fe(CN)_6]$$

$$5 \quad [(Me_3Sn)_4Ru(CN)_6]$$

$$6 \quad [(Me_3Sn)_4Os(CN)_6]$$
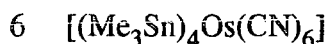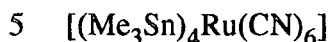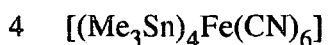
The NMR data are given in table 5.2.

5.2.1 ^{13}C spectra

The room temperature ^{13}C spectra for all three compounds contain two methyl signals

(figure 5.2.1) at comparable chemical shifts. Each has one signal between 1 ppm and

2 ppm, and a second signal at a higher frequency of between 4.0 ppm and 4.5 ppm. The

low-frequency signal in each case is at a similar chemical shift to those obtained

for the methyls of compound 1, all of which are bonded to tin atoms bound in the

lattice. It would therefore seem reasonable to assign the low-frequency signal in

each case to methyls bonded to tin atoms in the lattice. In each spectrum there is

only one such signal, which indicates only one type of chain in the lattice, unlike

the ^{13}C spectrum of compound 1, which distinguished two different chains. However,

the methyl signals for compounds 4, 5 and 6 are much broader than the signal for

compound 1, so any slight differences between the chains would not necessarily be

observed.

Logically, therefore, the second methyl signal in each spectrum would be due to the

fourth weakly co-ordinated trimethyl tin (see section 4.2). From this assignment the

relative intensities of the two signals would be expected to be 3:1, however, for all

three compounds it is close to 1:1. To investigate this discrepancy in intensity

ratios, spectra for all three compounds were obtained at elevated temperatures (see

section 5.2.4).

The two methyl signals are also much broader than those obtained for compound 1, with the satellites due to coupling only just visible. This broadening is possibly due to some type of exchange mechanism which has been investigated by low temperature NMR. The variable temperature spectra are discussed in section 5.2.4.

The only other signals in the three ^{13}C spectra are those due to the cyano groups (figure 5.2.2). Each spectrum contains a manifold of spinning-sidebands and a centreband, the position of which is shifted to a lower frequency as the metal atom is changed from Fe to Ru to Os. The carbon of the cyano group is directly bonded to the metal atom and so its environment is influenced by it. As this metal is changed from Fe to Ru to Os, the electron density around it increases, causing the carbon to be more shielded and hence the signal to be shifted to a lower frequency.

Each CN centreband is split into six lines in the approximate intensity ratio 2:1:2:1:2:1. The carbon of the cyano group is directly bonded to the metal atom and to nitrogen. Since the only spin-active nuclei of Fe, Ru and Os are of low abundance, no effect from these would be seen in the ^{13}C spectrum. Therefore any splitting of the signal can only be due to coupling of spin-1/2 ^{13}C to spin-1 ^{14}N. Coupling to one spin-1 nucleus would give three lines of equal intensity. However, due to quadrupolar effects, the three lines are all shifted, resulting in two lines in the intensity ratio 2:1 as discussed earlier (section 5.1.5). The centreband signal contains three such pairs of lines so it is concluded that there are three different environments for the CN groups.

A sample of 100% ^{15}N enriched [(Me$_3$Sn)$_4$Fe(CN)$_6$] was prepared to eliminate any splitting of the signal due to coupling of the ^{13}C to ^{14}N. The cyanide region of the ^{13}C spectrum contains only three signals in the centreband (178.9, 175.2 and 169.6 ppm) and in each spinning sideband (figure 5.2.2b) as expected, confirming that there are only three environments for the CN. The three signals are of almost equal intensity, with the central line in each case being slightly broader than the other two. ^{15}N enrichment had no effect on the methyl signals.

5.2.2 ^{119}Sn spectra

Similar conclusions can be drawn from the ^{119}Sn spectra to those from the ^{13}C. Each
compound gives a spectrum containing two centreband signals, separated by more than
120 ppm (figure 5.2.3), indicating two very different environments for the tin. The
low-frequency signal, in each case, occurs at a similar position to that obtained for
compound 1 and can therefore be assigned to the tin atoms in the three chains of the
lattice. The second, higher-frequency signal in each case would logically,
therefore, be assigned to the fourth weakly-bonded Me_3Sn group. From this assignment
it would be expected that the intensity ratio of the two signals for each compound
would be 3:1 but the ratios calculated from the spectra varied from 2.6:1, for the Fe
containing compound, to 1:1, for the Os compound. In order to investigate this a
single-pulse spectrum was acquired for $[(Me_3Sn)_4Fe(CN)_6]$, with a long relaxation
delay of 90 seconds, to allow the tin to fully relax before each pulse. This
resulted in a more accurate intensity ratio of 1:1. This experiment should in
principle be repeated for the Ru and Os containing compounds.

A ^{119}Sn spectrum was also obtained for the 100% ^{15}N-enriched sample, which contained
no apparent differences from the spectrum obtained from the natural abundance sample.

5.2.3 ^{15}N spectra

The nitrogen spectra of the Fe- and the Os- containing compounds are similar, each
containing three lines of approximately equal intensity (figure 5.2.4a). The
spectrum from the Ru- containing compound has a poor signal-to-noise ratio but three
signals are still observable. The signals are again shifted to lower frequencies as
the metal is changed from Fe to Ru to Os for the same reason as in the ^{13}C spectrum.
The appearance of three ^{15}N signals is in agreement with the CN region of the ^{13}C
spectrum, again indicating three different environments for the cyano groups.

A ^{15}N spectrum was also obtained of the 100% ^{15}N enriched sample (figure 5.2.4b). Because of the enrichment the signal-to-noise ratio of the spectrum is very good, enabling satellites to be seen due to the coupling of ^{15}N to ^{119}Sn for the two high frequency signals ($\delta = -109$ ppm, $J_{15N-119Sn} = 121$ Hz; $\delta = -124$ ppm, $J_{15N-119Sn} = 166$ Hz). The third signal is broader, as was seen in the cyanide region of the ^{13}C spectrum, which prevents the coupling from being seen. Any slight splitting of the spinning sidebands in figure 5.2.4b is due to unstable spinning.

5.2.4   Variable temperature studies

Variable temperature studies were carried out on the methyl region of the ^{13}C spectrum for the Fe, Ru and Os compounds over a range of temperatures from 51°C to $- 59^{\circ}$C. Figure 5.2.5 shows the spectra for the Ru compound. The other two compounds gave very similar results. At 51°C all three compounds gave two broad lines which were deconvoluted into two major signals and four low intensity satellites (figure 5.2.6), resulting in an intensity ratio for the two methyl environments of 1:1. The linewidths and coupling constants given in table 5.2 were obtained from these deconvoluted spectra.

As the temperature was lowered the methyl signals split into six lines of approximately equal intensity. The spectra also contain some lines of low intensity which are satellites due to the ^{13}C coupling to the ^{119}Sn. In both the high temperature methyl region of the ^{13}C spectrum, and the ^{119}Sn spectrum two signals are seen, indicating two different Me$_3$Sn groups; the three methyl groups attached to any one tin giving only one signal due to some form of exchange process. The six signals in the -37°C spectrum can therefore be divided into two groups of three, each group belonging to one of the room temperature signals. However it is not possible to distinguish which three signals should be grouped together. Sections 2.12 and 5.2.5 describe a two-dimensional spin-exchange experiment which overcomes this problem.

5.2.5   Two-dimensional spin-exchange experiment

The 2-D spin-exchange experiment as described in section 2.12 was used to investigate the methyl ^{13}C region of the compound $[(Me_3Sn)_4Fe(CN)_6]$. The experiment was run at a temperature of -26^oC using a mixing time of 0.5 s, recycle delay of 1 s, contact time of 1 ms, spin-rate of 2100 Hz and 198 transients. Figure 5.2.7 shows the result of this experiment as a contour plot and also the -37^oC and $+51^oC$ spectra obtained using an ordinary cross-polarisation experiment for comparison. The 2-D plot is symmetrical about the diagonal and the ordinary CP spectrum can be seen if the diagonal is projected along either axis. There are quite clearly six cross-peaks, each indicating an exchange process. Using the numbering scheme as in figure 5.2.7, these cross-peaks correspond to exchange processes between carbons 1 and 3, 1 and 5, 3 and 5, 2 and 4, 6 and 2, and 4 and 6. It is clear that the exchange processes are between two independent groups of three carbons, these two groups giving signals 1,3 and 5, and 2, 4 and 6. The 2-D experiment proves that the methyls around one tin atom undergo exchange with each other, on a timescale of approximately 0.5 s, but that there is no exchange between the two groups. The 2-D spectrum also resolved the signals from carbons 4 and 5 which overlapped in the CP spectrum obtained at -37^oC.

The transition from slow to fast exchange takes place at the coalescence temperature which in the case of $[(Me_3Sn)_4Fe(CN)_6]$ is approximately 7^oC. The exchange rate, k, at this temperature can be calculated using the following equation[31].

$$k = \frac{\pi \; \Delta v}{\sqrt{2}}$$

Δv is the separation of the two signals during slow exchange. The case of $[(Me_3Sn)_4Fe(CN)_6]$ is obviously more complicated since during slow exchange there are three signals and not two. If an average Δv is calculated for each group of three signals then an approximate exchange rate can also be calculated.

Signals 1,3,5   average Δv = 382 Hz   k = 848 Hz

Signals 2,4,6   average Δv = 317 Hz   k = 703 Hz

5.2.6 Proposal of a different structure for [(Me$_3$Sn)$_4$Fe(CN)$_6$]

Both the methyl region of the 51°C ^{13}C spectrum and the room temperature ^{119}Sn spectrum of [(Me$_3$Sn)$_4$Fe(CN)$_6$] suggest an equal number of two crystallographically different trimethyl tin groups. The initial structure proposed in section 4.2 does contain two crystallographically different trimethyl tin groups but they would be in the ratio 3:1. Therefore a different structure is suggested containing two chains of type A and one of type B.

Chain A $-\overset{|}{\underset{/}{Fe}}-C-N-\overset{\backslash/}{\underset{|}{Sn}}-N-C-\overset{|}{\underset{/}{Fe}}-$

Chain B $-\overset{|}{\underset{/}{Fe}}-C-N\overset{\overset{\backslash/}{Sn}}{\underset{\underset{/}{Sn}}{}}N-C-\overset{|}{\underset{/}{Fe}}-$
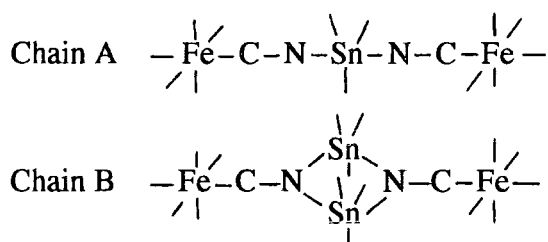
Chain A is similar to those chains of the Co containing compounds (1,2 and 3) but chain B contains Me$_3$Sn units in somewhat different chemical situations, the N atom becoming three-coordinate as opposed to two-coordinate in chain A. A 3-D lattice comprised of two chains of type A and one of type B would contain an equal number of each Me$_3$Sn environment. The observed ion-exchange reaction, as desribed in 4.2, is still possible. One of the Me$_3$Sn units can easily be removed from chain B leaving a chain similar to A and hence no further ion-exchange could take place.

The signals in the ^{13}C and ^{119}Sn spectra can therefore be reassigned as follows.

^{13}C	1.0 ppm	Chain A
	4.4 ppm	Chain B
^{119}Sn	-108 ppm	Chain A
	46 ppm	Chain B

The CN region of the ^{13}C spectrum of the 100% ^{15}N enriched sample contains three signals, one of which is broader than the other two. The broader signal can probably be assigned to the carbon attached to the three-coordinate nitrogen of chain B, since motion within this chain will be restricted.

Since compounds 5 and 6 give very similar ^{13}C and ^{119}Sn spectra to 4 it is suggested that their structures will be similar.

The ^{15}N spectra for all three compounds each contain two signals relatively close together and a third signal shifted substantially to a lower frequency. The spectrum of the ^{15}N-enriched sample also showed this low-frequency signal to be broader than the other two. Since in general it is known that an increase in co-ordination number causes a shift to lower frequency the third signal can probably be assigned to the 3-coordinate N of chain B. The increased coordination would also restrict any motion within the chain, broadening the signal. The two higher-frequency signals can therefore be assigned to the 2-coordinate N of the chains of type A. The fact that there are two signals implies that the CN groups of chain A are not equivalent.

The only snag with the present proposal is that methyl exchange in chain B would be expected to be more hindered than for chain A, since in the former the methyls could not all be equatorial. However, 'facial' exchange of an axial and two equatorial methyls is not impossible.

The ^{13}C, ^{119}Sn and ^{15}N NMR data for all three compounds appear now to be consistent with the second proposed structure.
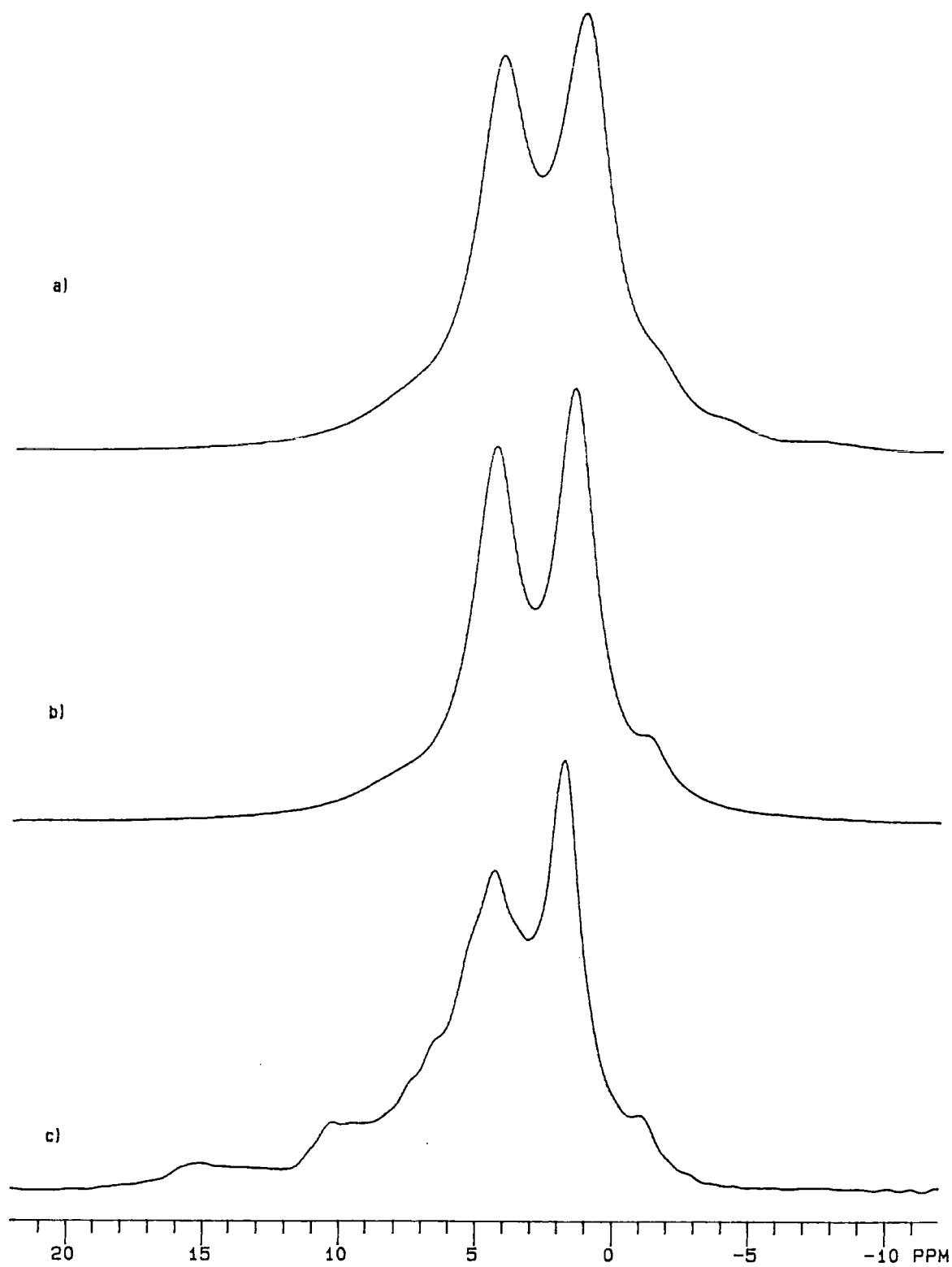
Figure 5.2.1   Methyl region form the room temperature ^{13}C spectrum of
a) $[(Me_3Sn)_4Fe(CN)_6]$ b) $[(Me_3Sn)_4Ru(CN)_6]$ and
c) $[(Me_3Sn)_4Os(CN)_6]$
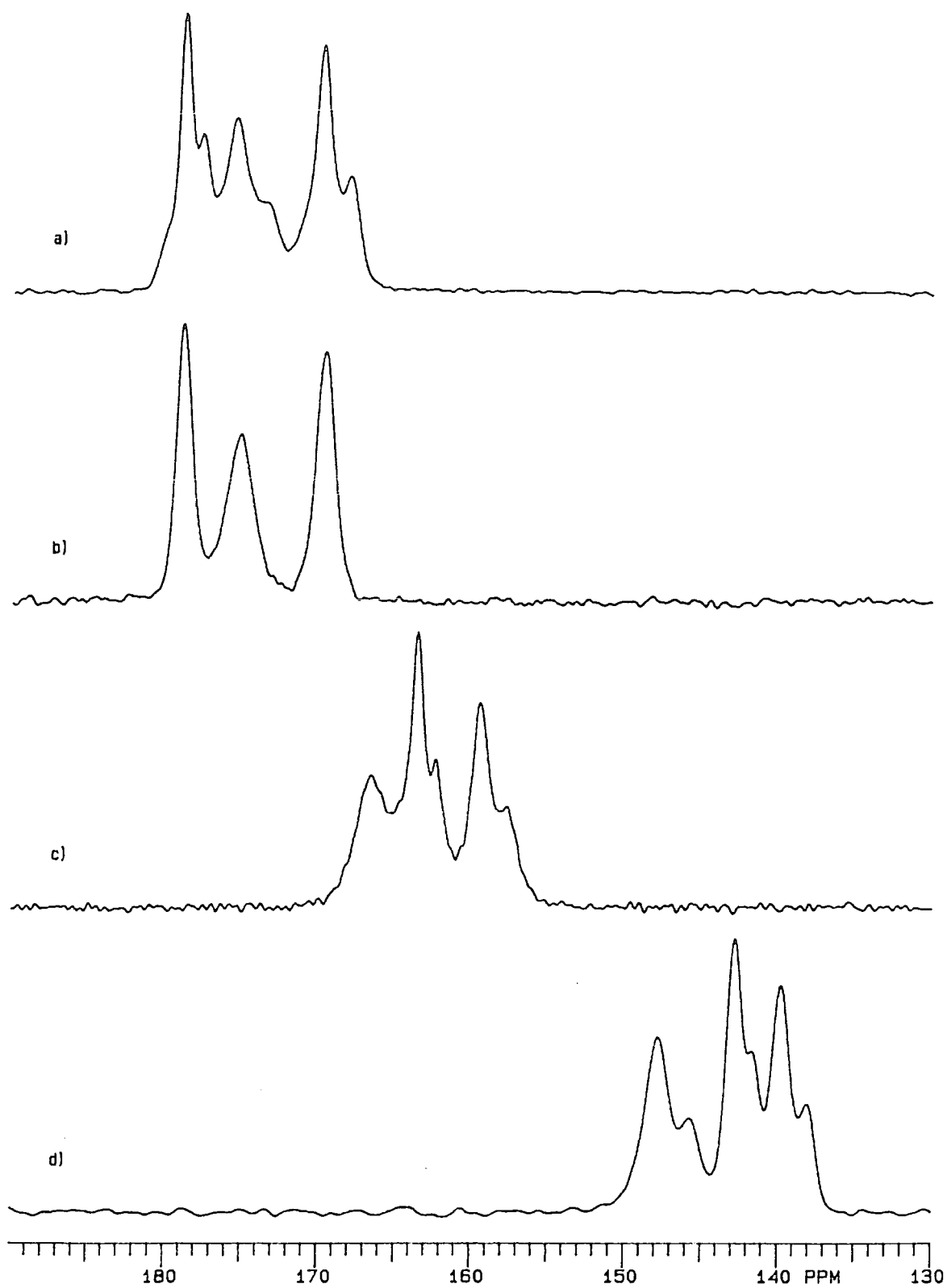
Figure 5.2.2   CN centreband from ^{13}C spectrum of a) $[(Me_3Sn)_4Fe(CN)_6]$
b) 100% ^{15}N enriched $[(Me_3Sn)_4Fe(CN)_6]$
c) $[(Me_3Sn)_4Ru(CN)_6]$ and d) $[(Me_3Sn)_4Os(CN)_6]$

105
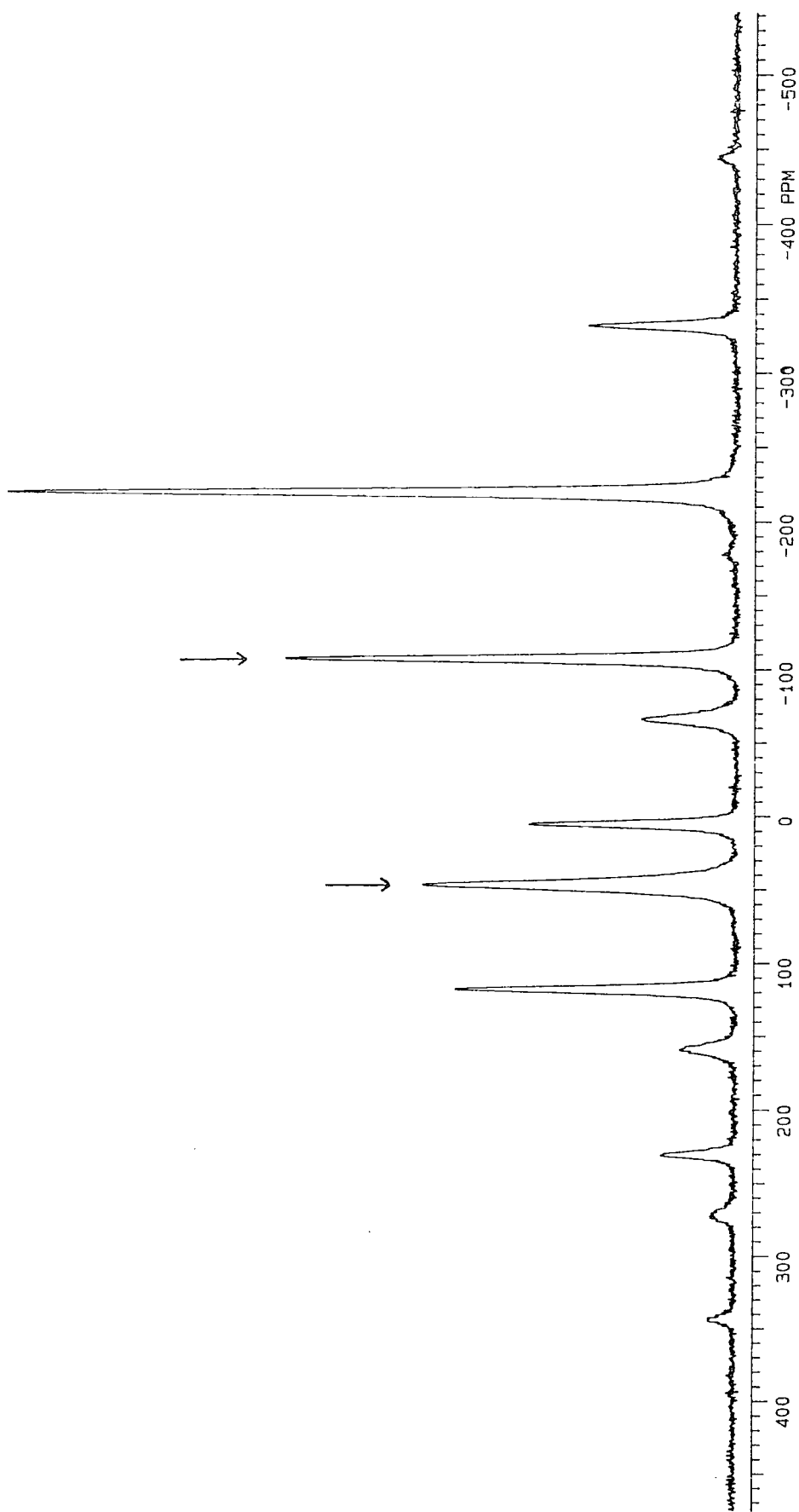
Figure 5.2.3 ^{119}Sn spectrum of $[(Me_3Sn)_4Fe(CN)_6]$
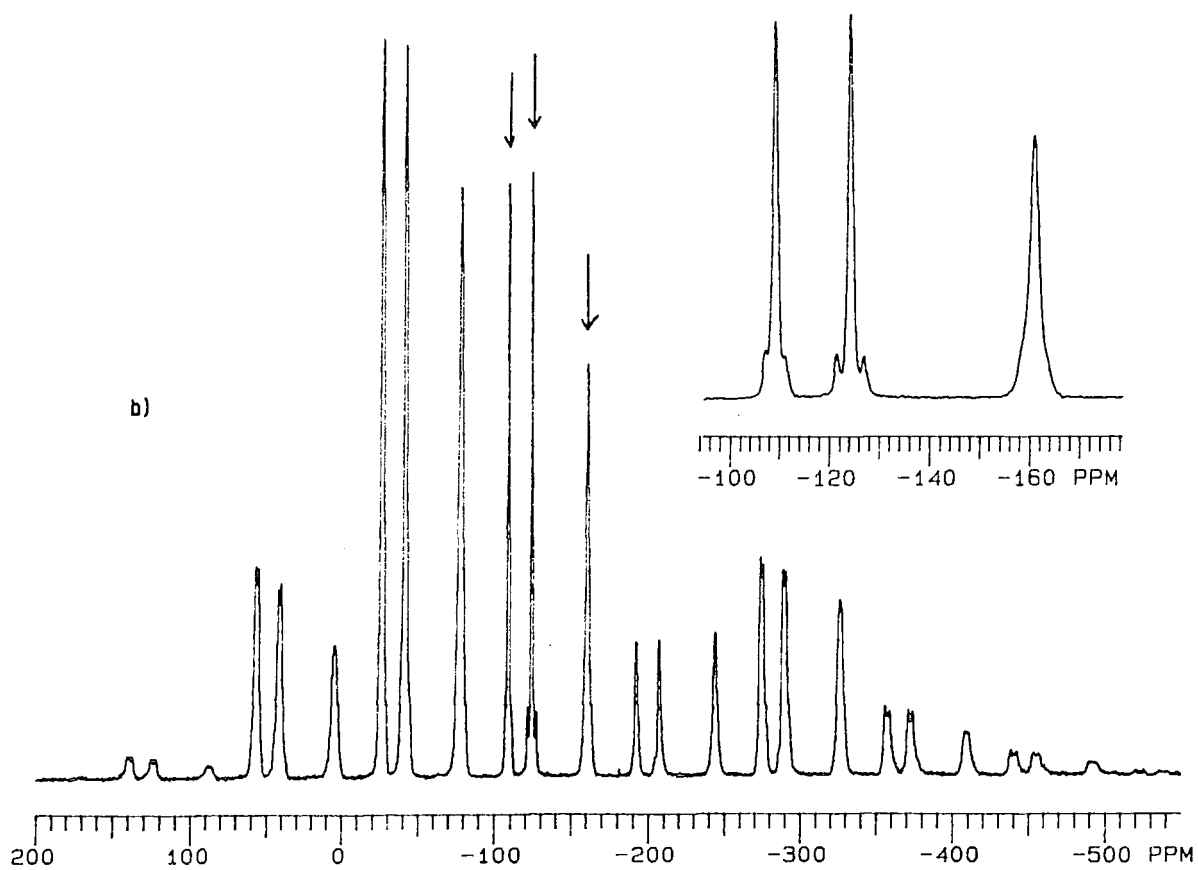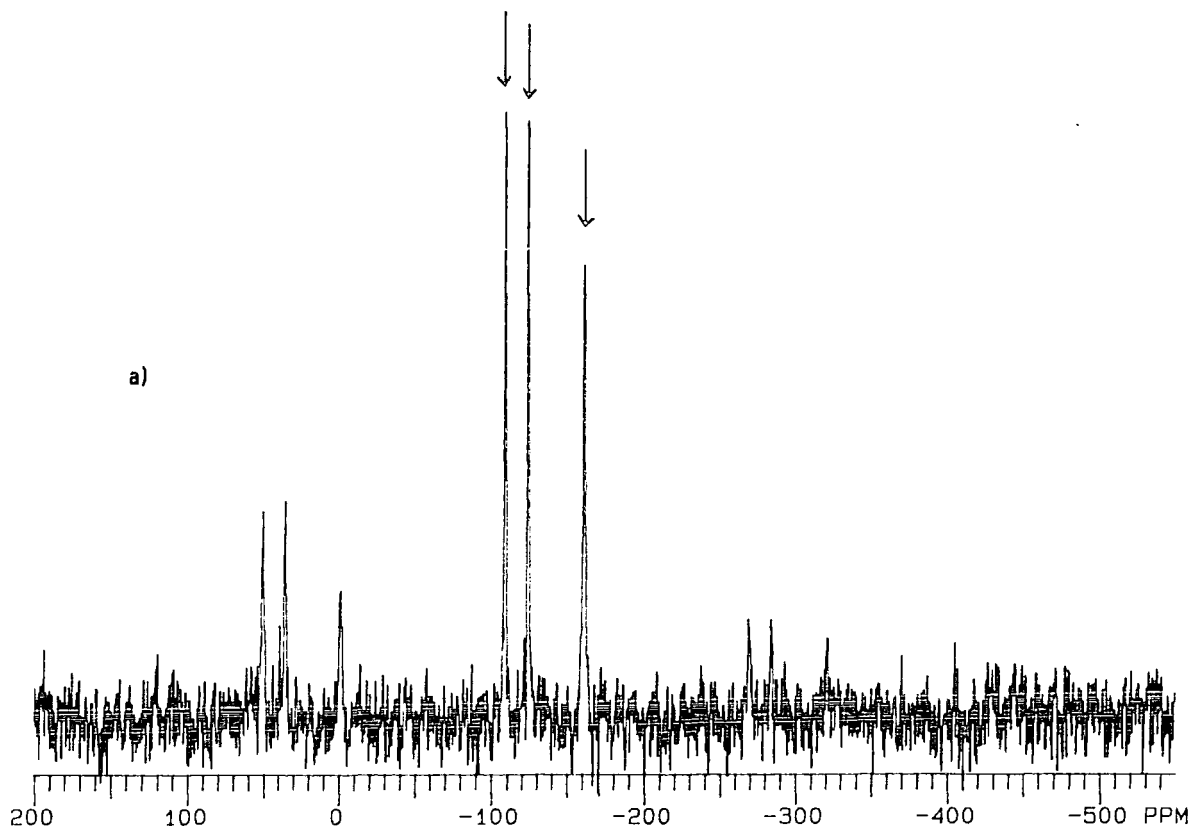
Figure 5.2.4 ^{15}N spectrum of $[(Me_3Sn)_4Fe(CN)_6]$ at a) natural abundance
and b) 100% ^{15}N enriched

107
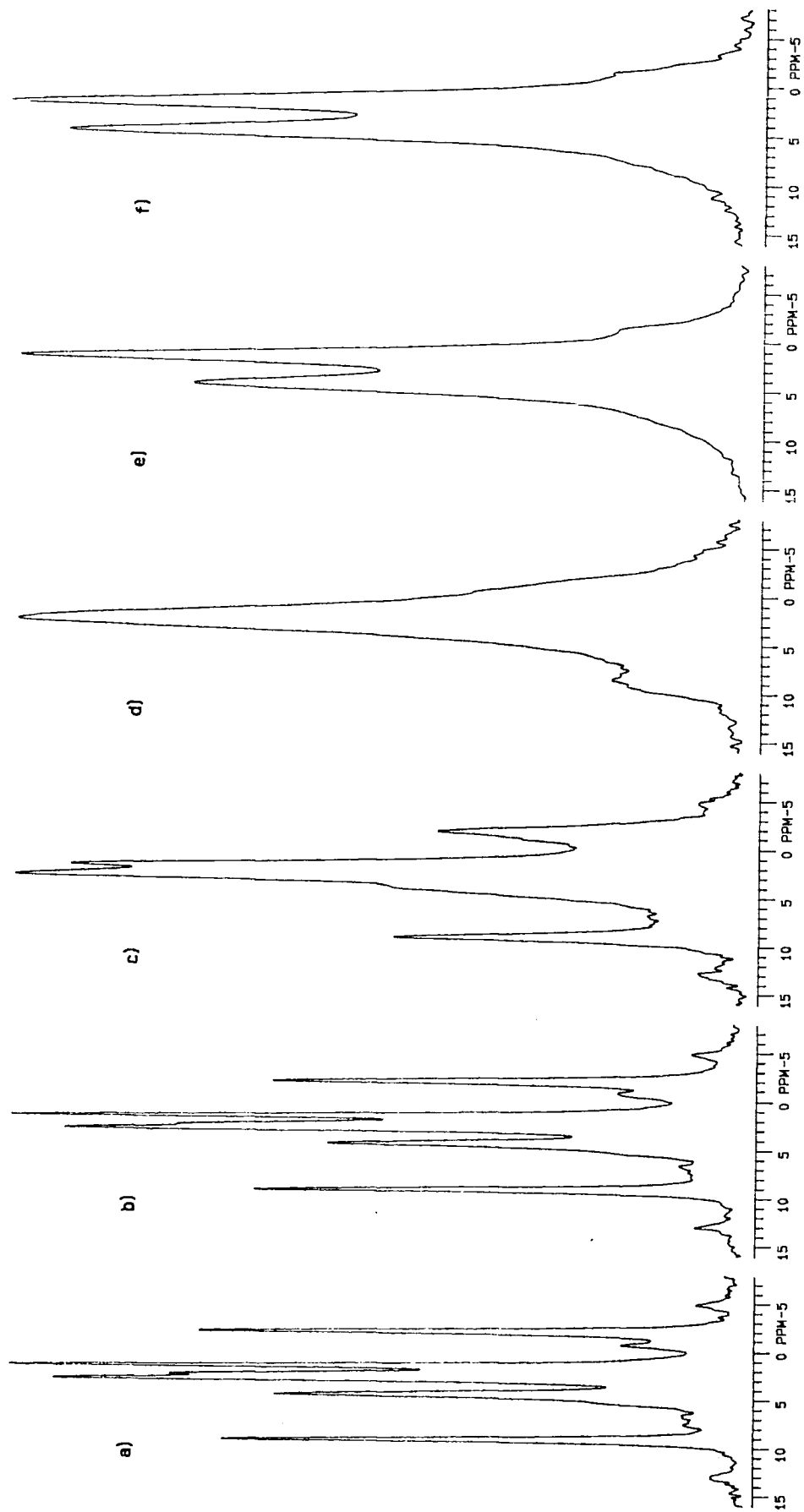
Figure 5.2.5   Variable temperature ^{13}C spectra of the methyl region of [(Me$_3$Sn)$_4$Ru(CN)$_6$] at a) −59 b) −37 c) −15 d) 7 e) 31 and f) 51°C

108
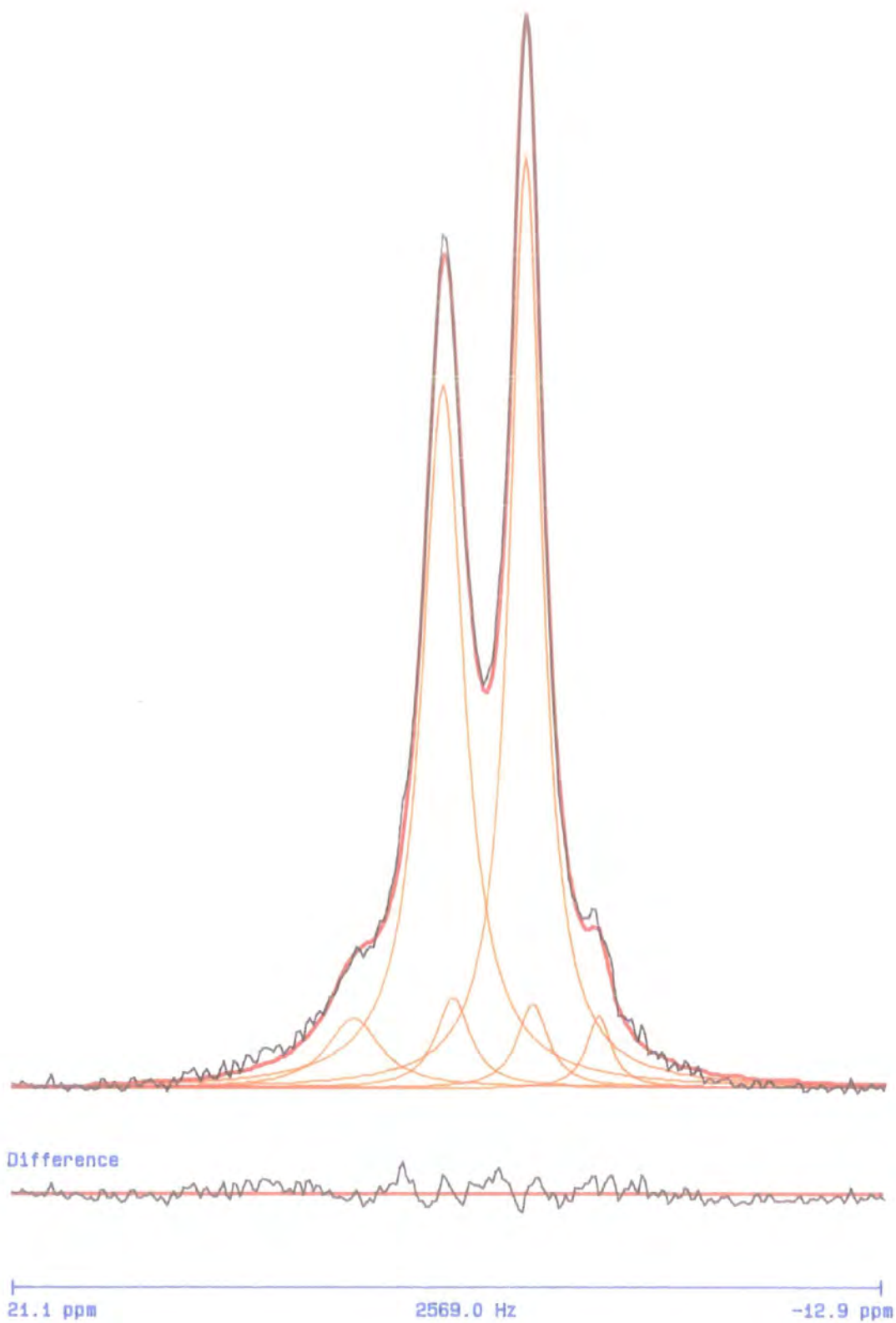
Figure 5.2.6   Deconvolution of the methyl region from the 51°C 13C spectrum of [(Me3Sn)4Fe(CN)6]

109
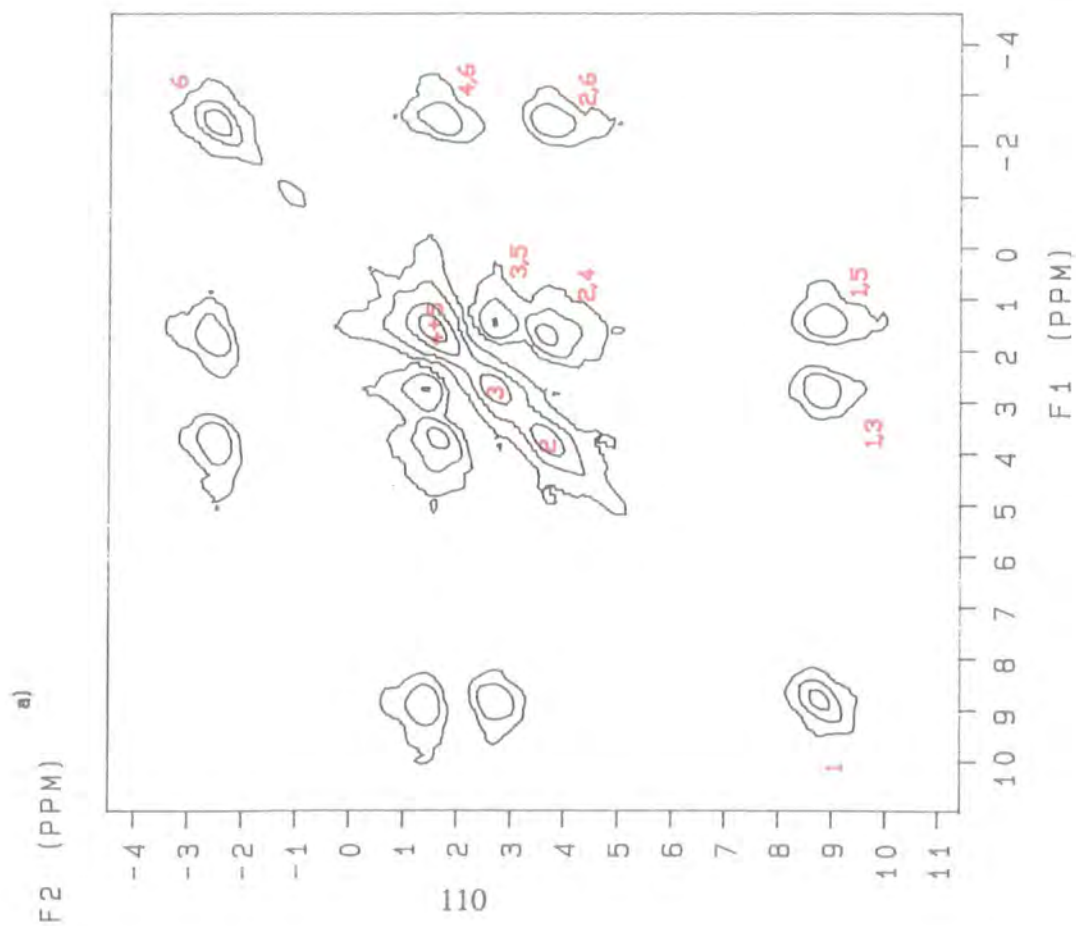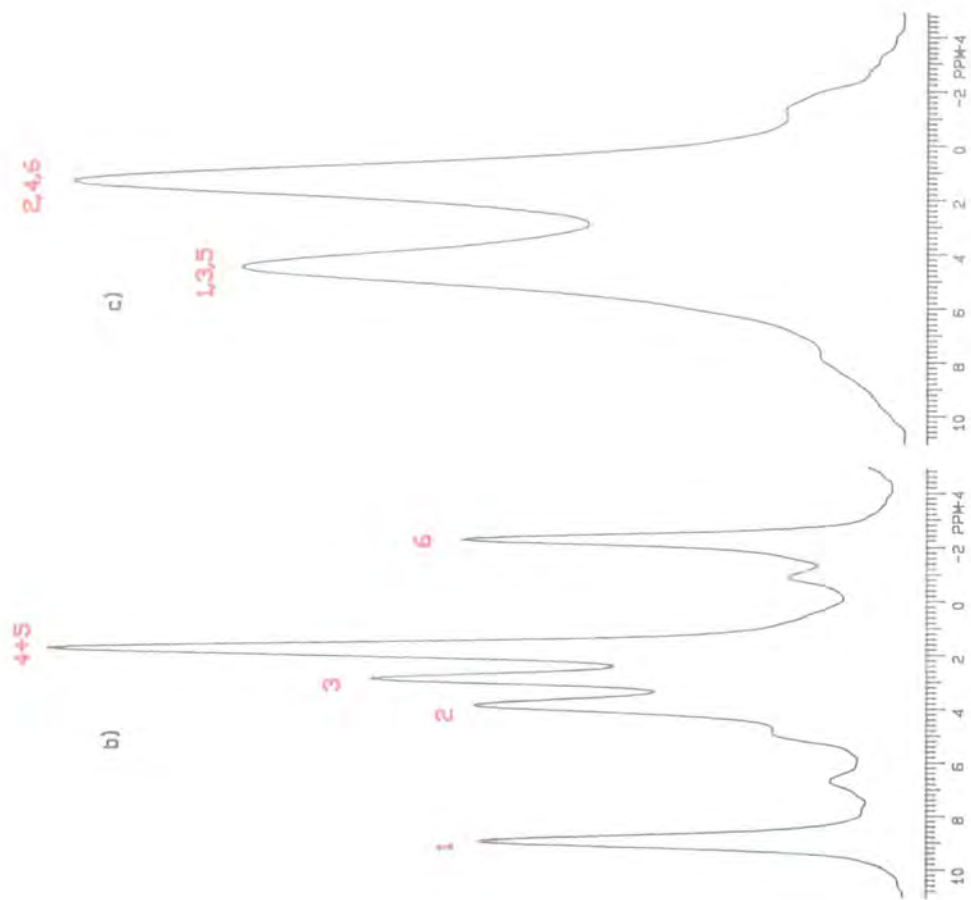
Figure 5.2.7   Spectra of $[(Me_3Sn)_4Fe(CN)_6]$ from a) 2-D spin-exchange experiment b) CPMAS at $-37°C$ and c) CPMAS at $51°C$

110

Table 5.2   NMR data for **4**, **5** and **6**

<div style="text-align:center">

4 $[(Me_3Sn)_4Fe(CN)_6]$

5 $[(Me_3Sn)_4Ru(CN)_6]$

6 $[(Me_3Sn)_4Os(CN)_6]$

</div>
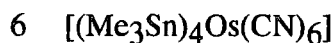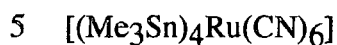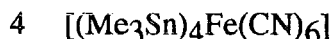
	δ/ppm	I_{rel}	J/Hz	$\Delta\upsilon_{1/2}$/Hz	assignment
^{13}C					
4	1.0	1.0	430	118	CH_3
	4.2	1.0	550	152	CH_3
	175[a]				CN
5	1.4	1.1	415	137	CH_3
	4.3	1.0	410	155	CH_3
	163[a]				CN
6	1.8	1.0	440	129	CH_3
	4.4	1.2	560	180	CH_3
	140[a]				CN
^{119}Sn					
4	–108	2.6[f] 1.0[g]		600	Chain A
	46	1.0[f] 1.0[g]		930	Chain B
5	–97	2.1		550	Chain A
	32	1.0		1020	Chain B
6	–94	1.1		460	Chain A
	26	1.0		790	Chain B
^{15}N					
4	–161	1		43	Chain B
	–124	1		28	Chain A
	–109	1		23	Chain A
5	–165	1			Chain B
	–136	1			Chain A
	–118	1			Chain A
6	–171	1		72	Chain B
	–144	1		38	Chain A
	–126	1		42	Chain A

[a]   multiplet, therefore only approximate δ

[f]   ratio calculated from CP experiment

[g]   ratio calculated from SP experiment

5.3 Derivatives of $[(Me_3Sn)_4Fe(CN)_6)]$

7    $[(Me_3Sn)_4Fe(CN)_6).C_4H_8O_2/H_2O]$

8    $[(Me_3Sn)_4Fe(CN)_6).2H_2O]$

9    $[(Me_3Sn)_4Fe(CN)_6).D(+)glucose]$

The NMR data for these three compounds are given in table 5.3.

5.3.1 ^{13}C Spectrum of $[(Me_3Sn)_4Fe(CN)_6.C_4H_8O_2/H_2O]$

The methyl region of the ^{13}C spectrum of compound 7 contains two signals, with coupling of the carbon of the methyl to tin seen as satellite peaks (figure 5.3.1). The X-ray crystal structure indicates two different types of chains, A and B, (section 4.3) so it would be expected for the ^{13}C NMR spectrum to indicate two different environments for the methyls, as is the case. Even though there are twice as many chains of type A as there are B, chain B contains two trimethyl tin units between each pair of Fe atoms, whereas chain A contains only one. Consequently there are equal numbers of each of the two different methyl environments, which should lead to two signals of equal intensity. When this compound was first looked at using a cross-polarisation experiment the intensity ratio of the two methyls was 1:2.2. Since this does not agree with the crystallographic data a single-pulse spectrum was also obtained, using a recycle time of 60 seconds to ensure the methyls were fully relaxed. This gave an improved intensity ratio of 1:1.3. It is assumed that the correct ratio is 1:1.

If the chemical shifts of the methyl signals are compared to those obtained for compound 4, both of the signals from 7 appear close to the low-frequency signal obtained for 4 (section 5.2.6). The A type chains in compound 7 are similar to the A type chains of 4, so the signal closest to that obtained for 1 at 0.9 ppm could be assigned to chain A and the signal at 2.2 ppm to methyls in chain B (which contains the dioxane molecules). The different methyls around one tin atom are again not distinguishable by NMR, presumably due to exchange processes as described earlier.

112

The remainder of the ^{13}C spectrum for 7 contains a signal at 67.5 ppm due to the four equivalent carbon atoms of the dioxane. Since there is only one signal, this also indicates that all the dioxane molecules within chain B are equivalent, as predicted by the crystal structure.

The only other signals in the spectrum are due to the carbon of the CN groups (figure 5.3.2). There is a centreband at approximately 172 ppm which is split into six signals in three groups of two in the approximate intensity ratio 2:1:2:1:2:1. This is the same pattern as was seen for $[(Me_3Sn)_4Fe(CN)_6]$ and is at a similar chemical shift, indicating three different environments for the cyanides, the splittings being caused by coupling of ^{13}C to ^{14}N (section 5.1.5). This is in agreement with crystallographic data, which predicts one environment for CN in chain B and two different environments in chain A.

5.3.2 ^{119}Sn spectrum of $[(Me_3Sn)_4Fe(CN)_6.C_4H_8O_2/H_2O]$

The tin spectrum clearly shows two different tin signals with an intensity ratio of 1:1 (figure 5.3.3), indicating an equal number of two crystallographically different environments. This is consistent with the crystallographic data, which indicate an equal number of tin atoms in the two different environments of chain A and chain B. The two signals are separated by 63 ppm showing that the two environments are quite different. The tin atom in chain B is directly bonded to an oxygen atom which will draw electron density away from the tin atom, deshielding it and causing it to resonate at a higher frequency. Therefore the high-frequency signal at -73 ppm can probably be assigned to the tin atoms of chain B and the signal at -136 ppm to the tin atoms of chain A. This assignment would also be in agreement with that given for 4, where the low-frequency signal at -108 ppm was assigned to the tin atoms in chain A (which are in a similar environment to those in chain A of compound 7).

5.3.3 ^{15}N spectrum of $[(Me_3Sn)_4Fe(CN)_6 \cdot C_4H_8O_2/H_2O]$

The ^{15}N spectrum of 7 (figure 5.3.4) contains two signals in the ratio 2:1 indicating two environments with twice as many nitrogens in one as the other. The signal of double intensity at −116 ppm must be from the nitrogens of chain A since there are twice as many of these and therefore the other signal can be assigned to the nitrogen in chain B. It is interesting to note that the ^{15}N NMR spectrum does not distinguish the two different CN groups of chain A as the ^{13}C spectrum did. This implies that the two nitrogen environments in the CN of chain A are much more alike than the two carbon environments.

The ^{15}N spectrum contains no low-frequency signal at −161 ppm as was the case for 4. This confirms the assignment of this signal to a postulated 3 co-ordinate nitrogen of chain B since the structure of 7 does not contain such an environment.

To conclude, the NMR data is consistent with the crystallographic data. Also in comparing the structures of compounds 4 and 7, it can be seen that they both contain similar A-type chains but very different B-type chains. This is as expected by comparing the known structure of 7 with the proposed structure of 4.

5.3.4 ^{13}C spectra for 8 and 9

The methyl regions of the carbon spectra for 8 and 9 are similar (figure 5.3.5), containing only one major peak at 1.6 ppm, with satellites due to coupling of the carbon of the methyl to the tin ($J_{(13C-119Sn)}$ = 565 Hz). However, both also have a much broader signal underneath the major peak, suggesting a second methyl environment different from the first.

The centreband signal for the carbon in the CN groups (figure 5.3.6), for both compounds 8 and 9, appears at approximately the same frequency (175 ppm) which is also at a similar position to that obtained for compounds 4 and 7. The signals are

split into complicated patterns, partly due to to coupling to the ^{14}N, but here there is even more complication indicating more than three crystallographically different environments for the CN.

The spectrum of 9 also clearly shows six signals of approximately equal intensity due to the six carbons of D(+)glucose (figure 5.3.5). The glucose must be in cyclic form since there is no high-frequency peak, between 195 and 205 ppm as would be expected from the carbonyl of a straight chain glucose[32]. A solution-state assignment of D(+)glucose[33] allows the following assignments to be made.

92.8 ppm C6
72.9 ppm ⎫
71.8 ppm ⎬ C2,3,4,5
70.9 ppm ⎪
69.9 ppm ⎭
60.7 ppm C1
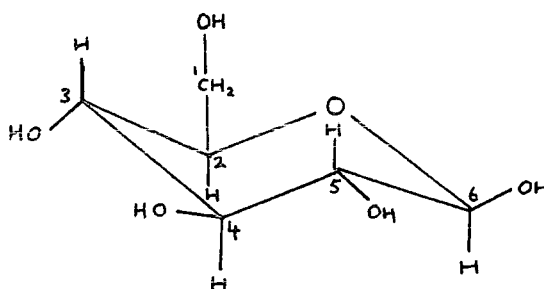
5.3.5 ^{119}Sn spectra for 8 and 9

The first tin spectra obtained for compounds 8 and 9 (figures 5.3.7a and 5.3.8a) each contained three overlapping spinning-sideband manifolds, indicating three tin environments. However, when the second spin-rates were recorded, in order to establish the centrebands, a fourth tin species became apparent (figures 5.3.7b and 5.3.8b). The centreband positions of the four species are similar for the two compounds (table 5.3). Each contains centrebands at approximately -107 and 47 ppm which are very similar to those of compound 4. The structures of 8 and 9 can therefore be predicted to contain two tin environments similar to those in 4 with the following assignments.

Chain A $-$ C$-$N$-$Sn$-$N$-$C $-$ -107 ppm

Chain B $-$ C$-$N   N$-$C $-$ 47 ppm
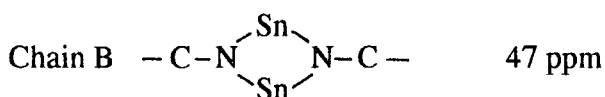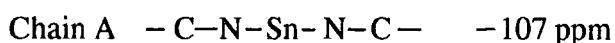
The tin environment in 8 at -29 ppm probably involves bonding to the H_2O molecule.

$$\text{Chain C} \quad \text{C}-\text{N}-\text{Sn}-\text{O}\begin{smallmatrix} \nearrow \text{H} \\ \searrow \text{H} \end{smallmatrix} \quad -29 \text{ ppm}$$
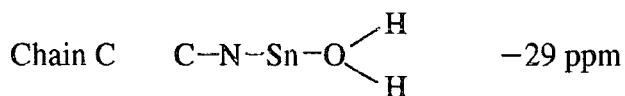
The oxygen is directly bonded to the tin which draws electron density away from ^{119}Sn, deshielding it, and causing it to resonate at a higher frequency than the tin in chain A.

The centreband at a similar position in 9 (-30 ppm) is most likely due to tin bonded to the most exposed oxygen of the glucose molecule.

$$\text{Chain C} \quad \text{C}-\text{N}-\text{Sn}-\text{O}\overset{\nearrow \text{H}}{\underset{\underset{\text{CH}_2}{|}}{|}}$$
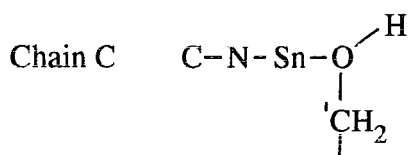
The fourth centreband in each (-138 ppm) case could be another chain of type A although this is unlikely since it is shifted by 30 ppm to a lower frequency. Alternatively this fourth signal could be an impurity.

The relative intensities of the SSB manifolds were obtained from the first spin-rate spectrum and are given in table 5.3. Since the manifolds for the signals at -29 and -138 ppm are overlapping the intensity given is a total for both of these environments. The most intense signal for compound 8 is at 47 ppm (chain B) and for compound 9 is at -107 ppm (chain A).

5.3.6 ^{15}N spectra for 8 and 9

The ^{15}N spectra for both compound 8 and 9 (figure 5.3.9) are very similar each containing three main signals indicating three different environments for the nitrogen of the CN. Two of the signals (-124 ppm and -109 ppm) are comparable to those obtained for 7 (-125 ppm and -116 ppm), but the third signal is at a lower frequency (-161 ppm), indicating some sort of shielding effect.

All three signals are very similar to those obtained for 4 and so the same assignments can be made. The low-frequency signal (-161 ppm) to the three co-ordinate nitrogen of chain B and the other two signals to the two co-ordinate nitrogens of chain A and C.

The NMR data for 8 and 9 indicate many similarities between the two compounds as expected from their chemical formulae. However their structures are obviously quite different from that of 7 and contain the doubly bridged chain and three-coordinate nitrogen characteristic of compound 4.
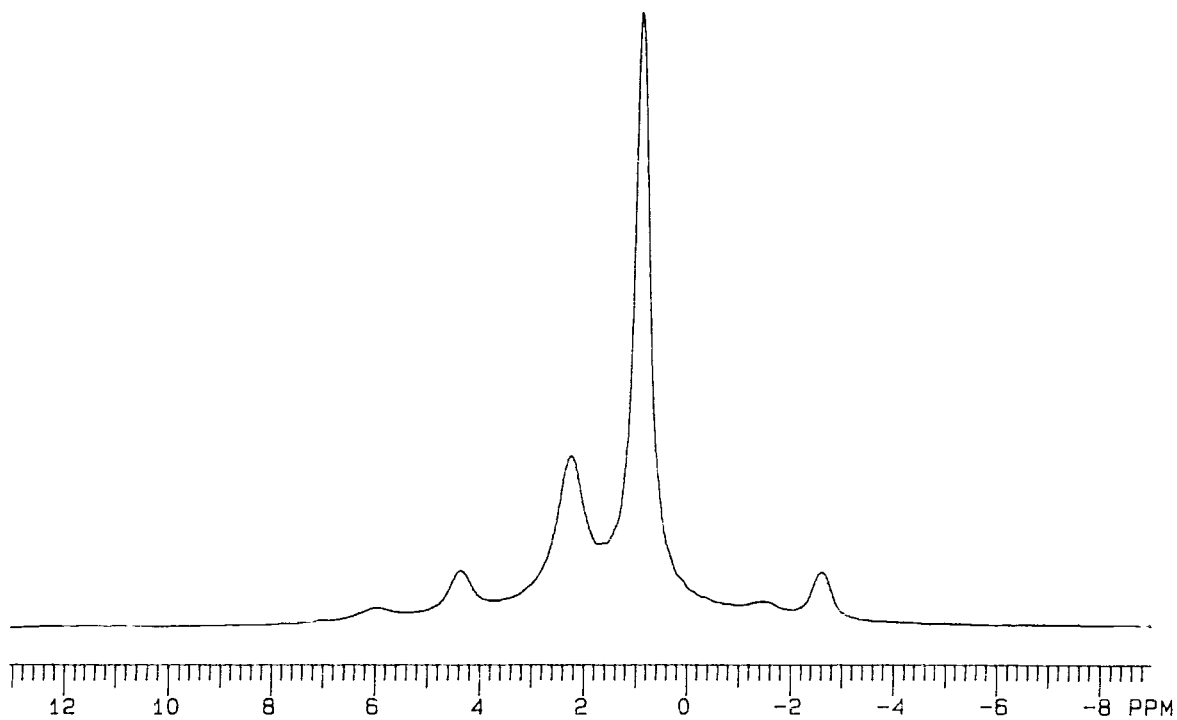
Figure 5.3.1   Methyl region from ^{13}C spectrum of [(Me$_3$Sn)$_4$Fe(CN)$_6$·C$_4$H$_8$O$_2$/H$_2$O]
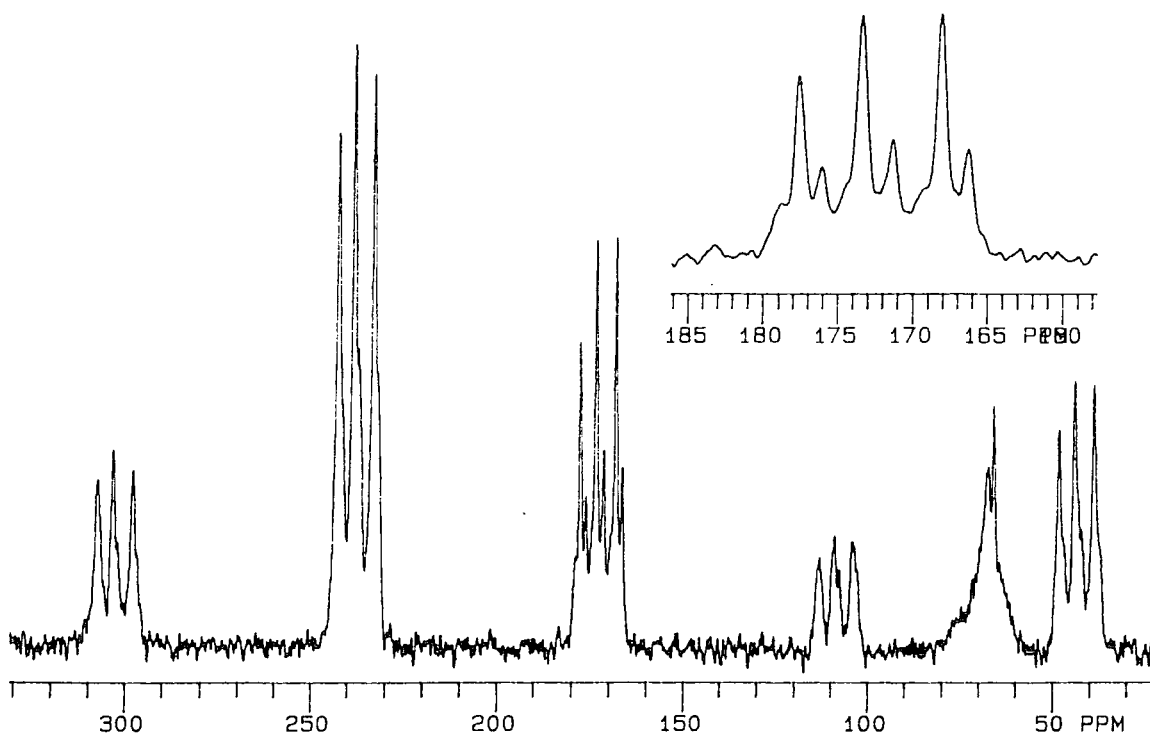
Figure 5.3.2   CN region from ^{13}C spectrum of [(Me$_3$Sn)$_4$Fe(CN)$_6$·C$_4$H$_8$O$_2$/H$_2$O] and an expansion of the centreband
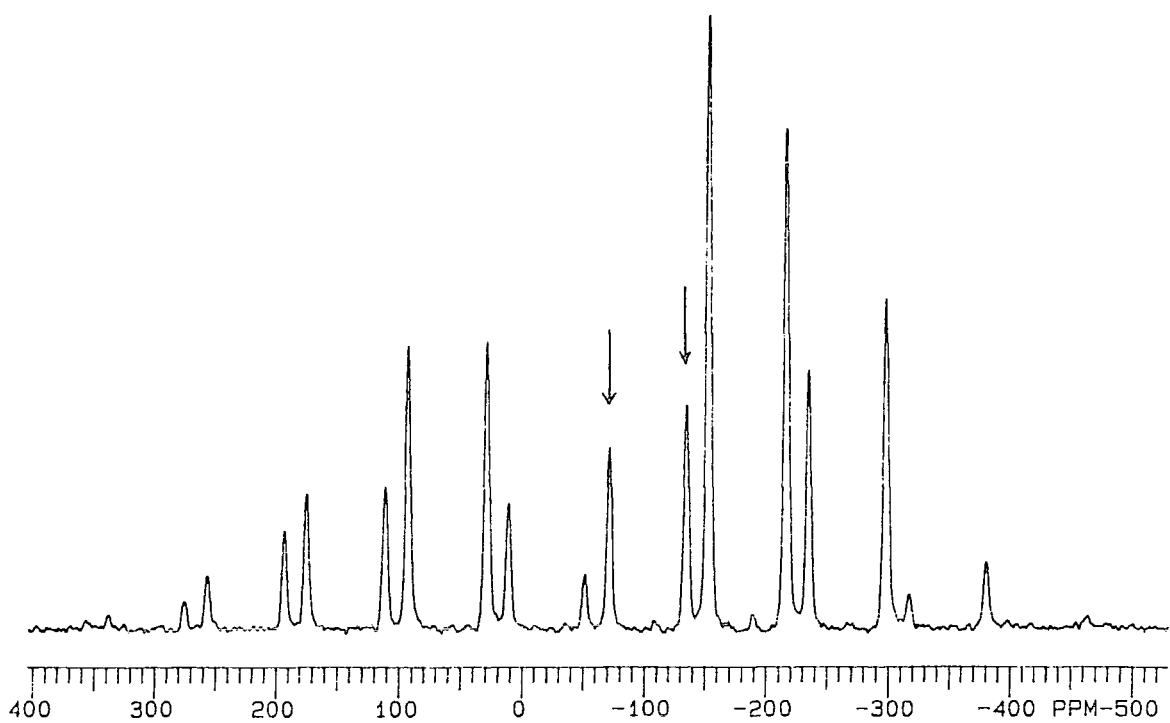
Figure 5.3.3 ^{119}Sn spectrum of $[(Me_3Sn)_4Fe(CN)_6 \cdot C_4H_8O_2/H_2O]$
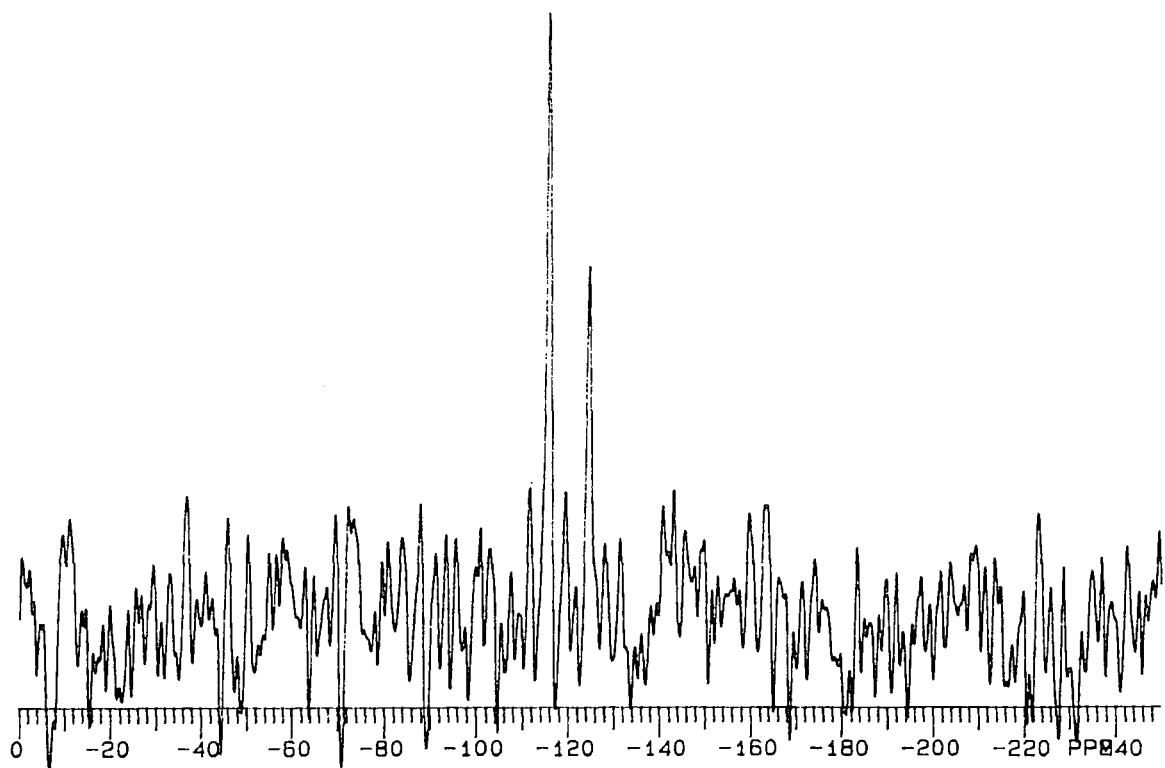
Figure 5.3.4 ^{15}N spectrum of $[(Me_3Sn)_4Fe(CN)_6 \cdot C_4H_8O_2/H_2O]$
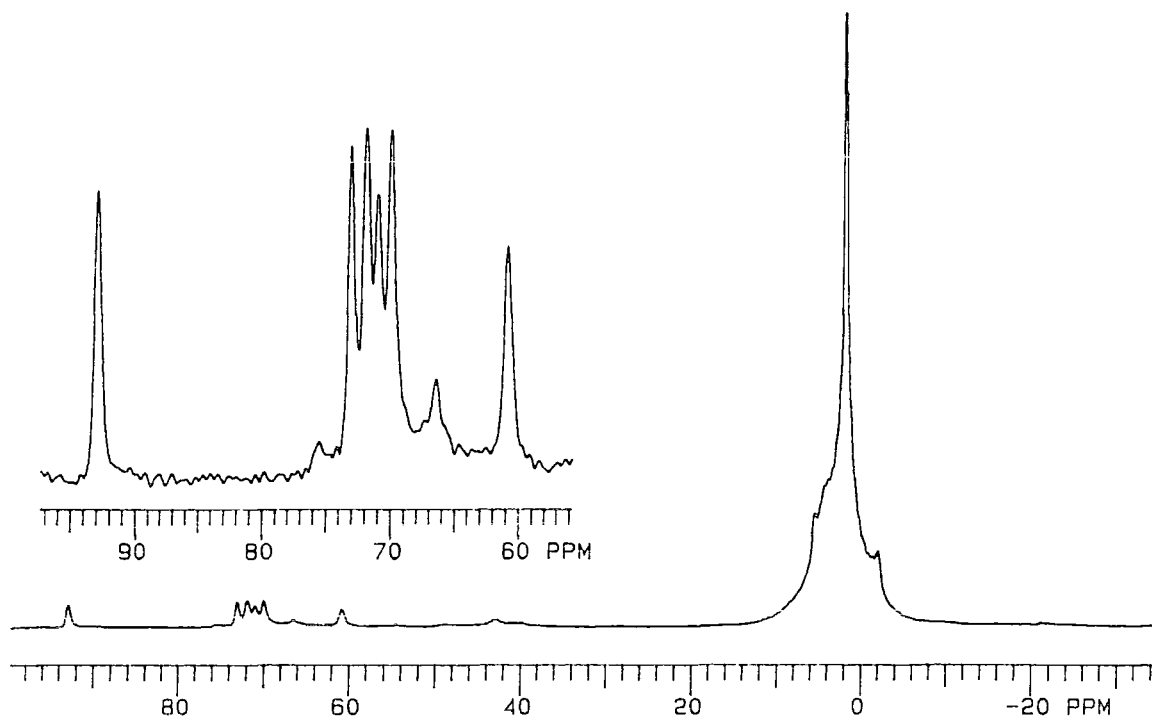
Figure 5.3.5   Low frequency region of ^{13}C spectrum of $[(Me_3Sn)_4Fe(CN)_6.2H_2O]$
and an expansion of the D(+)glucose signals
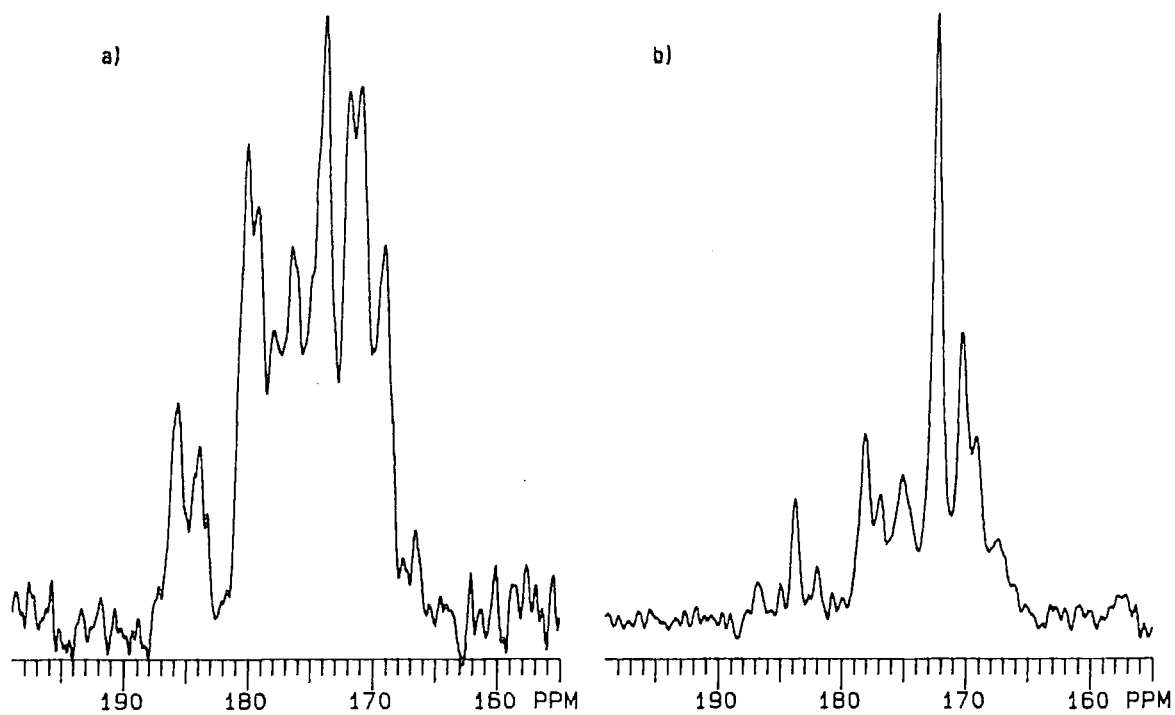
Figure 5.3.6   CN centreband from the ^{13}C spectrum of a) $[(Me_3Sn)_4Fe(CN)_6.2H_2O]$
b) $[(Me_3Sn)_4Fe(CN)_6.D(+)glucose]$
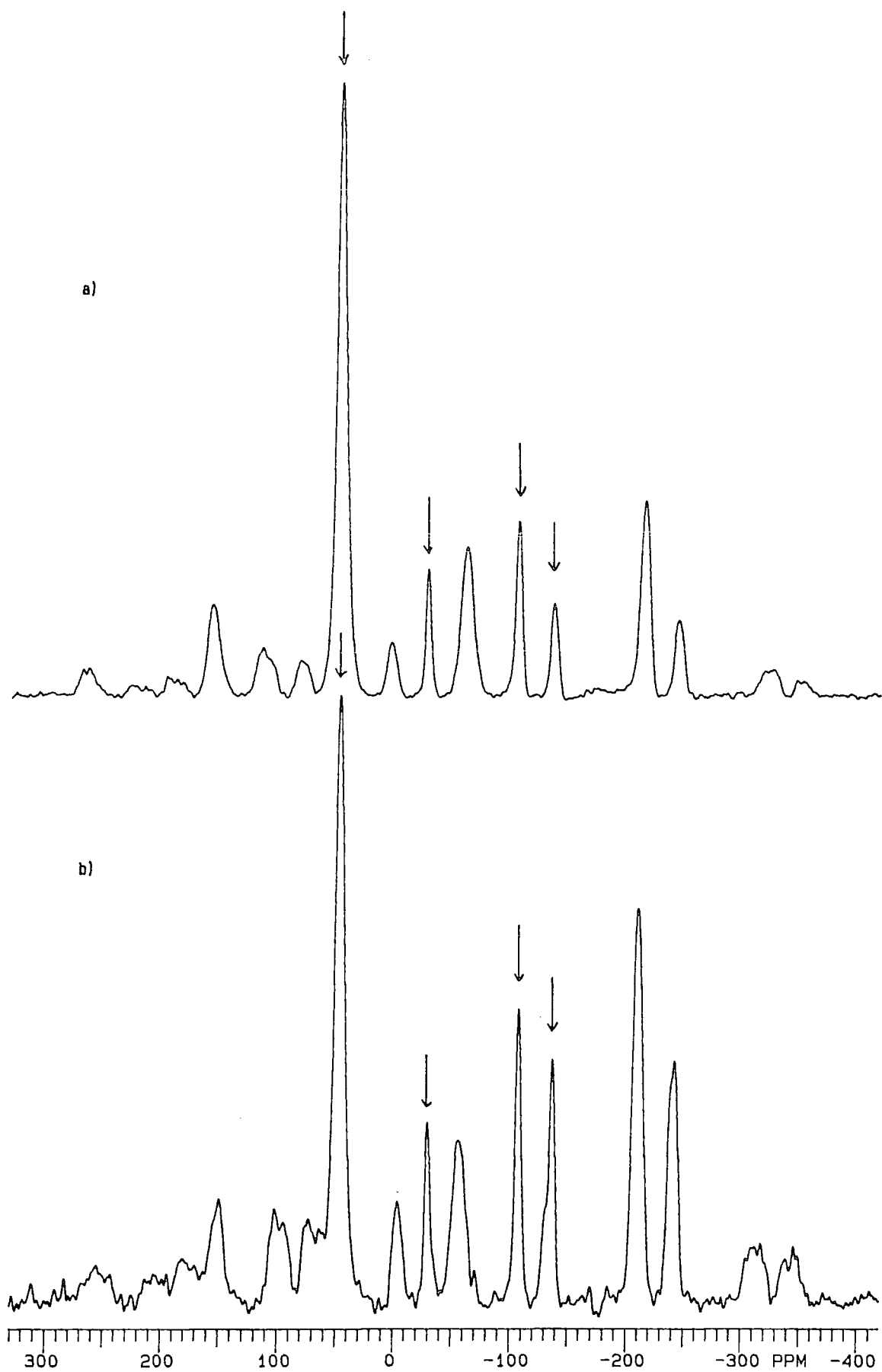
Figure 5.3.7 ^{119}Sn spectra of [$(Me_3Sn)_4Fe(CN)_6 \cdot 2H_2O$] at spin-rates of a) 12650 Hz
and b) 12000 Hz
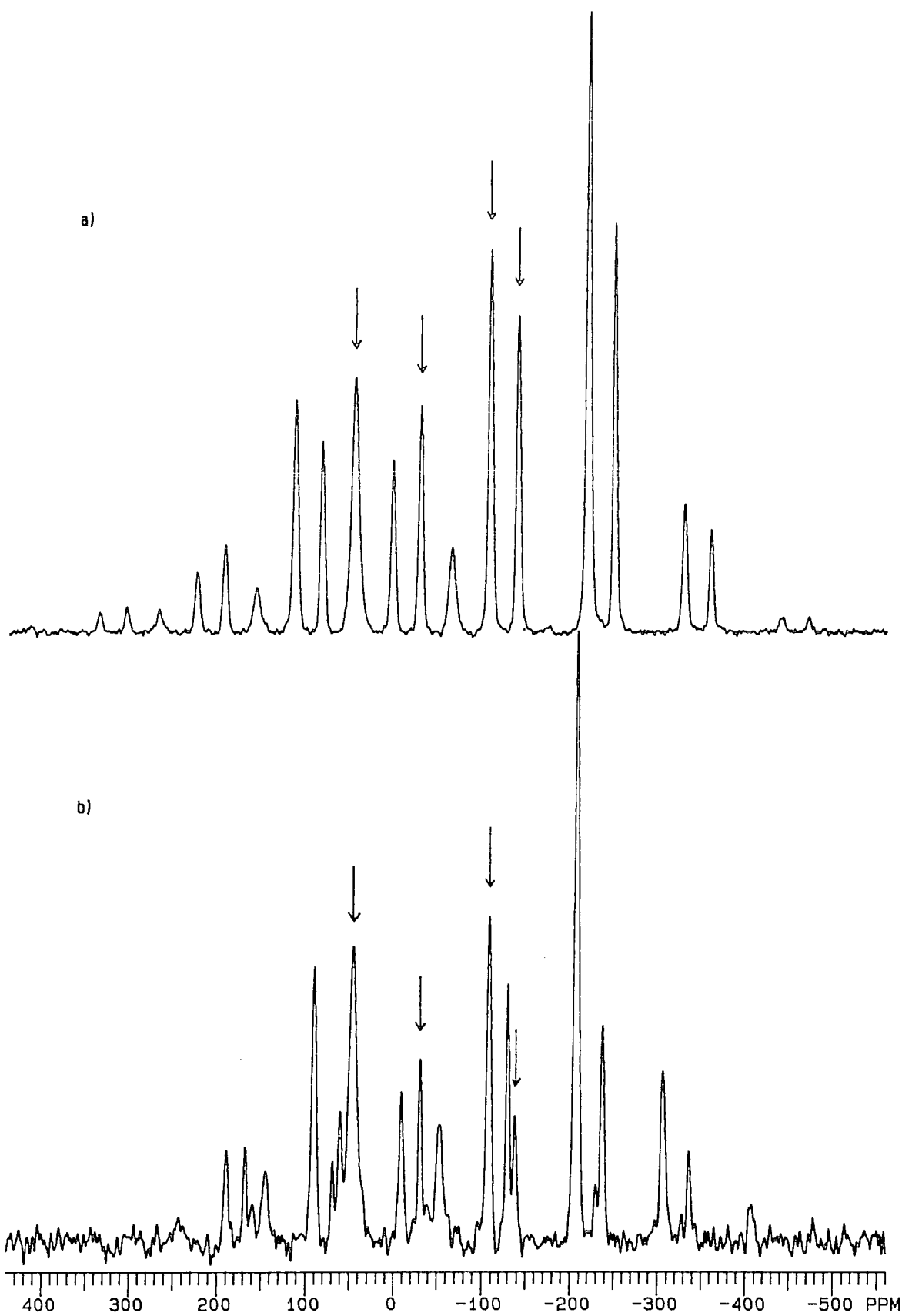
Figure 5.3.8 ^{119}Sn spectra of [(Me$_3$Sn)$_4$Fe(CN)$_6$.D(+)glucose] at spin-rates of
                a) 12600 Hz and b) 11100 Hz
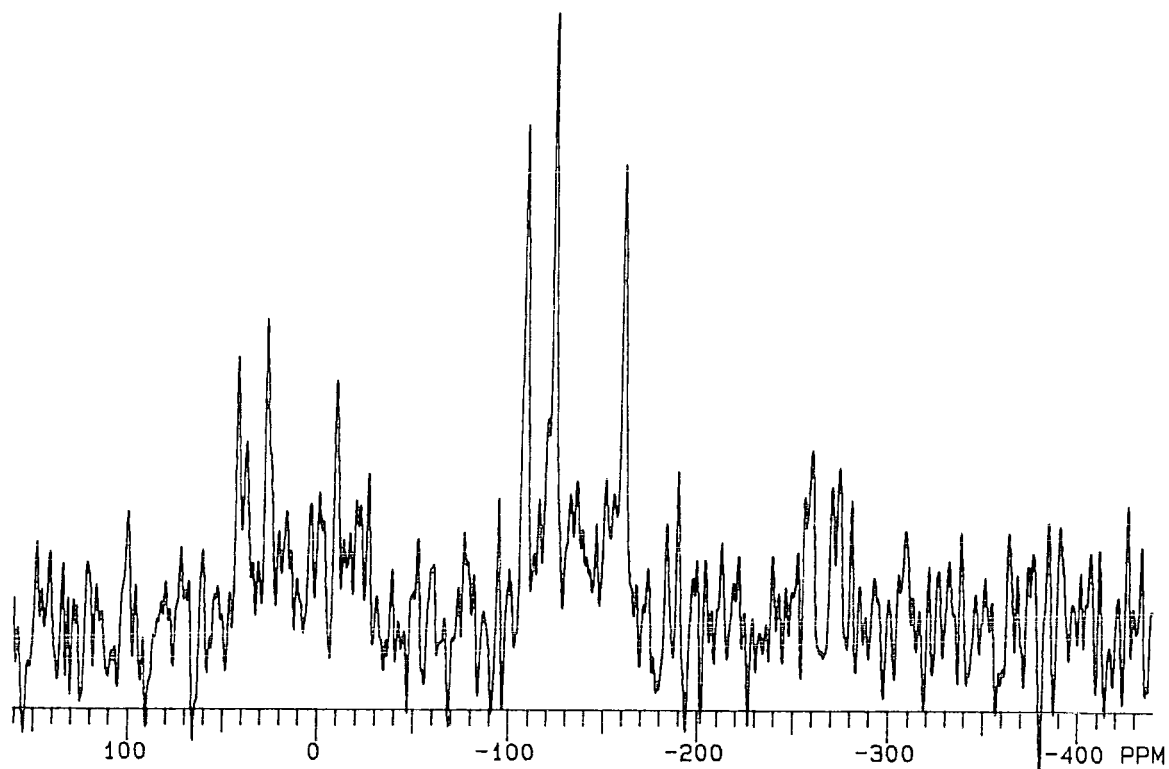
Figure 5.3.9 ^{15}N spectrum of $[(Me_3Sn)_4Fe(CN)_6.D(+)glucose]$

Table 5.3　NMR data for 7, 8 and 9

7　$[(Me_3Sn)_4Fe(CN)_6.C_4H_8O_2/H_2O]$
8　$[(Me_3Sn)_4Fe(CN)_6.2H_2O]$
9　$[(Me_3Sn)_4Fe(CN)_6.D(+)glucose]$

	δ/ppm	I_{rel}	J/Hz	$\Delta\upsilon_{1/2}$/Hz	assignment
^{13}C					
7	0.9	2.2^f　1.3^g	520	23	CH_3
	2.2	1.0^f　1.0^g	566	56	CH_3
	67.5				$C_4H_8O_2$
	172^a				CN
8	1.7		566		CH_3
	4.4				CH_3
	175^a				CN
9	1.6		565	43	CH_3
	60-93				D(+)glucose
	175^a				CN
^{119}Sn					
7	−136	1.0		470	Chain A
	−73	1.0		410	Chain B
8	−107	1.0		540	Chain A
	47	2.0		950	Chain B
	−29 }	0.6		370	Chain C
	−138 }				
9	−108	2.6		530	Chain A
	46	1.0		830	Chain B
	−30 }	2.0		470	Chain C
	−138 }			570	
^{15}N					
7	−125	1		15	Chain B
	−116	2		15	Chain A
8	−161	1		50	Chain B
	−124	1		34	} Chains A+C
	−109	1		38	}
9	−161	1		90	Chain B
	−124	1		50	} Chains A+C
	−109	1		60	}

a　multiplet, therefore only approximate δ

f　ratio calculated from CP experiment

g　ratio calculated from SP experiment

5.4   Lead containing compounds

$$10 \quad [(Me_3Pb)_3Co(CN)_6]$$

$$11 \quad [(Me_3Pb)_4Ru(CN)_6 \cdot 2H_2O]$$

$$12 \quad [(Me_3Pb)_4Fe(CN)_6 \cdot 2H_2O]$$

The NMR data for these lead-containing compounds are given in table 5.4.

5.4.1 ^{13}C Spectrum of [(Me$_3$Pb)$_3$Co(CN)$_6$]

From the crystallographic data given in section 4.4.1 it is known that this compound contains nine inequivalent methyl environments and six cyanides. The methyl region of the ^{13}C spectrum (figure 5.4.1) contains three signals of equal intensity indicating only three different environments. It is most likely that each signal arises from the methyls in one of the chains A, B or C. The three methyls attached to the same lead atom are again not distinguishable by NMR due to rotation of the trimethyl-lead fragment about the N-Pb-N axis. Each methyl signal has satellites due to the coupling of the ^{13}C of the methyl to the spin-1/2 ^{207}Pb, the value of which is about 400 Hz (slightly smaller than the ^{13}C-^{119}Sn coupling constants).

Variable temperature spectra were obtained of the methyl region of the ^{13}C between room temperature and $-37^{\circ}C$ but no differences were seen apart from a slight change in the chemical shifts.

The CN region of the spectrum contains a manifold of spinning sidebands with a centreband at approximately 135 ppm which is split into many signals. The pattern of the splitting is similar to that seen in the ^{13}C spectrum of the cobalt- containing compounds. This is as expected since ^{207}Pb is a spin-1/2 nuclei, like ^{119}Sn. The pattern does, however, look slightly more complicated, possibly indicating more differences between the CN groups.

If this ^{13}C spectrum is compared to that obtained for the tin analogue [(Me$_3$Sn)$_3$Co(CN)$_6$], it may be seen that the methyl regions are different. In the tin compound only two signals were resolved even though the crystallographic data indicated three different chains, but in the lead compound signals from all three chains can be seen. This indicates that in the lead compound all three chains are quite different whereas in the tin compound chains A and B are very similar. This is in agreement with the crystallographic data. The chemical shifts of the methyl-lead signals are at a higher frequency than the methyl-tin signals. The signals due to the carbon of the cyanide group appear at approximately the same frequency for the two compounds.

5.4.2 ^{207}Pb spectrum of [(Me$_3$Pb)$_3$Co(CN)$_6$]

The crystallographic data indicate the presence of three different environments for the lead in the chains A, B and C. The ^{207}Pb spectrum (figure 5.4.2), however, contains only two signals but one is double the intensity of the other. This indicates that two of the environments are very similar and NMR cannot distinguish between them. From the crystallographic data it can be seen that chain C contains a more asymmetric N-Pb-N bridge (Pb-N = 0.252, 0.246 nm) compared to chain A (Pb-N = 0.252, 0.252 nm) and chain B (Pb-N = 0.252, 0.254 nm). Therefore the signal of double intensity at 172 ppm can be assigned to the lead in chains of types A and B, and the signal at 78 ppm to chain C. This is in agreement with that given for the ^{119}Sn spectrum of 1, where the low-frequency signal was assigned to the asymmetric bridge. An alternative assignment would be that the signal of double intensity was due to chains A and C, which are both not as bent as chain B (which has a Pb-N-C angle of 125°). However this is not so likely, since the angle at the nitrogen atom will not affect the environment of the lead very much. The signal assigned to chain C is at a lower frequency than that assigned to chains A and B. This could be due to the short Pb-N bond length of 0.246 nm causing the lead atom to be more shielded, hence shifting the signal to a lower frequency.

5.4.3 ^{15}N spectrum of $[(Me_3Pb)_3Co(CN)_6]$

The ^{15}N spectrum has a poor signal-to-noise ratio but appears to contain only one signal. This indicates only one environment whereas the X-ray studies predicted six. The Pb-N and N-C bond lengths in chains A, B and C are all very similar and although the bond angles (Pb-N-C) vary from 125° to 154° this apparently does not cause enough differences in the nitrogen environments to be detected by NMR.

5.4.4 ^{59}Co spectrum of $[(Me_3Pb)_3Co(CN)_6]$

The spectrum contains only a single intense line with many spinning sidebands of much lower intensity and is very similar to spectra obtained for 1,2 and 3. The crystal structure indicates two environments but none of the previously discussed ^{59}Co spectra have distinguished this difference so the result is not inconsistent.

The spectra of all the different nuclei studied indicate that the number of crystallographically different environments in the asymmetric unit differs from the number of observed resonance lines in the NMR spectra as shown below.

	CH_3	CN	N	Pb	Co
XRS	9	6	6	3	2
NMR	3		1	2	1

5.4.5 ^{13}C spectrum of $[(Me_3Pb)_4Ru(CN)_6.2H_2O]$

The ^{13}C spectrum of the methyl region (figure 5.4.3a) contains two signals in the approximate intensity ratio 2:1. This is not in agreement with the crystallographic data, which predicted that the two Me_3Pb environments should be equal in number. Each signal has satellites due to the coupling to the ^{207}Pb of approximately 350 Hz, which is comparable to the coupling constant measured from the spectrum of 10. The lower-frequency methyl signal (17.6 ppm) is at a similar chemical shift to those observed for compound 10 which only contains chains of type A. The signal at 17.6 ppm can therefore probably be assigned to methyls in chain A.

Chain B of compound 11 is very different from chain A, with the Me_3Pb unit bonded between an oxygen and a nitrogen atom. Compared to chain A, the Me_3Pb unit in chain B is more deshielded due to the oxygen drawing electrons away shifting the methyl signal to a higher frequency. This methyl signal is also broader than that for chain A. Variable temperature spectra may help to explain why this is so and a high temperature spectrum may also give a more correct intensity ratio for the two signals.

The cyanide region of the ^{13}C spectrum contains a centreband at approximately 160 ppm (figure 5.4.4a) and a manifold of spinning sidebands. The centreband signal is quite clearly split into three groups of lines, each group containing two signals in the intensity ratio of 2:1. This is characteristic of splitting due to coupling to the quadrupolar spin-1 ^{14}N as explained in 5.2.1. The CN region is therefore indicating three different CN environments; one in chain B and two in the two chains of type A.

The chemical shifts of the signals in the centreband are approximately the same as those measured for the anhydrous Ru compound (5) except that the pair of low-frequency signals is shifted to an even lower frequency. The structure of 11 contains a weak bond from a hydrogen atom at the end of chain B onto the nitrogen of the CN of chain A which could account for this low-frequency signal. This should show up even more in the ^{15}N spectrum.

128

The lead spectrum (figure 5.4.5a) shows two intense overlapping spinning sideband manifolds with centrebands at 200 ppm and 150 ppm. This is consistent with the crystallographic data which predicts two environments one in each of chain A and B. However, the structure contains the same number of lead atoms in each environment, whereas the signals in the spectrum have an intensity ratio of approximately 3:1. This discrepancy could be due to differences in the cross-polarisation rates between the two Pb environments. This could be investigated further by a single-pulse experiment or a variable contact time CP experiment, but these would occupy much spectrometer time.

The lead atoms in chain B are directly bonded to both oxygen and nitrogen whereas those in chain A are bonded to two nitrogens. Since the electronegativity of oxygen is greater than that of nitrogen, the lead atoms in chain B are deshielded to a greater extent than those in chain A. Therefore the higher-frequency (200 ppm) signal can probably be assigned to the lead in chain B and the signal at 150 ppm to the lead in chain A.

The centreband at approximately 200 ppm is split, as is the third sideband to the high-frequency side. This could indicate a third, very similar, Pb environment which is not apparent in the other spinning sidebands because the other signal swamps it. There are also some other low-intensity signals, either indicating more different lead environments, or impurities within the lattice.

5.4.7 ^{15}N spectrum of [(Me$_3$Pb)$_4$Ru(CN)$_6$.2H$_2$O]

The ^{15}N spectrum (figure 5.4.6a) contains three major signals indicating three environments for the CN groups , the same as the ^{13}C spectrum. There are also a few smaller peaks possibly indicating coupling of the nitrogen to ^{207}Pb of approximately 350 Hz, but the signal-to-noise ratio is not good enough to be sure. As expected

from the structure one of the signals is shifted to a much lower frequency (-158 ppm) due to the weak bond from the hydrogen of chain B to the nitrogen of chain A. This is also in agreement with the CN region of the carbon spectrum. The intensity ratio of the signals is approximately 1:1:1 which is consistent with the X-ray data. There is one environment in chain B and two in the two chains of type A.

The NMR data is to a certain extent consistent with the crystallographic data. However, it does indicates more equivalence of the cyanide groups and the methyls as was seen in some of the earlier compounds.

5.4.8 ^{13}C spectrum of [(Me$_3$Pb)$_4$Fe(CN)$_6$.2H$_2$O]

The crystallographic data indicate that this is very similar to the ruthenium compound but the spectra are quite different.

The methyl region of the ^{13}C spectrum (figure 5.4.3b) contains many signals ranging from 14 ppm to 28 ppm. There are two sharp signals of reasonably large intensity at 18.1 ppm and 18.3 ppm with satellites indicating a coupling constant $J_{13C-207Pb} = 360$ Hz. Comparison of these two signals with that assigned to the methyls in chain A for compound 11 shows they are at roughly the same chemical shift with the same linewidth and the same coupling constant. This suggests that compound 12 contains two chains of type A which are slightly different. The ^{13}C spectrum of 12 also contains a signal at 22 ppm, as the spectrum of the Ru compound did, indicating the structure also contains chains of type B. There are also many other broader signals in the range 14-25 ppm, of a similar intensity, suggesting that the structure is disordered, containing many different methyl environments.

Variable temperature spectra may help to simplify this complicated methyl region if some of the signals become sharper.

130

The CN region (figure 5.4.4b) is also far more complicated than that recorded for the Ru compound. The chemical shift of the centreband is at a higher frequency - the same trend as was seen in the series of compounds 4, 5 and 6. Taking only the signals of greatest intensity gives six lines in three groups of two, similar to the pattern obtained for the Ru compound and indicating three major CN environments. There is, however, a difference in their relative chemical shifts. Here there is a larger gap between the two higher frequency groups rather than between the two lower frequency groups as in the Ru compound. The many other signals of smaller intensity also seem to indicate a disordered structure.

5.4.9 ^{207}Pb spectrum of [(Me$_3$Pb)$_4$Fe(CN)$_6$.2H$_2$O]

The ^{207}Pb spectrum (figure 5.4.5b) contains three signals suggesting three environments for the lead although the crystallographic data indicated only two. The three signals at 139, 64 and 195 ppm are in the ratio 2.8 : 2.6 : 1 respectively.

If the chemical shifts for compounds 11 and 12 are compared, it can be seen that the two higher-frequency signals of 12 are at similar chemical shifts to the two signals of 11. Compound 12 also contains a third environment with a signal at a lower frequency (64ppm).

The ^{207}Pb spectrum of 12 does not predict such a disordered structure as the ^{13}C spectrum did, although any minor signals would probably be hidden under the three major signals.

5.4.10 ^{15}N spectrum of [(Me$_3$Pb)$_4$Fe(CN)$_6$.2H$_2$O]

The ^{15}N spectrum (figure 5.4.7b) has a surprisingly good signal-to-noise ratio compared to other nitrogen spectra obtained and clearly contains three signals of approximately equal intensity. The chemical shifts of the signals are evenly spaced in contrast to the Ru compound. There are possibly some signals of lower intensity

hidden in the noise but like the ^{207}Pb spectrum it predicts a much more ordered structure than the ^{13}C suggested, with three CN environments.

There do not appear to be many similarities at all between the structures predicted by the NMR and the crystallographic data. The ^{13}C spectrum, especially, seems to indicate a disordered structure very different to that of compound 11.
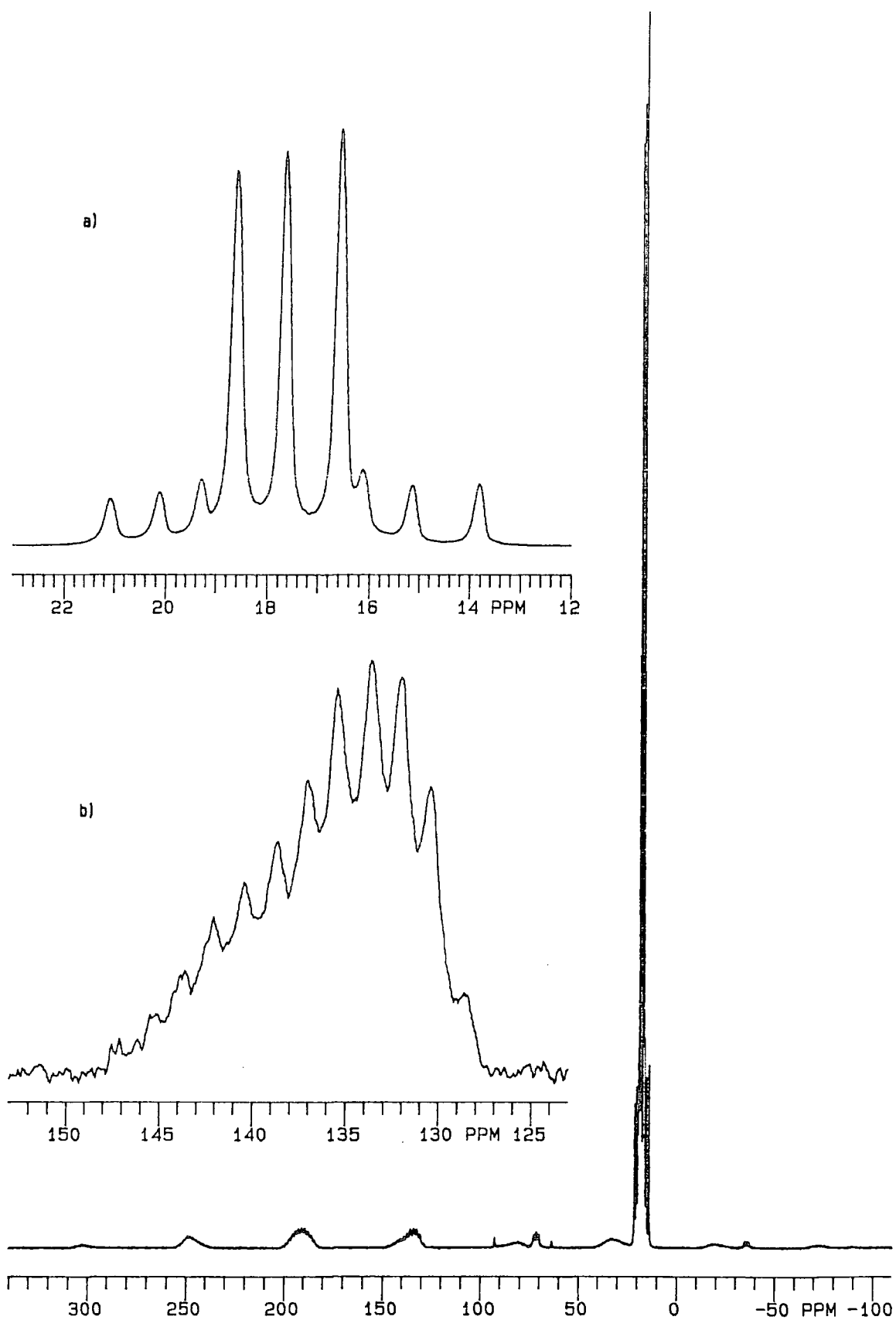
Figure 5.4.1 ^{13}C spectrum of $[(Me_3Pb)_3Co(CN)_6]$ and expansions of a) the methyl region and b) the CN centreband
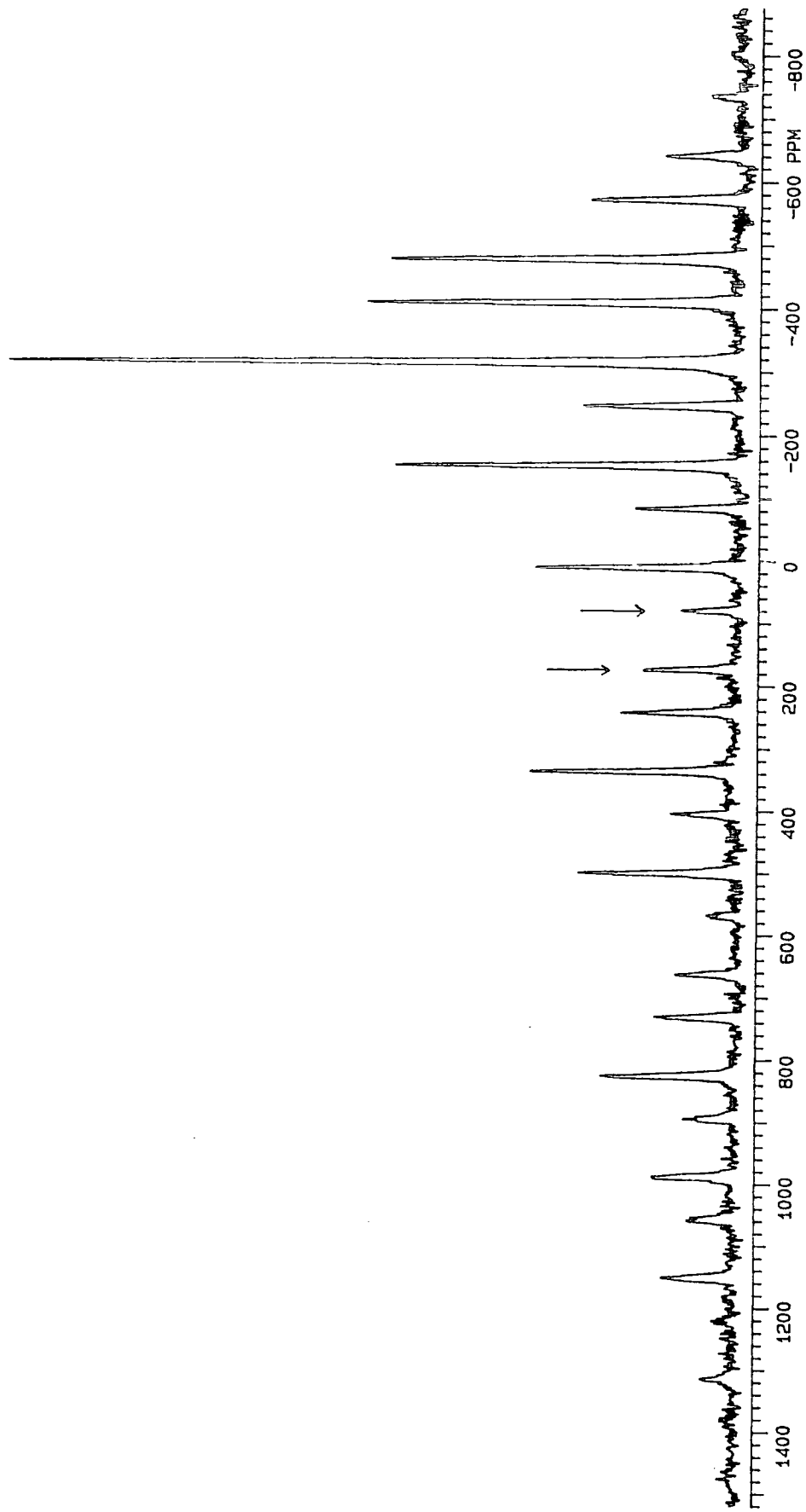
Figure 5.4.2 ^{207}Pb spectrum of $[(Me_3Pb)_3Co(CN)_6]$
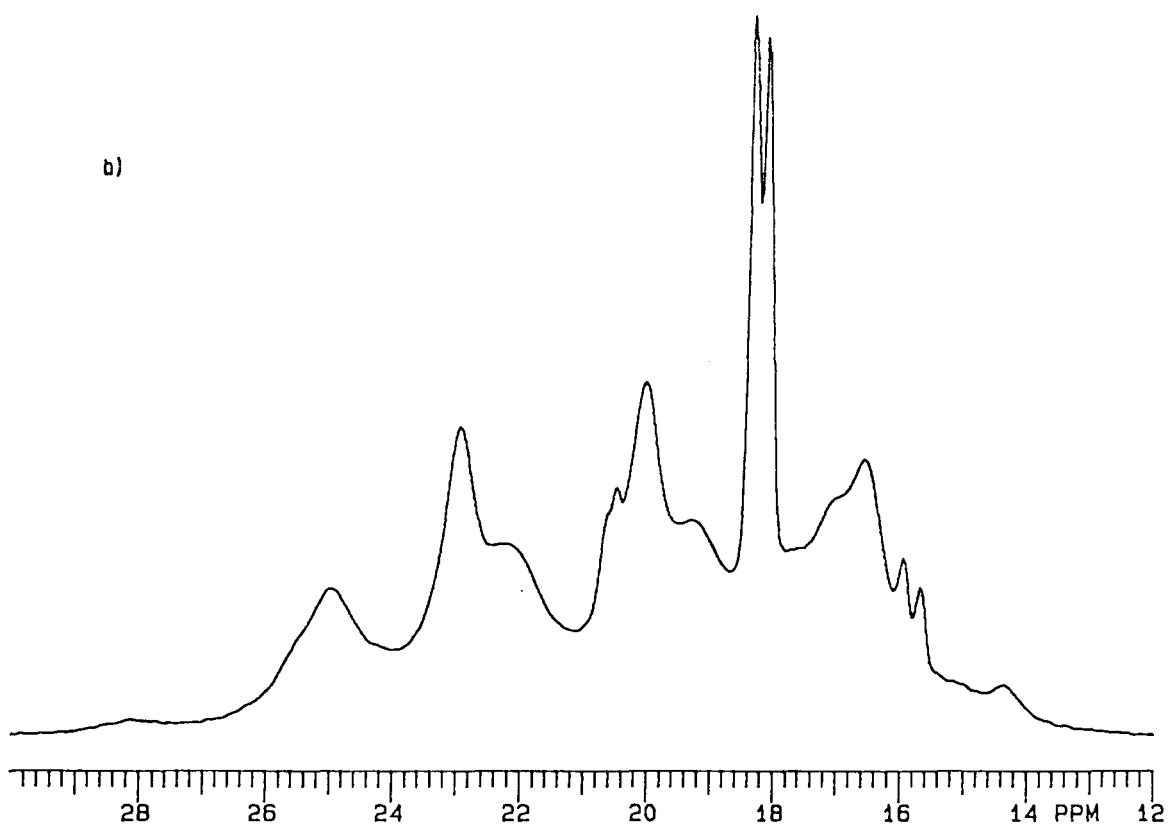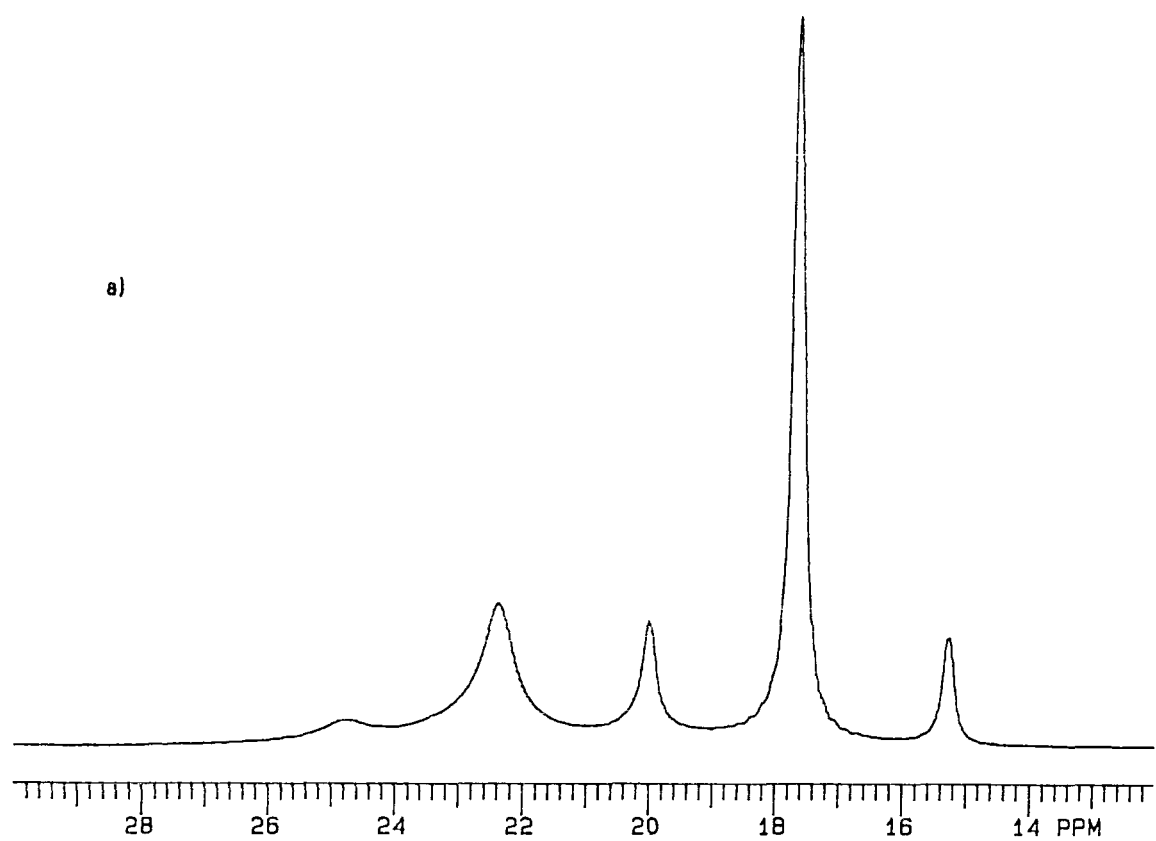
Figure 5.4.3   Methyl regions from the ^{13}C spectra of a) $[(Me_3Pb)_4Ru(CN).2H_2O]$
and b) $[(Me_3Pb)_4Fe(CN).2H_2O]$

135
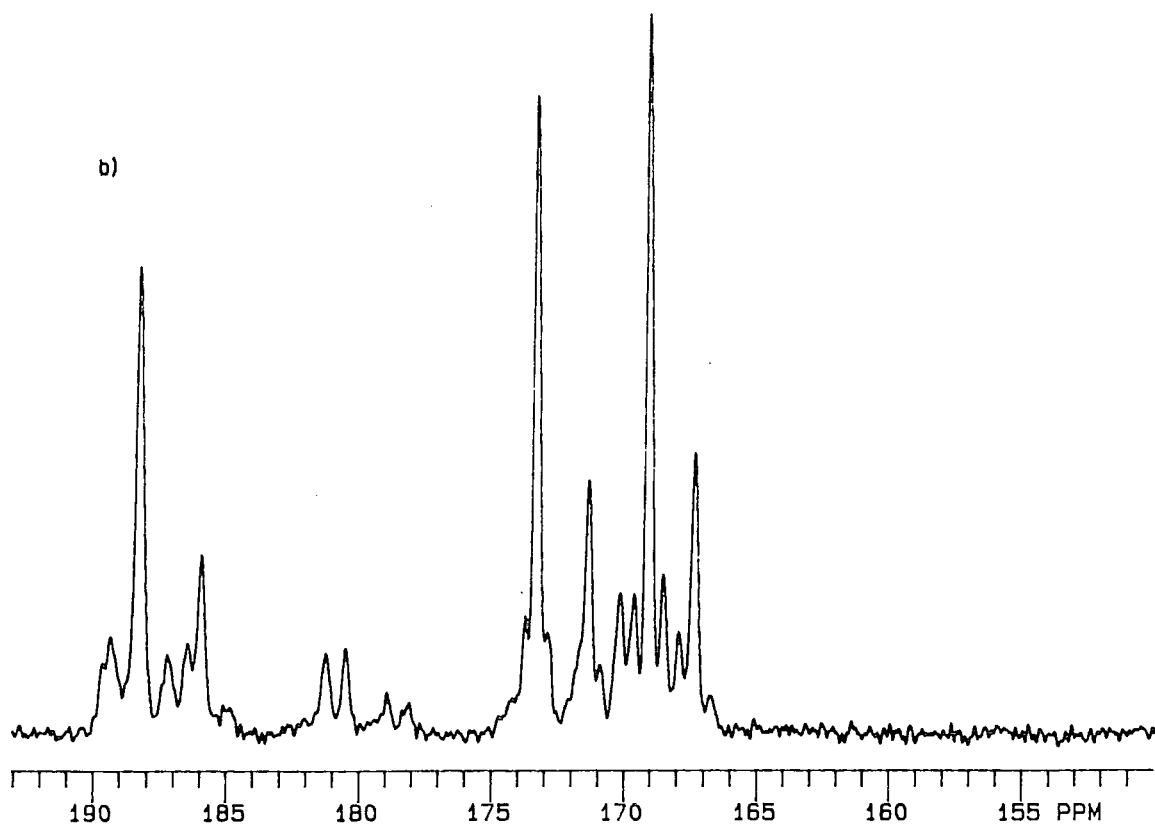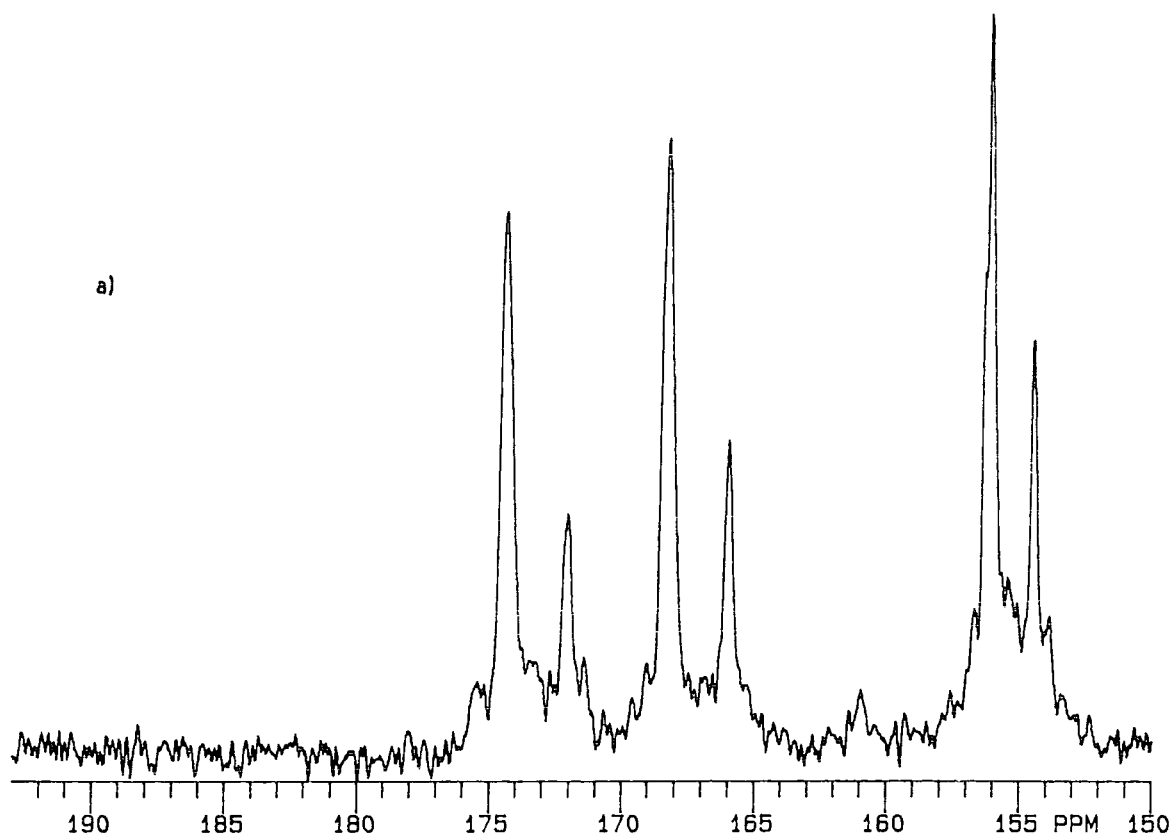
Figure 5.4.4 CN centrebands from the ^{13}C spectrum of a) $[(Me_3Pb)_4Ru(CN).2H_2O]$ and b) $[(Me_3Pb)_4Fe(CN).2H_2O]$

136
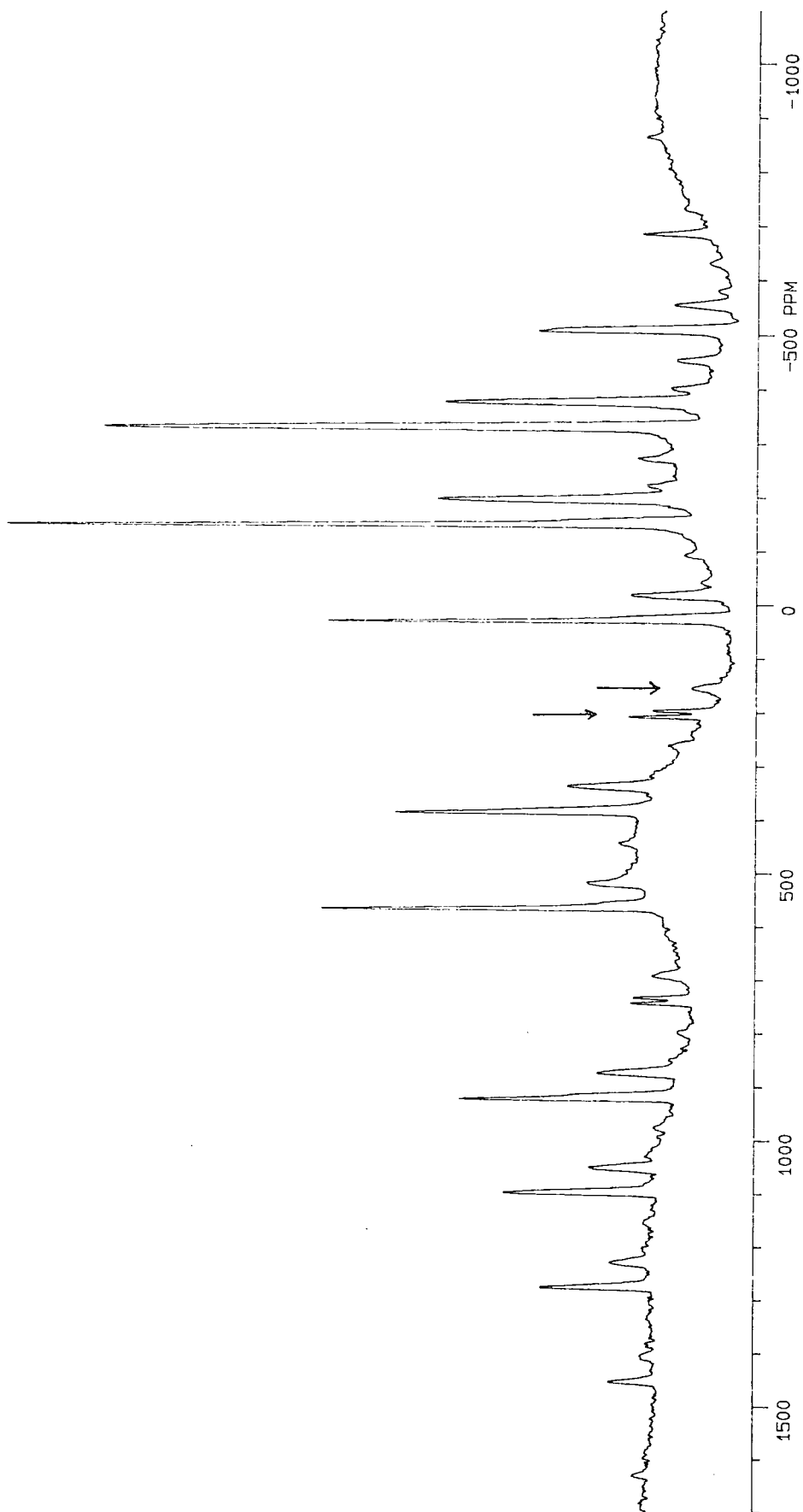
Figure 5.4.5 ^{207}Pb spectrum of $[(Me_3Pb)_4Ru(CN).2H_2O]$
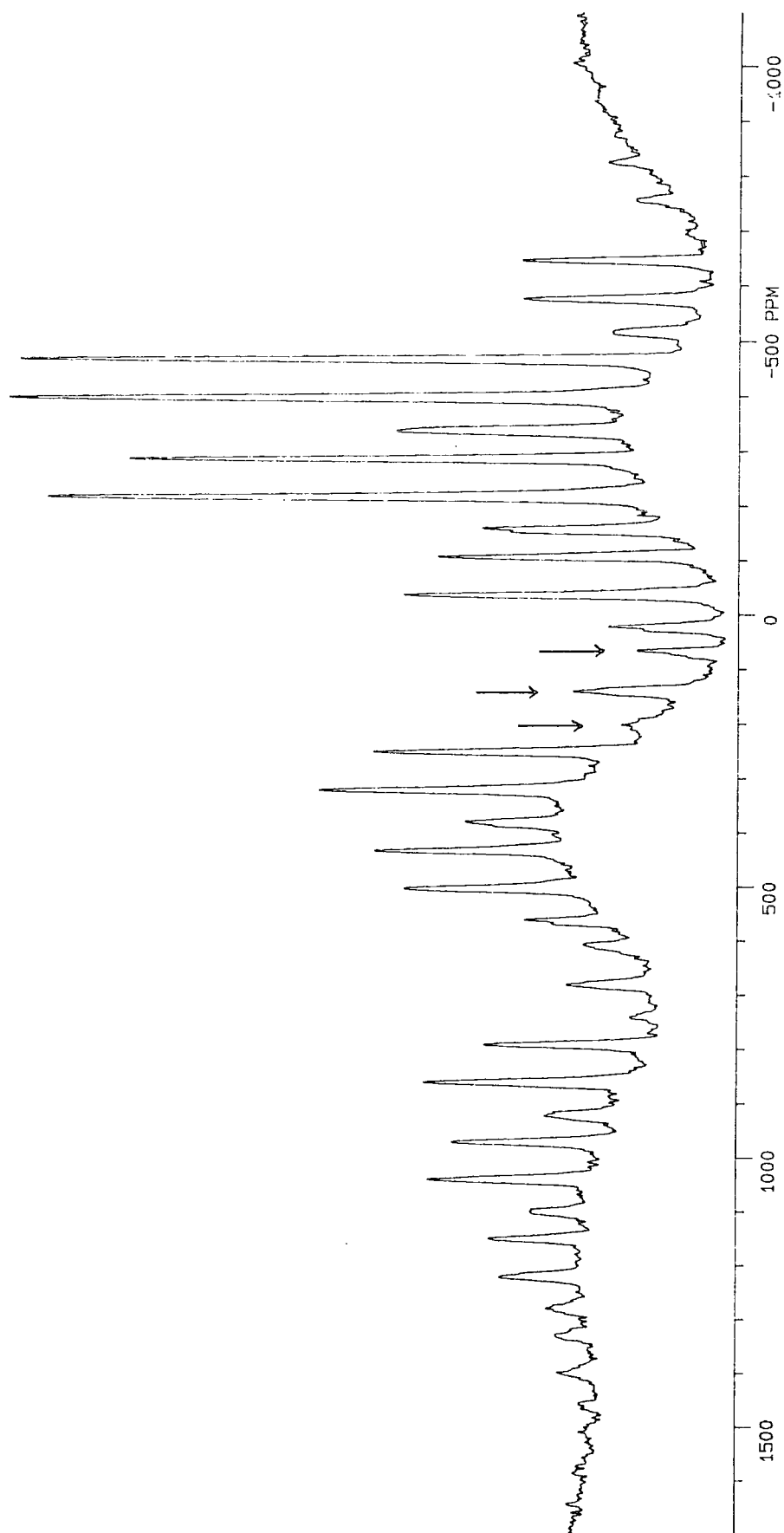
Figure 5.4.6 ^{207}Pb spectrum of $[(Me_3Pb)_4Fe(CN)_6].2H_2O]$
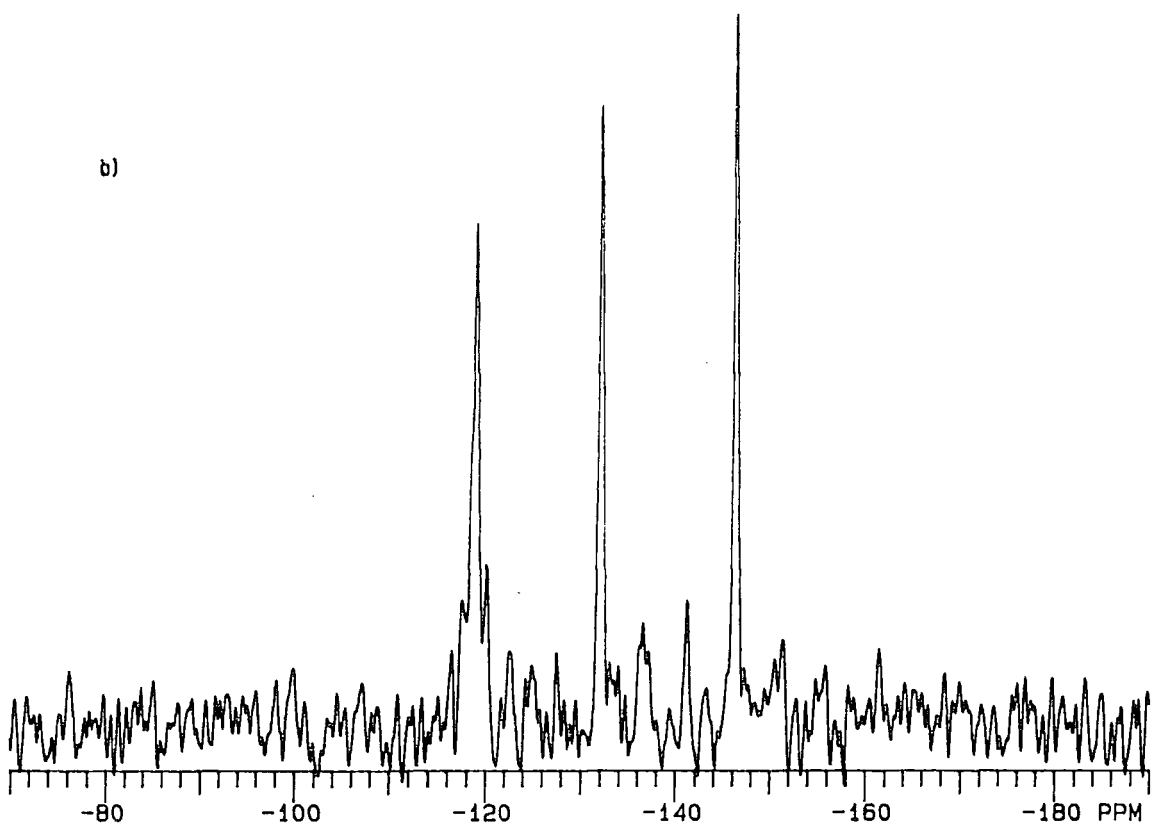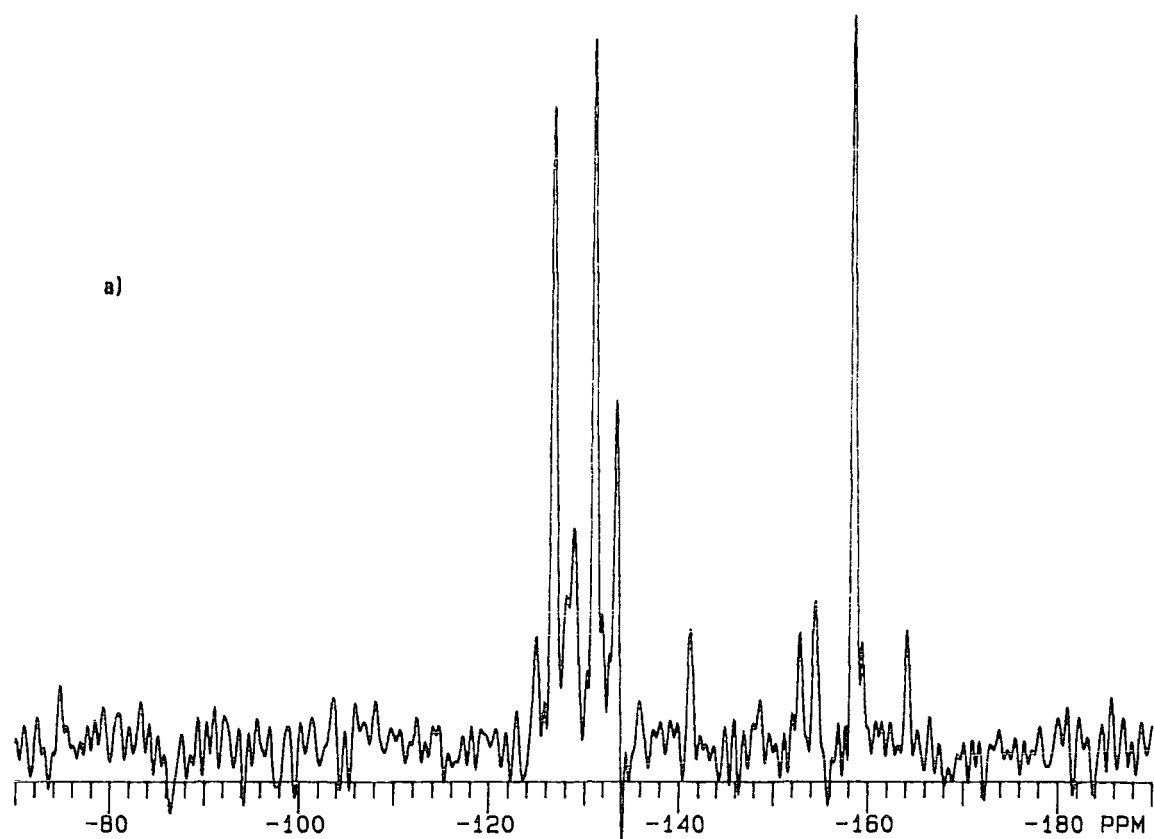
Figure 5.4.7 ^{15}N spectrum of a) $[(Me_3Pb)_4Ru(CN).2H_2O]$ and
                b) $[(Me_3Pb)_4Fe(CN).2H_2O]$

Table 5.4 NMR data for 10, 11 and 12

10    $[(Me_3Pb)_3Co(CN)_6]$
11    $[(Me_3Pb)_4Ru(CN)_6.2H_2O]$
12    $[(Me_3Pb)_4Fe(CN)_6.2H_2O]$
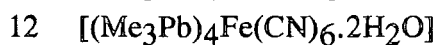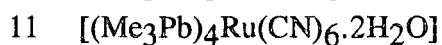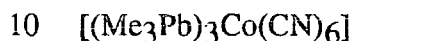
	δ/ppm	I_{rel}	J/Hz	$\Delta\upsilon_{1/2}$/Hz	assignment
^{13}C					
10	16.5	1	414	17	CH_3
	17.6	1	375	18	CH_3
	18.6	1	373	18	CH_3
	135[a]				CN
	93 63				impurity
11	17.6	2	357	15	CH_3
	22.4	1	347	50	CH_3
	165[a]				CN
12	18.1		354	20	CH_3
	18.3		364	20	CH_3
	14-25				CH_3's
	175[a]				CN
^{207}Pb					
10	172	2		500	Chains A+B
	78	1		520	Chain C
11	200	3			Chain B
	149	1		450	Chain A
12	195	1.0		1200	
	139	2.8		1000	
	64	2.6		780	
^{15}N					
10	−124				
11	−127	1		17	
	−131	1		16	
	−158	1		15	
12	−119			11	
	−132			10	
	−146			10	
^{59}Co					
10	−157			800	

[a] multiplet, therefore only approximate δ

13    $[(Cp_2Co)(Me_3Sn)_3Fe(CN)_6]$

14    $[(Et_4N)(Me_3Sn)_3Fe(CN)_6]$

The NMR data for both these compounds can be found in table 5.5.

5.5.1 $[(Cp_2Co)(Me_3Sn)_3Fe(CN)_6]$

^{13}C spectrum

The low frequency region of the ^{13}C spectrum (figure 5.5.1a) contains one major methyl signal at 4.1 ppm with satellite peaks $(J_{13C-119Sn} = 565$ Hz). There is another signal of much lower intensity to a slightly lower frequency. The crystal structure predicts six crystallographically different methyl groups, however, it is most likely that only two would be seen at ambient temperatures due to exchange processes as described earlier (section 5.2.5). These two signals would be expected to be in the ratio 2:1 but the room temperature spectrum shows clearly that this is not the case. It is possible that a more accurate intensity ratio would be achieved at an elevated temperature of 51°C as was the case for compounds 4,5 and 6 in section 5.2.4.
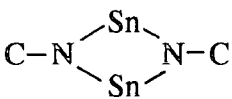
The signal at 86 ppm is due to the carbons of the Cp_2Co. The crystal structure predicted that the five carbons of the Cp were different but the NMR spectrum indicates that they are equivalent. This is probably due to rotation of the molecule resulting in an average position for the NMR signal.

The higher frequency region of the spectrum contains the signals due to CN groups. The centreband (figure 5.5.1b) is split into at least seven lines which, when the splitting due to coupling to ^{14}N is taken into account, indicates at least four different CN environments. This is one more than the crystal structure suggests.

^{119}Sn spectrum

The ^{119}Sn spectrum (figure 5.5.2) contains three overlapping sideband manifolds with centrebands at 48, −105, and −139 ppm, however, the crystal structure predicted only two different tin environments. If the chemical shifts are compared to those of compound 4 it can be seen that two of the signals are at very similar positions.

		Compound 4	Compound 13
Chain A	C−N−Sn−N−C	−108 ppm	−105 ppm
Chain B	C−N⟨Sn Sn⟩N−C	46 ppm	48 ppm

It can be concluded that the structure of 13 contains two tin environments very similar to the two in compound 4.

The third signal at −139 ppm is at a similar chemical shift to the low frequency ^{119}Sn signals for compounds 8 and 9. It is possibly due to a tin atom in a straight chain, such as A, but the tin must be more shielded since it is shifted by approximately 30 ppm to a lower frequency.

^{15}N spectrum

Again, the signal-to-noise ratio of the ^{15}N spectrum (figure 5.5.3) is not very good but a weak signal can be seen at −122 ppm. This is in the region previously found to contain the signals due to the CN groups. A much improved spectrum would be needed before any comparisons could be made.

^{59}Co spectrum

It was attempted to acquire a ^{59}Co spectrum for 14 but due to the non-octahedral environment it was not possible.

The NMR data appears to predict a different structure to the crystallographic data. The CN region of the ^{13}C spectrum contains an extra signal, as does the tin spectrum. The ^{119}Sn chemical shifts are also more characteristic of compound 4 rather than the simple lattice of compound 1.

5.5.2 [(Et$_4$N)(Me$_3$Sn)$_3$Fe(CN)$_6$]

^{13}C spectrum

The low frequency region of the ^{13}C spectrum of 14 (fig 5.5.4a) clearly shows two methyl signals at 2.9 ppm and 9.2 ppm. The lower-frequency signal has satellite peaks due to coupling to the tin and can therefore be assigned to the methyls of the (Me$_3$Sn) groups. The second methyl signal has no satellites and must arise from the methyls of the (Et$_4$N) groups. There is also a signal at 53.6 ppm due to the CH$_2$ groups of (Et$_4$N). The appearance of only one signal for each type of protonated carbon implies equivalence in each of the different sites.

The only other signals present in the spectrum are those due to the CN groups and are relatively broad. The centreband (figure 5.5.4b) and each spinning sideband is split into two in the ratio 2:1. This is because the spin-1/2 ^{13}C is dipolar-coupled to the spin-1 ^{14}N as seen before in the ^{13}C spectrum of [(Me$_3$Sn)$_4$Fe(CN)$_6$] (4) (section 5.2.1).

The ^{13}C spectrum looked at as a whole suggests that the structure of 14 is more ordered than that of 13. Spectra obtained at a lower temperature might give more information.

The ^{119}Sn spectrum (figure 5.5.5) contains two sideband manifolds with centrebands at −158 ppm and −181 ppm. Their relative intensities are approximately 2.5:1 but this value could be inaccurate if the cross-polarisation rates are different (see section 2.11.2). For this reason a single-pulse spectrum was also obtained and gave an intensity ratio of 2.4:1. The two signals indicate two different environments and if they are compared with those obtained for compound 13 they are both at a lower frequency. This implies that the two environments are similar to each other but are quite different from those in 13. It is difficult to see how this result can be reconciled with the ^{13}C spectrum which predicted only one type of chain. It is possible that there are motional processes influencing ^{13}C but not ^{119}Sn at ambient probe temperatures.

^{15}N spectrum

This spectrum (figure 5.5.6) has a very low signal-to-noise ratio and apparently contains only one signal at −373 ppm. It is most likely due to the ^{15}N of the (Et$_4$N) groups, since all other nitrogen signals seen have been in the range −100 to −170 ppm. Any signals from the CN groups must have been lost in the noise.

Both the ^{13}C and ^{119}Sn spectra suggest a structure for 14 containing much equivalence and order compared to that of 13. It is also difficult to make any comparisons to compound 4 since the chemical shifts, especially of the tin atoms, are very different.
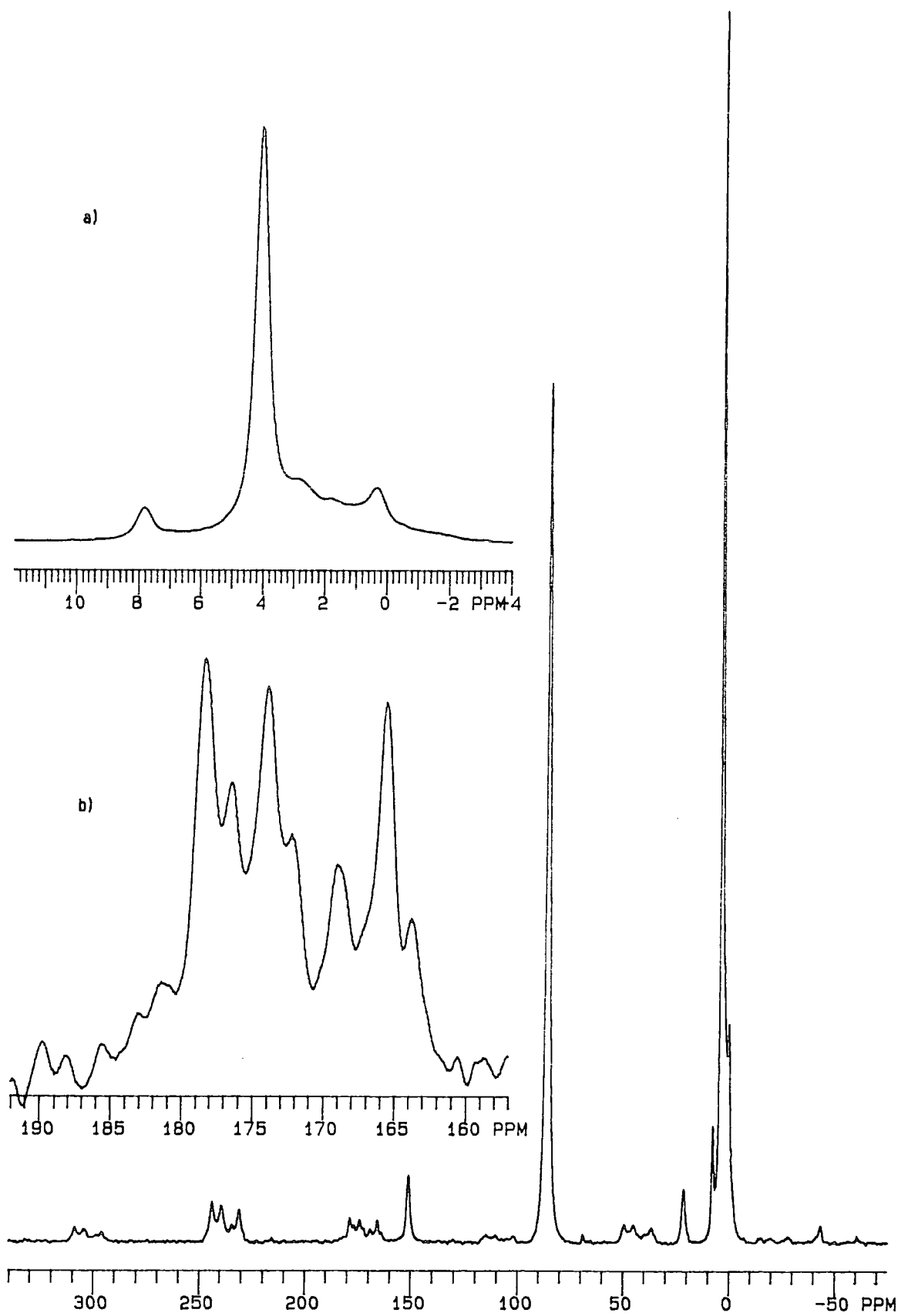
Figure 5.5.1 ^{13}C spectrum of $[(Cp_2Co)(Me_3Sn)_3Fe(CN)_6]$ and expansions of a) the alkyl region and b) the CN centreband
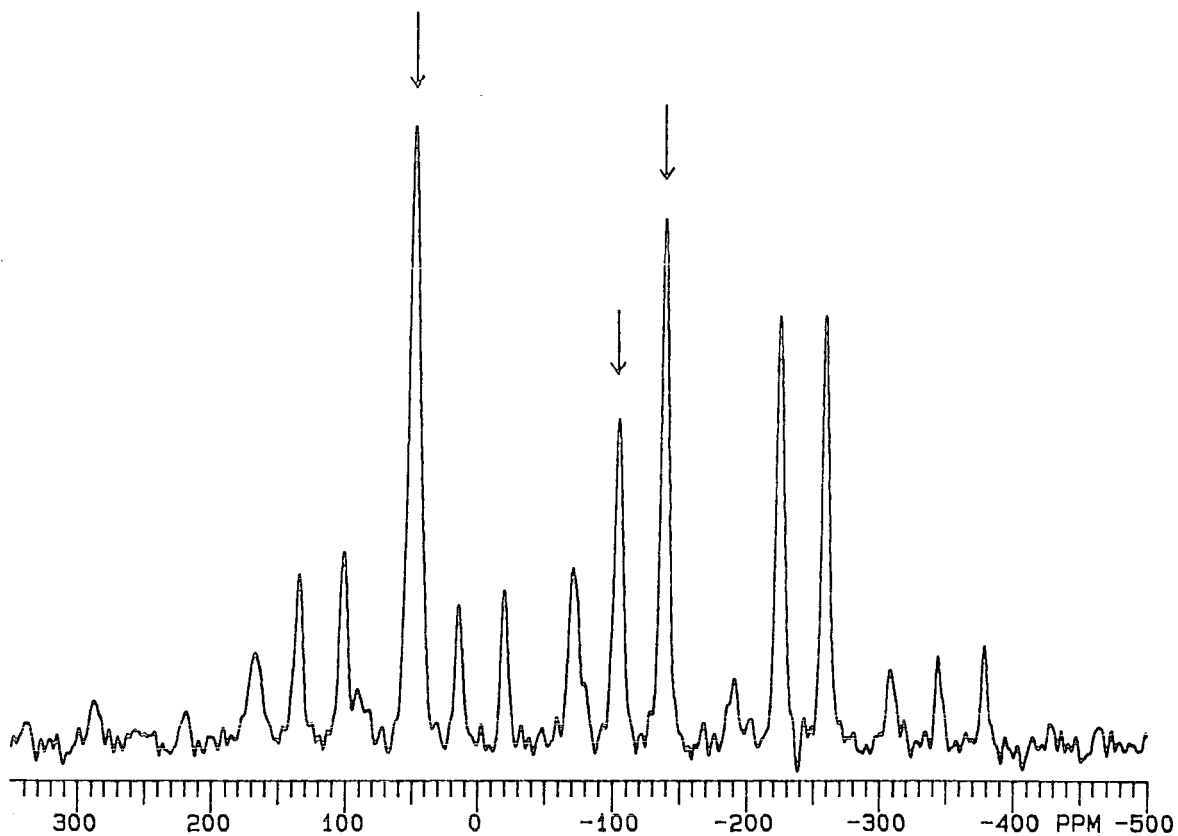
Figure 5.5.2 ^{119}Sn spectrum of $[(Cp_2Co)(Me_3Sn)_3Fe(CN)_6]$
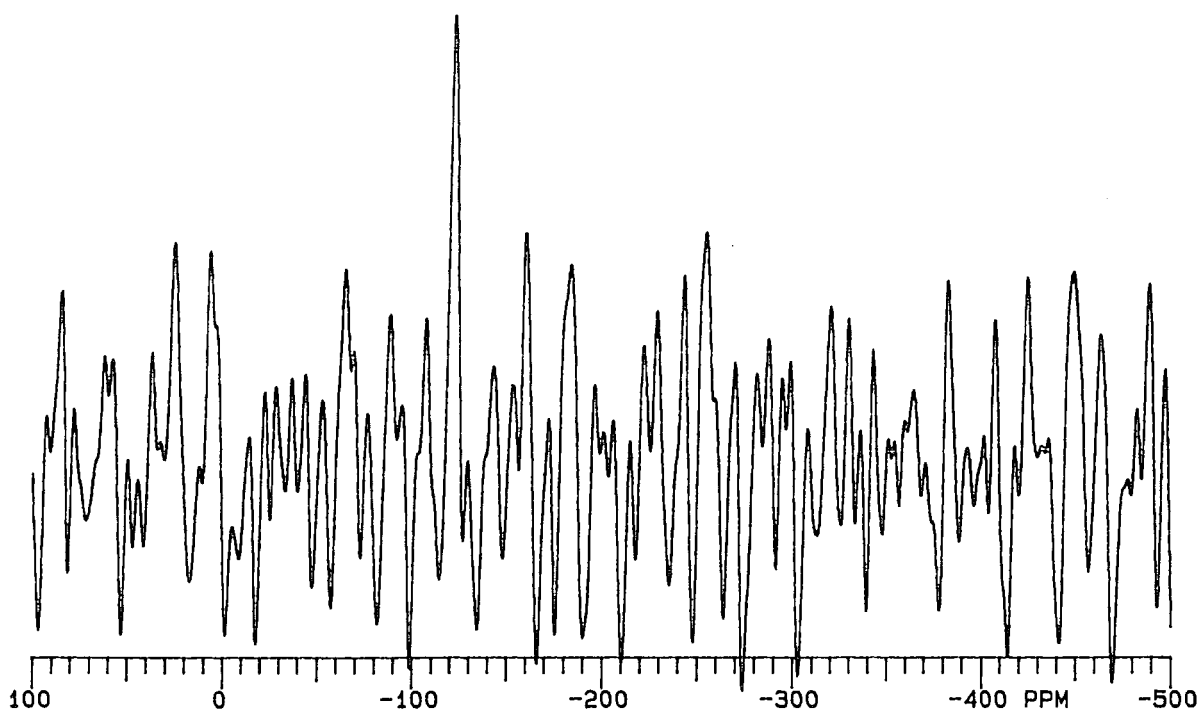
Figure 5.5.3 ^{15}N spectrum of $[(Cp_2Co)(Me_3Sn)_3Fe(CN)_6]$
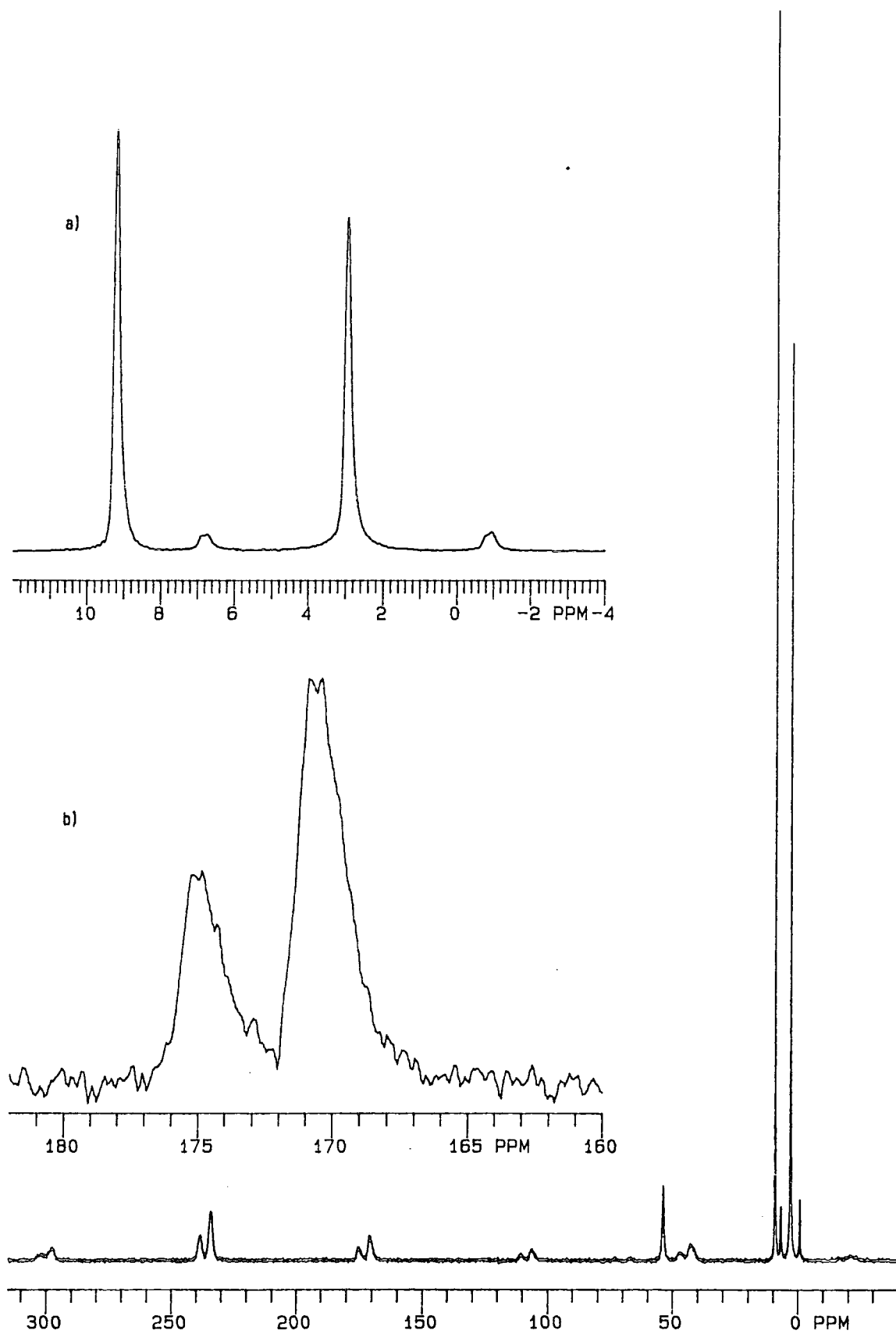
Figure 5.5.4 ^{13}C spectrum of $[(Et_4N)(Me_3Sn)_3Fe(CN)_6]$ and expansions of
a) the methyl region and b) the CN centreband
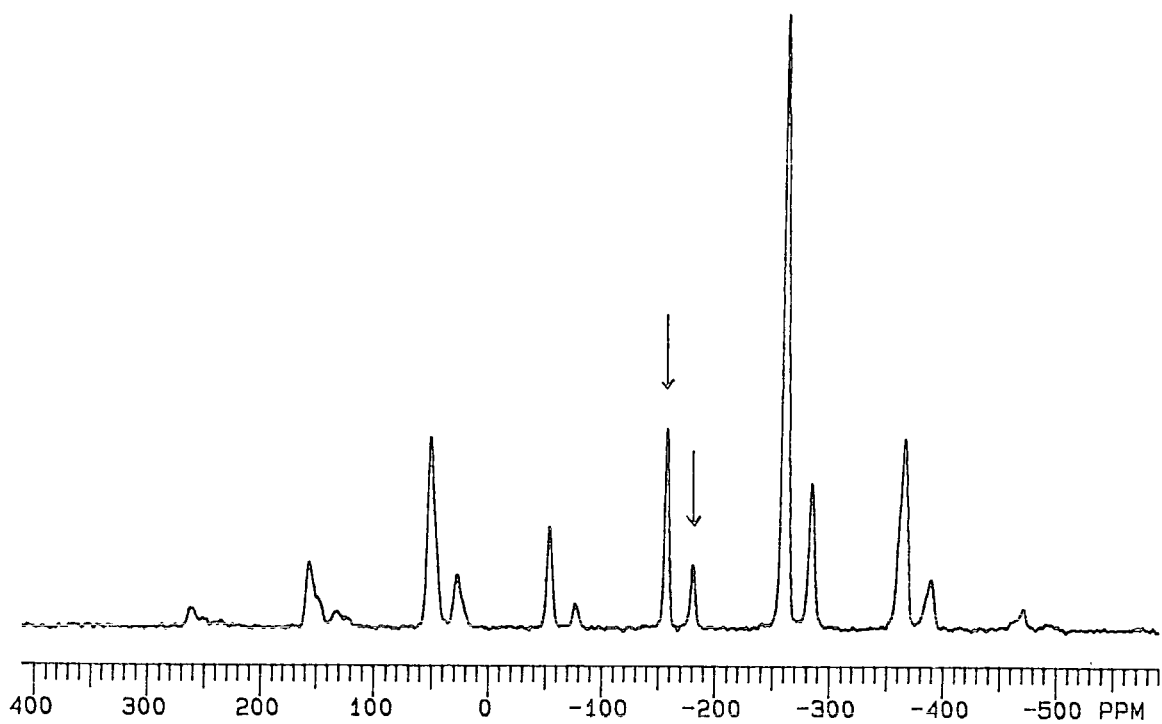
Figure 5.5.5 ^{119}Sn spectrum of $[(Et_4N)(Me_3Sn)_3Fe(CN)_6]$
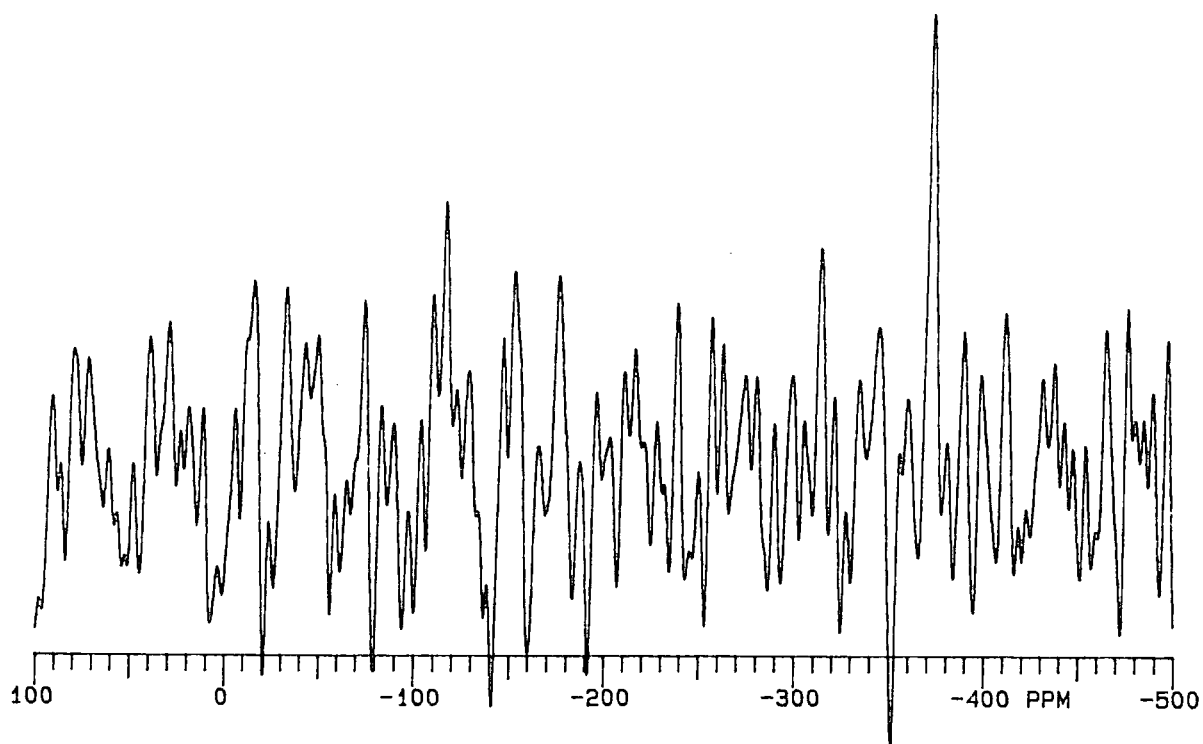
Figure 5.5.6 ^{15}N spectrum of $[(Et_4N)(Me_3Sn)_3Fe(CN)_6]$

148

Table 5.5   NMR data for 13 and 14

13    $(Cp_2Co)(Me_3Sn)_3Fe(CN)_6$
14    $(Et_4N)(Me_3Sn)_3Fe(CN)_6$

	δ/ppm	I_{rel}	J/Hz	$\Delta\upsilon_{1/2}$/Hz	assignment
^{13}C					
13	4.1	1	565	37	CH_3
	86.0	1		124	Cp
	172[a]				CN
14	2.9	1	580	14	CH_3
	9.2	1		13	CH_3
	53.6			51	CH_2
	172[a]				CN
^{119}Sn					
13	48	1.2		1040	
	−105	1.0		510	
	−139	1.1		620	
14	−158	2.5		380	
	−181	1.0		360	
^{15}N					
13	−122				
14	−373				

[a] multiplet, therefore only approximate δ

5.6 Anisotropies and asymmetries of both tin and lead containing compounds

The data for all the tin compounds can be found in table 5.6.

5.6.1 Tin and cobalt containing compounds

1 $[(Me_3Sn)_3Co(CN)_6]$

2 $[(Et_3Sn)_3Co(CN)_6]$

3 $[(Bu_3Sn)_3Co(CN)_6]$

As discussed earlier (4.1), compound 1 contains three crystallographically different tin environments, but the NMR spectrum indicates only two and the spectra for both 2 and 3 indicate only one. All the environments are very similar with the tin being penta-coordinate within an infinite non-linear chain, creating an almost axially symmetric environment.

The asymmetry values calculated for all the environments are in the range 0.1-0.2 and are close enough to zero to imply axial symmetry (see section 3.7). The anisotropy values range from −360 to −277 ppm.

The two different environments within 1 have anisotropies of −360 ppm for the low-frequency signal, which was assigned to tin atoms in the more asymmetric bridges of chain C, and −341 ppm for the higher-frequency signal assigned to the more symmetric bridges of chains A and B (see section 4.1 for structure). The values calculated for the anisotropies tend to confirm this assignment with the more asymmetric environment having a marginally larger anisotropy.

If the anisotropy of the symmetric environment (−341 ppm) in 1 is compared to the anisotropies for 2 and 3 (−305 ppm and −277 ppm) it can be seen that as the R group is changed from methyl to ethyl to butyl, the magnitude of the anisotropy decreases, i.e. the tin environment is becoming slightly more spherically symmetric as the R group becomes more bulky. It is difficult to see a similar trend in the asymmetries.

5.6.2 Trimethyl tin compounds with different metal atoms

$$4 \quad [(Me_3Sn)_4Fe(CN)_6]$$

$$5 \quad [(Me_3Sn)_4Ru(CN)_6]$$

$$6 \quad [(Me_3Sn)_4Os(CN)_6]$$
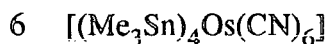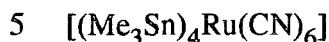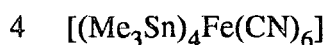
Two structures have been proposed for this series of compounds. The first, in section 4.2, consists of a three-dimensional lattice involving three of the trimethyl tin groups, with the fourth being only weakly bonded in the cages of the lattice. The second, in section 5.2.6, incorporates all four trimethyl tin groups within the lattice in two different environments, A and B, as shown below.

A   C−N−Sn−N−C   B   C−N⟨Sn⟩N−C (Sn above and below)
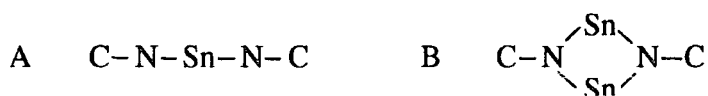
In general, the asymmetry value of the high-frequency signal for each compound is greater than that for the low-frequency signal, indicating that the environment of the tin corresponding to the high-frequency signal is moving away from axial symmetry. This is in agreement with the assignment of the high-frequency signal to environment B and the low-frequency signal to A as given in section 5.2.6.

A much larger difference is seen in the anisotropies of the two different environments. For each compound the value for the low-frequency signal is approximately -340 ppm and for the high-frequency signal approximately -200 ppm. This decrease in magnitude for the anisotropy implies that the high-frequency signal is due to an environment which has moved away from spherical symmetry such as B, which is in agreement with the above assignment. It is probably significant that the anisotropy data for the lower-frequency signals are close to those for compound 1, whereas the values for the higher-frequency resonances are substantially different.

Both the anisotropy and the asymmetry data are more consistent with the second proposed structure. It might be expected that the fourth, weakly-bound Me_3Sn group, in the first proposed structure would have a larger asymmetry and smaller anisotropy than the values calculated.

$$5.6.3 \quad \text{Derivatives of } [(Me_3Sn)_4Fe(CN)_6]$$

    7    $[(Me_3Sn)_4Fe(CN)_6.Dioxan/H_2O]$

    8    $[(Me_3Sn)_4Fe(CN)_6.2H_2O]$

    9    $[(Me_3Sn)_4Fe(CN)_6.D(+)glucose]$
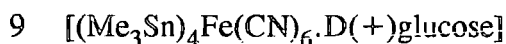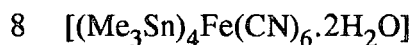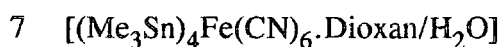
The crystal structure for 7 is given in section 4.3 and contains two chains with similar tin environments as shown below.

Chain A

$$\begin{array}{c} \text{Me} \quad \text{Me} \\ \diagdown \;\; \diagup \\ -C-N-Sn-N-C- \\ | \\ \text{Me} \end{array}$$

Chain B

$$\begin{array}{c} \text{Me} \quad \text{Me} \\ \diagdown \;\; \diagup \\ -C-N-Sn-O- \\ | \\ \text{Me} \end{array}$$
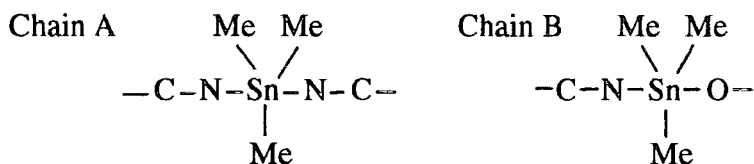
The asymmetry values calculated for both environments are zero within experimental error, indicating axial symmetry, as expected for the two structures above. There is, however, a difference in the anisotropies of 46 ppm implying one of the environments is less spherically symmetric than the other. In section 5.3.2 the higher-frequency signal is assigned to the tin in chain B which has the smaller anisotropy. This decrease is probably due to the oxygen directly bonded to the tin.

The structures of 8 and 9 are not known but the ^{119}Sn NMR spectrum indicates four different environments for each. The anisotropies and asymmetries were calculated from the second spin-rate spectra. It was difficult to integrate the peak areas because of overlapping lines therefore intensities were found by measuring the peak heights. The results are given in table 5.6.1.

The tin environment of chain A in both 8 and 9 (-107 ppm) has an asymmetry of zero indicating axial symmetry as expected from the structure below.

Chain A $-C-N-Sn-N-C-$
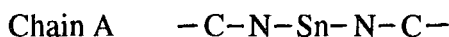
The corresponding anisotropies (-317 and -353 ppm) are both similar to that calculated for the similar environment in 4.

In 8, the environment of chain B (47 ppm) has an asymmetry of zero but in 9 it is 0.3.

$$\text{Chain B} \quad -\text{C}-\text{N}\overset{\diagup\text{Sn}\diagdown}{\underset{\diagdown\text{Sn}\diagup}{}}\text{N}-\text{C}-$$
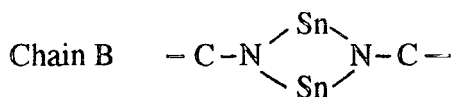
A non zero asymmetry value would be expected for this environment since there is no longer axial symmetry. The value of 0.3 is also in agreement with that calculated for the similar environment in 4. The corresponding anisotropies for both 8 and 9 (-171 and -190 ppm) are smaller in magnitude than those calculated for chain A and are in agreement with that calculated for the similar environment in 4. This reflects the different environment in chain B where the N-Sn-N angle is quite bent.
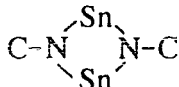
In the third environment the tin is directly bonded to an oxygen atom (chain C, -30 ppm). The calculated asymmetry for 8 is 0.96 indicating a highly asymmetric environment and the possibility that the N-Sn-O angle is very bent. For 9 the asymmetry of 0.16 again indicates an environment no longer axially symmetric but one not as asymmetric as in 8. The anisotropy for 8 is smaller in magnitude than that for 9 and implies that although the two environments are asymmetric, the one in 8 is slightly more spherically symmetric than that in 9.

The fourth environment in each case is axially symmetric (asymmetry = 0) and has an anisotropy greater than -300 ppm. This appears to indicate an environment similar to that in chain A, of a tin atom in a relatively straight chain.

153

13   $[(Cp_2Co)(Me_3Sn)_3Fe(CN)_6]$

14   $[(Et_3N)(Me_3Sn)_3Fe(CN)_6]$
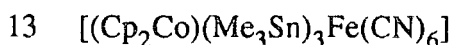
The crystallographic data for compound 13 indicate two different tin environments but the ^{119}Sn spectrum contains three signals. The chemical shifts of two of the signals are very close to those obtained for compound 4 and it can be seen that the anisotropies are also very similar.

		4		13	
		δ/ppm	⅃/ppm	δ/ppm	⅃/ppm
Chain A	C–N–Sn–N–C	−108	−347	−105	−359
Chain B	C–N(Sn)(Sn)–N–C	46	−184	48	−188

It can therefore be concluded that both compounds contain tin environments of the type in chain A and chain B.

The asymmetry values calculated for the two sites are in agreement with this assignment. The environment of chain A has an asymmetry of zero indicating axial symmetry and that of chain B has a larger asymmetry since the environment is no longer axially symmetric.

The third environment in compound 13 has an anisotropy of −382 ppm and an asymmetry of 0.28. This indicates near axial symmetry and an environment possibly similar to that in chain A.

For compound 14 no crystallographic studies have been possible but the ^{119}Sn spectrum indicates two similar tin environments. Both have asymmetries close to zero indicating axial symmetry. Their anisotropies are also similar and are greater in magnitude than those calculated for any of the other tin containing compounds. It can be concluded that compound 14 contains two very similar tin environments which are different to those of compound 13.

10    $[(Me_3Pb)_3Co(CN)_6]$

11    $[(Me_3Pb)_4Ru(CN)_6.2H_2O]$

12    $[(Me_3Pb)_4Fe(CN)_6.2H_2O]$

The ^{207}Pb spectra were run at two different spin-rates and a SSB analysis was carried out on each one. The results were then averaged and can be seen in table 5.6.2. The values of asymmetry calculated for all the lead environments are zero within experimental error, indicating axial symmetry. The anisotropies are all in the range -1200 ppm to -1400 ppm, substantially greater than any found for ^{119}Sn in the present work.

Compound 10 contains two lead environments separated by 100 ppm but their anisotropies are the same within experimental error. The analogous compound $[(Me_3Sn)_3Co(CN)_6]$, by comparison, showed a more significant difference between the anisotropies of the two tin environments.

Compound 11 also contains two lead environments with the same anisotropies but of a slightly smaller magnitude than in 10.

Compound 12 contains three environments, two of which have the same anisotropies and the third is slightly smaller.

To conclude, the SSB analyses on all three lead-containing compounds indicate all the environments to be very similar.

Due to the ^{15}N-enrichment of this sample the signal-to-noise ratio of the ^{15}N spectrum is very good (figure 5.2.6). This enabled a slow-spinning spectrum to be obtained suitable for SSB analysis. Two different spin-rates were used and the results were averaged and can be seen in table 5.6.3.

The spectrum indicates three different environments all of which have an asymmetry of zero implying axial symmetry. According to the structure suggested in section 5.2.6, the nitrogen can be either two- or three- coordinate. The two higher-frequency signals assigned to the two-coordinate nitrogens have asymmetries of zero and similar anisotropies of approximately 330 ppm. The signal at −161 ppm assigned to the three-coordinate nitrogen also has an asymmetry of zero but the anisotropy is somewhat smaller (300 ppm). The lack of asymmetry for the −161 ppm signal is not as expected from the assignment to a site with substantially different coordination from the others.

5.6.7   CN groups of selected compounds

3   [(Bu$_3$Sn)$_3$Co(CN)$_6$]

5   [(Me$_3$Sn)$_4$Ru(CN)$_6$]

10   [(Me$_3$Pb)$_3$Co(CN)$_6$]
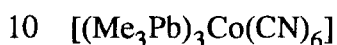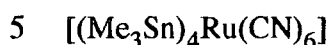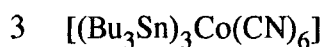
SSB analysis of the CN signals in the ^{13}C spectra is more difficult due to the signals overlapping with the lower frequency peaks from the R (Me,Et,Bu) groups. However, three spectra were chosen where there was a reasonable number of sidebands with no overlap. Since the sidebands are not all the same shape, and are also split, their intensities were found by integrating the signals using the spectrometer. The results of the SSB analyses can be found in table 5.6.4.

Both compounds 3 and 5 gave asymmetries of zero, indicating axial symmetry, which is an understandable result since the carbon is only bonded to two other atoms (Co or Ru

and N). However, the CN groups in 10 have a calculated asymmetry value of 0.4. This is not as expected since the values calculated for the anisotropy are all approximately the same (200 ppm), indicating the environments of the CN groups within the three compounds are very similar.

It is interesting to note that the anisotropies calculated for both ^{15}N and ^{13}C are positive whereas for ^{119}Sn and ^{207}Pb they are all negative.

Table 5.6.1   Anisotropy and asymmetry values for tin compounds

		SR/Hz	δ/ppm	⅃/ppm	η	SDSQ
1	[(Me₃Sn)₃Co(CN)₆]	4500	−118	−360	0.2	10
			−88	−341	0.16	8
2	[(Et₃Sn)₃Co(CN)₆]	4000	−75	−305	0.11	10
3	[(Bu₃Sn)₃Co(CN)₆]	5110	−45	−277	0.13	7
		10110	−45	−298	0.0	10
4	[(Me₃Sn)₄Fe(CN)₆]	4620	−108	−347	0.15	6
			46	−184	0.3	1
5	[(Me₃Sn)₄Ru(CN)₆]	4480	−97	−340	0.22	29
			32	−210	0.29	2
6	[(Me₃Sn)₄Os(CN)₆]	8980	−94	−338	0.11	7
			26	−219	0.23	2
7	[(Me₃Sn)₄Fe(CN)₆ .Dioxan/H₂O]	9170	−136	−374	0.0	7
			−73	−328	0.0	45
8	[(Me₃Sn)₄Fe(CN)₆ .2H₂O]	12650	−107	−317	0.0	58
			47	−171	0.0	34
			−29	−229	0.96	48
			−138	−301	0.0	56
9	[(Me₃Sn)₄Fe(CN)₆ .D(+)glucose]	12350	−108	−353	0.0	8
			46	−190	0.3	6
			−30	−312	0.16	10
			−139	−369	0.0	39
13	[(Cp₂Co)(Me₃Sn)₃ Fe(CN)₆]	11000	−139	−382	0.28	20
			−105	−359	0.0	12
			48	−188	0.47	21
14	[(Et₄N)(Me₃Sn)₃ Fe(CN)₆]	10000	−181	−428	0.1	14
			−158	−419	0.0	40

Table 5.6.2   Anisotropy and asymmetry values for lead compounds

		SR/Hz	δ/ppm	$\beth$/ppm	η	SDSQ
10	[(Me$_3$Pb)$_3$Co(CN)$_6$]	10360	172	−1360	0.0	115
			78	−1365	0.0	93
		12310	172	−1331	0.0	204
			78	−1338	0.0	75
		average	172	−1345	0.0	
			78	−1351	0.0	
11	[(Me$_3$Pb)$_4$Ru(CN)$_6$ .2H$_2$O]	11180	200	−1273	0.0	14
			149	−1285	0.0	76
		12850	200	−1305	0.0	25
			149	−1305	0.0	57
		average	200	−1289	0.0	
			149	−1295	0.0	
12	[(Me$_3$Pb)$_4$Fe(CN)$_6$ .2H$_2$O]	11300	195	−1345	0.0	21
			139	−1300	0.0	21
			64	−1362	0.0	44
		12280	195	−1370	0.0	34
			139	−1314	0.0	26
			64	−1350	0.0	35
		average	195	−1357	0.0	
			139	−1307	0.0	
			64	−1356	0.0	

Table 5.6.3   Anisotropy and asymmetry for ^{15}N enriched [(Me$_3$Sn)$_4$Fe(CN)$_6$]

		SR/Hz	δ/ppm	⅃/ppm	η	SDSQ
4a	[(Me$_3$Sn)$_4$Fe(CN)$_6$]	2540	−109	335	0.0	11
			−124	328	0.0	12
			−161	300	0.0	8
		3690	−109	333	0.0	7
			−124	327	0.0	6
			−161	293	0.0	3
		average	−109	334	0.0	
			−124	328	0.0	
			−161	297	0.0	

Table 5.6.4   Anisotropies and asymmetries for ^{13}C in CN groups

		SR/Hz	δ/ppm	⅃/ppm	η	SDSQ
3	[(Bu$_3$Sn)$_3$Co(CN)$_6$]	4930	128	189	0.0	74
5	[(Me$_3$Sn)$_4$Ru(CN)$_6$]	5000	162	233	0.0	7
10	[(Me$_3$Pb)$_3$Co(CN)$_6$]	4140	135	208	0.39	73

160

CHAPTER 6

SUMMARY AND CONCLUSION

The ^{13}C spectra of all the systems studied contain fewer methyl signals than that predicted by X-ray studies. A 2-D experiment described in 5.2.5 shows that an exchange process is taking place between the three methyl groups attached to one tin atom. In most cases, therefore, the number of methyl signals seen in the NMR spectrum can be multiplied by three.

All the ^{59}Co spectra obtained only contain one signal even though the X-ray data indicate two different cobalt atoms in the asymmetric unit. It is unlikely that different signals are obscured by the substantial linewidths since cobalt chemical shifts are very sensitive to changes in the environment.

All tin and lead atoms have trigonal bipyramidal symmetry with two nitrogens in the axial positions and three R groups (R =Me, Et, Bu) in the equatorial positions. The chemical shifts are typical of such five coordinate environments.

A summary and some conclusions are given below for each of the compounds studied.

6.2 [(Me$_3$Sn)$_3$Co(CN)$_6$]   1

The structure of this compound is known to consist of three intersecting chains A, B and C of the general form :-

$$-\overset{|}{\underset{|}{Co}}-C-N-\overset{\backslash/}{\underset{|}{Sn}}-N-C-\overset{|}{\underset{|}{Co}}-$$
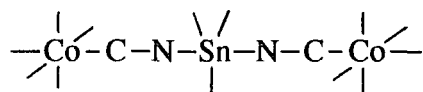
There are differences in bond lengths and bond angles between the chains. Chains A and B are similar. Chain C has a more asymmetric N-Sn-N bridge and is more bent at the nitrogen atom in comparison to A and B. The number of crystallographically different sites in the asymmetric unit is given in the table below with the number of sites found from the NMR data.

	C(CH₃)	C(CN)	Sn	N(CN)	Co
X-ray data	9	6	3	6	2
NMR data	3^1	?	2^2	3	1

^{1} at temperature of $-59^\circ C$
^{2} in the intensity ratio 2:1

There appears to be a certain amount of discrepancy between the X-ray data and the NMR data. The cyanide region of the ^{13}C spectrum is very complicated but if coupling to both ^{14}N and ^{59}Co are taken into account it probably indicates more than one CN but not as many as six. NMR does not appear to be able to distinguish between the tin atoms in chain A and B or the methyls except at low temperature. The nitrogen spectrum, however, indicates three different chains but is unable to distinguish between the two different CN groups within each chain. The asymmetry data confirms the axially symmetric nature of the tin environment.

6.3 [(Et₃Sn)₃Co(CN)₆] 2

	C(CH₃)	C(CH₂)	C(CN)	Sn	N(CN)	Co
NMR data	1	1	1^1	1	1	1

^{1} see section 5.1.5

All the NMR data appear to indicate that the chains are equivalent. By comparison of chemical shifts, the chains are probably most similar to A and B of compound 1, having more symmetrical bridges and being less bent than chain C. The asymmetry data again confirms an axially symmetric environment for the tin. A small decrease in magnitude of the anisotropy, in comparison to 1, indicates a slightly more spherical tin environment due to the increase in the steric bulk of the R group.

6.4 $[(Bu_3Sn)_3Co(CN)_6]$ 3

	Butyl	C(CN)	Sn	N(CN)	Co
NMR data	2	$?^1$	1	1	1

^{1} no resolution in centreband signal

The NMR data again indicate the chains are all equivalent; the two butyl signals arising from differences in the butyls on one particular tin atom. The exchange process described earlier has been slowed down enough by the increase in steric bulk of the butyl to allow differences to be seen at room temperature. The asymmetry implies axial symmetry for the tin and there is a further decrease in the magnitude of the anisotropy implying a more spherical environment due to the increase in size of the R group.

6.5 $[(Me_3Sn)_4Fe(CN)_6]$ 4

The structure of 4 is not known. It was originally thought that the $(Me_3Sn)_3Fe(CN)_6$ formed a lattice similar to that of $[(Me_3Sn)_3Co(CN)_6]$ with the fourth Me_3Sn only weakly bonded in the cavities. The number of crystallographically different sites in the asymmetric unit, as suggested by the NMR data, is given in the table below.

	$C(CH_3)$	C(CN)	Sn	N(CN)
NMR data	2^1	3	2	3

^{1} 6 at temperature of $-37°C$

These numbers are in agreement with the proposed structure but the relative intensities of the NMR signals do not reflect the 3:1 ratio of the numbers of Me_3Sn groups in the two different sites. A different structure is therefore proposed which contains two chains of type A and one of type B.

Chain A   Fe—C—N—Sn—N—C—Fe

Chain B   Fe—C—N\<$_{Sn}^{Sn}$>N—C—Fe
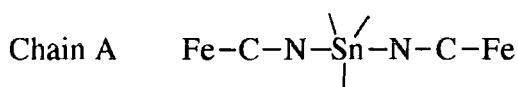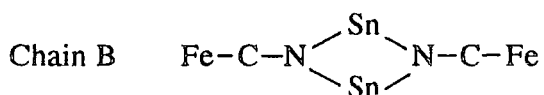
This structure results in the intensity ratio of 1:1 as found in the methyl region of the ^{13}C spectrum and the ^{119}Sn spectrum.

The high frequency region of the ^{13}C spectrum, and the ^{15}N spectrum, indicate that the structure contains an equal number of three different cyanide groups. This probably indicates that the two A type chains are slightly different.

Both the ^{15}N and ^{119}Sn spectra show a substantial difference in the chemical shifts between the N and Sn atoms in chains A and B and those in chain C reflecting their very different environments. The anisotropy and asymmetry data for the tin environments also show a large difference enabling the chemical shift assignments to be confirmed. The corresponding data for the nitrogen do not show such a marked difference.

6.6   [(Me$_3$Sn)$_4$Ru(CN)$_6$] 5 and [(Me$_3$Sn)$_4$Os(CN)$_6$] 6

The spectra for 5 and 6 are very similar to those obtained for the Fe containing compound and therefore similar conclusions can be made concerning their structures. There is, however, a shift of both the ^{13}C and the ^{15}N signals of the cyanide groups to lower frequency as the metal atom is changed from Fe to Ru to Os. This is due to an increase in electron density as the metal atom gets larger resulting in the C and N being more shielded.

6.7 [(Me$_3$Sn)$_4$Fe(CN)$_6$.Dioxane/H$_2$O] 7

The crystal structure of compound 7 is known and contains two different non-linear chains.

Chain A   Fe - C — N — Sn — N — C — Fe

Chain B   Fe - C — N — Sn — O — H ⋯ O⟨⟩O ⋯ H — O — Sn — N — C — Fe
with H below the two Sn–O groups.

There are twice as many chains of type A as there are of type B which creates an equal number of the two different Me$_3$Sn environments. The numbers of crystallographically different sites in the asymmetric unit are given in the table below with the numbers obtained from the NMR data.

	C(CH$_3$)	C(CN)	Sn	N(CN)
X-ray data	6	3	2	3
NMR data	2	3	2	2[1]

[1] in the ratio 2:1

It would appear that the NMR data agree very closely with the X-ray data except for not being able to distinguish between the nitrogens of the two different CN groups of chain A. The asymmetry data confirm the axially symmetric nature of both tin environments and a difference in their anisotropies is in agreement with one tin bonded to two nitrogens and the other bonded to a nitrogen and an oxygen.

6.8 [(Me₃Sn)₄Fe(CN)₆.2H₂O] 8 and [(Me₃Sn)₄Fe(CN)₆.D(+)glucose] 9

The structures of these two compounds are not known but the table below indicates the results obtained from the NMR spectra.

|	$C(CH_3)$	$C(CN)$	Sn	N(CN)
NMR data for 8 and 9	1^1	$?^2$	4	3

1 possibly a second indicated by a broader signal
2 signal is very complicated

The NMR data does not give a clear number of crystallographically different sites within the asymmetric unit, however, the two compounds give similar spectra indicating that they have similar structures. Both the ^{119}Sn and the ^{15}N spectra contain signals at very similar chemical shifts to those obtained for compound 4. The anisotropy and asymmetry data for two of the tin environments are also similar to 4. It can therefore be concluded that the structures of both 8 and 9 contain chains of type A and B like those in 4. There are also two other tin signals, one probably due to bonding to H_2O or D(+)glucose and the other to an A type chain but different from that of 4.

6.9 [(Me₃Pb)₃Co(CN)₆] 10

The crystal structure of 10 is known and is similar to that of 1 with three intersecting non-linear chains A, B and C forming a three-dimensional lattice.

Chains A, B and C $-\overset{|}{\underset{/}{C}o}-C-N-\overset{\diagdown}{\underset{|}{P}b}-N-C-\overset{|}{\underset{/}{C}o}-$
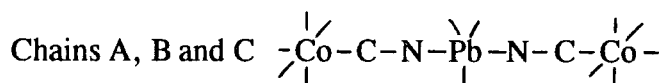
Differences between the three chains arise from differences in the bond lengths and angles. Chains A and B are similar having more symmetrical N-Pb-N bridges than chain C. The chains are bent at the nitrogen atom by more than in the tin analogue with chain B being the most bent. The numbers of crystallographically different sites in the asymmetric unit as obtained from both the X-ray and NMR data are given in the table below.

	C(CH$_3$)	C(CN)	Pb	C(CN)	Co
X-ray data	9	6	3	6	2
NMR data	3	?	2	1	1

The NMR data do not appear to agree too closely with the X-ray data. The ^{13}C spectrum is very similar to that of compound 1 with a complicated CN region making it difficult to distinguish how many different CN groups there are within the asymmetric unit. The three methyl environments of the three different chains are easily distinguished but only two ^{207}Pb NMR signals (ratio 2:1) indicates that two of the lead environments, probably in chains A and B, are very similar. The poor signal-to-noise ratio of the ^{15}N spectrum results in only one signal being seen. The asymmetry data for the lead environments confirm that they are both axially symmetric.

6.10 [(Me$_3$Pb)$_4$Ru(CN)$_6$.2H$_2$O] 11 and [(Me$_3$Pb)$_4$Fe(CN)$_6$.2H$_2$O] 12

The crystal structures of both 11 and 12 are known and they both consist of a three-dimensional lattice of non-linear chains A and B.

Chain A   M−C−N−Pb−N−C−M−   M = Ru, Fe

Chain B   H₂O−Pb−N−C−M−C−N−Pb−OH₂
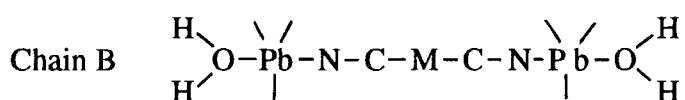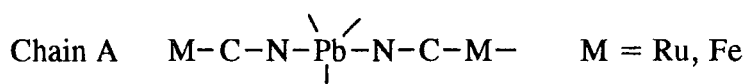
There are twice as many chains of type A as there are B resulting in an equal number of each of the two PbMe$_3$ environments and chain A contains two different cyanide groups. Hydrogen bonds form between the water of chain B and the closest nitrogen of a cyanide group. The numbers of crystallographically different sites in the asymmetric unit as determined from both X-ray and NMR data are given below.

168

	C(CH$_3$)	C(CN)	Pb	N(CN)
X-ray data for both 11 and 12	6	3	2	3
NMR data for 11	2	3	2	3
NMR data for 12	?	?	3	3

The NMR data for 11 agree very well with the X-ray data as regards the number of crystallographically different atoms. There is, however, a discrepancy in the relative intensities of both the methyl (ratio 2:1) and the lead signals (ratio 3:1). From the crystal structure, both were expected to have relative intensities in the ratio 1:1. The asymmetry data confirm the axially symmetric nature of the two lead environments and their anisotropies indicate that they are similar.

The NMR data for 12 are very different from the X-ray data. The ^{13}C spectrum is complicated in both the methyl and the cyanide regions possibly indicating a disordered structure. The ^{207}Pb spectrum indicates one extra lead environment than the X-ray data although two of the signals are at similar chemical shifts to those of compound 11. The ^{15}N spectrum contains three signals at similar chemical shifts to those obtained for 11 which is in agreement with the X-ray data and appears to predict a more ordered structure than the ^{13}C spectrum. The anisotropy and asymmetry data confirm the axially symmetric nature of the lead environment.

6.11 [Cp$_2$Co(Me$_3$Sn)$_3$Fe(CN)$_6$] 13

The table below indicates the number of crystallographically different sites in the asymmetric unit as predicted by the X-ray and NMR data.

|	C(CH$_3$)	C(CN)	Sn	N(CN)
X-ray	6	3	2	3
NMR	1[1]	>4	3	1

[1] plus a second broader signal of lower intensity

It is thought that the $(Me_3Sn)_3Fe(CN)_6$ forms a lattice similar to that of compound 1 consisting of three intersecting non-linear chains of the form:

$$-\overset{|\diagup}{Fe}-C-N-\overset{\diagdown\diagup}{Sn}-N-C-\overset{|\diagup}{Fe}-$$
$$\diagup| \qquad\qquad | \qquad\quad \diagup|$$
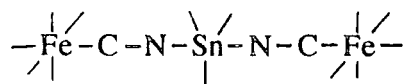
The lattice acts as a 'host' to the Cp_2Co - the 'guest'.

The NMR data do not agree with the crystallographic data. There is an extra signal in both the cyanide region of the ^{13}C spectrum and the ^{119}Sn spectrum. The methyl region of the ^{13}C spectrum does contain two signals but they are of different intensity and one is broader than the other. It is possible that ^{13}C spectra recorded at elevated temperatures would give a different picture as was the case for compounds 4, 5 and 6. Two of the tin signals have similar chemical shifts and anisotropy and asymmetry values to those obtained for compound 4. This implies that the structure contains both a straight chain (A) and a doubly bridged chain (B).

Chain A $Fe-C-N-Sn-N-C-Fe$

Chain B $Fe-C-N\diagup^{Sn}\diagdown_{Sn}\diagup N-C-Fe$
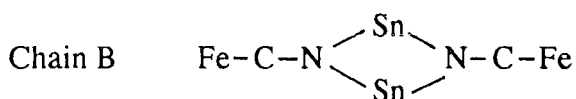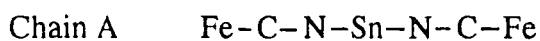
It would seem that exchange of the fourth (Me_3Sn) group has not been fully completed.

6.12 $[Et_4N(Me_3Sn)_3Fe(CN)_6]$ 14

Compound 14 is also thought to be a host-guest system although no X-ray crystallographic studies have been done. The NMR spectra are very simple in comparison to 13 and suggest the following number of crystallographically inequivalent sites in the asymmetric unit.

	$C(CH_3\text{-}Sn)$	$C(CH_3\text{-}CH_2\text{-}N)$	$C(CN)$	Sn	$N(CN)$	$N(Et_4N)$
NMR	1	2	1	2	?[1]	1

[1] signal to noise ratio poor

170

The ^{13}C spectrum contains only one signal for each type of carbon present indicating that all the chains of the lattice are equivalent. The ^{119}Sn spectrum, however, contains two signals which seems to predict a difference in the chains not seen in the ^{13}C spectrum. The chemical shifts of the ^{119}Sn signals are at a lower frequency than those for compound 4 and possibly indicate that complete ion-exchange has taken place.

The anisotropy and asymmetry values for the tin environments indicate they are similar and both axially symmetric.

6.13   Conclusion

Multinuclear NMR spectroscopy has proved to be a very useful tool in the investigation of three-dimensional organometallic polymers. The NMR results have sometimes confirmed the structural information obtained from X-ray crystallography and have also been used to predict structures for those compounds where X-ray crystallography has not yet been possible. There are also many more NMR experiments, including variable temperature studies, which could provide much more information.

REFERENCES

Chapter 1

1. B. F. Hoskins and R. Robson, J. Am. Chem. Soc., 112, 1546-1554 (1990).

2. R. Uson, J. Fornies, M. A. Uson and E. Lalinde, J. Organomet. Chem., 185, 359-366 (1980).

3. T. M. Garrett, U. Koert, J. Lehn, A. Rigualt, D. Meyer and J. Fischer, J. Chem. Soc. Chem. Comm., 557-558 (1990).

Chapter 2

4. E. R. Andrew, Philos. T. Roy. Soc. A, 299, 505-520 (1981).

5. A. Pines, M. G. Gibby and J. S. Waugh, J. Chem. Phys., 59(2), 569-590 (1973).

6. S. R. Hartmann and E. L. Hahn, Phys. Rev., 128(5), 2042-2053 (1962).

7. High-Resolution NMR Spectroscopy of Synthetic Polymers in Bulk (Methods in Stereochemical Analysis 7), p. 42, edited by R. A. Komoroski, VCH publishers, Florida (1986)

8. N. M. Szeverenyi, M. J. Sullivan and G. E. Maciel, J. Magn. Reson., 47, 462-475 (1982).

9. J. Jeener, B. H. Meier, P. Bachmann and R. R. Ernst, J. Chem. Phys., 71, 4546 (1979).

Chapter 3

10. R. D. Kendrick, R. A. Wind and C. S. Yannoni, J. Magn. Reson., 40, 585 (1980).

11. G. J. Martin, M. L. Martin and J. Gouesnard, NMR Basic Principles and Progress 18, ^{15}N NMR spectroscopy, p52, Springer-Verlag Berlin Heidelberg (1981).

12. A. Samoson and E. Lippmaa, Phys. Rev. B, 28, 6567 (1983)

13. J. S. Waugh, J. Mol. Spectrosc., 35, 298-305 (1970).
    A. E. Derome, Modern NMR Techniques for Chemistry Research, p. 165, Pergamon Press (1987).

14. Sideband fitting program written by Larry Merwin and Xiao Ping, University of Durham.

15. M. M. Maricq and J. S. Waugh, J. Chem. Phys., 70(7), 3300-3315 (1979).

16. N. J. Clayden, C. M. Dobson, L. Lian and D. J. Smith, J. Magn. Reson., 69, 476-487 (1986).

17. J. F. Haw, G. C. Campbell and R. C. Crosby, Anal. Chem., 58(14), 3172-3177 (1986).

18. Alan Jeffrey, Mathematics for Engineers and Scientists, p. 705, Van Nostrand Reinhold (UK) Co. Ltd. (1979).

19. Internal communication, D. C. Apperley, University of Durham.

20. P. W. Atkins, Physical Chemistry, p801, Oxford University Press 1982.

Chapter 4

21. K. Yunlu, N. Hock and R. D. Fischer, Angew. Chem. Int. Edit., 24(10), 879-881 (1985).

22. A. K. Brimah, Doctoral Dissertation, University of Hamburg, Germany, 1991.

23. P. Brandt, A. K. Brimah and R. D. Fischer, Angew. Chem. Int. Edit., 27(11), 1521-1522 (1988).

24. S. Eller, P. Brandt, A. K. Brimah, P. Schwarz and R. D. Fischer, Angew. Chem. Int. Edit., 28(9), 1263-1265 (1989).

25. M. Adam, A. K. Brimah, R. D. Fischer and Li Xing Fu, Inorg. Chem., 29(9), 1595-1597 (1990).

26. D. C. Apperley, N. A. Davies, R. K. Harris, A. K. Brimah, S. Eller and R. D. Fischer, Organometallics, in press.

27. Internal communication, R. D. Fischer, Universtiy of Hamburg, Germany.

Chapter 5

28. J. P. Lockhart, W. F. Manders and J. J. Zuckerman, J. Am. Chem. Soc., 107, 4546-4547 (1985).

29. D. C. Apperley, B. Haiping and R. K. Harris, Mol. Phys., 68(6), 1277-1286 (1989).

30. R. Gobetto, R. K. Harris and D. C. Apperley, J. Magn. Reson., 96, 119-130 (1992).

31. J.K.M.Sanders and B.K.Hunter, Modern NMR Spectroscopy - A Guide for Chemists, p. 210, Oxford University Press (1987).

32. F. W. Wehrli and T. Wirthlin, Interpretation of C-13 NMR Spectra, Heyden & Sons Ltd., London, 1976.

33. L. F. Johnson and W. C. Jankowski, C-13 NMR Spectra, John Wiley & Sons (1972).

BIBLIOGRAPHY

A. E. Derome, *Modern NMR techniques for Chemistry Research*, Pergamon Press (1987).

J.K.M.Sanders and B.K.Hunter, Modern NMR Spectroscopy - A Guide for Chemists, Oxford University Press (1987).

C. A. Fyfe, Solid-State NMR for Chemists, CFC Press (1983).

G. Engelhardt and D. Michel, High-Resolution Solid-State NMR of Silicates and Zeolites, John Wiley & Sons (1987).

M. Mehring, NMR 11 Basic Priciples and Progress - High-Resolution NMR spectroscopy in Solids.

C. Brevard and P. Granger, Handbook of High-Resolution Multinuclear NMR, Jon Wiley & Sons (1981).